The Pennsylvania State University

The Graduate School

College of Earth and Mineral Sciences

EXPLORING A 60-YEAR RECORD OF MANGANESE DEPOSITION IN MARIETTA OHIO USING SOIL CHEMISTRY AND ATMOSPHERIC DISPERSION MODELING

A Thesis in

Geosciences

by

Megan R. Carter

Submitted in Partial Fulfillment
of the Requirements
for the Degree of

Master of Science

August 2013

The thesis of Megan R. Carter was reviewed and approved* by the following:

Susan Brantley
Distinguished Professor of Geosciences
Thesis Advisor

James Kubicki
Professor of Geosciences

Timothy White
Senior Research Associate

Chris Marone
Professor of Geosciences
Associate Head for Graduate Programs and Research

*Signatures are on file in the Graduate School.

Abstract

Atmospheric deposition of metals emitted by anthropogenic activities has contributed metals to soils worldwide. A ferromanganese refinery, located in Marietta, OH, is currently the largest source of manganese (Mn) emitted into the atmosphere in the U.S.A. Particulate emissions during production are up to 35% manganese oxide (MnO_2) by weight and are dominantly in the size range of 0.05 to 0.4 µm diameter. Particles of that size are both highly mobile and respirable. In order to understand how emissions of Mn and another emitted metal, Cr, has varied over the lifetime of the refinery, a series of soil cores were collected at sites located from 1 to 47 km from the refinery. Concentrations of soil-surface Mn and Cr are enriched 9 and 3 times that of the parent material within 1.2 km of the refinery, respectively. Total mass of Mn added to soils per unit land area integrated over the soil depth was calculated to be 77 mg Mn cm^{-2} near the refinery. The geographic extent of Mn deposition due to EMI as indicated by a positive integrated Mn mass flux value extends up to 25 km or possibly even beyond 47 km from EMI, depending on assumed composition of the parent material. Mn deposition rates were also simulated with an atmospheric dispersion model (SCIPUFF) using meteorological data from a local weather station and emission rates for the refinery, though the model under-predicted recent deposition. Soil-derived integrated mass flux values for Mn coupled with recent estimates of Mn deposition in Marietta suggest that deposition rates in the past may have been 3 orders of magnitude greater than today's rates. Such a higher historic emission rate cannot be tested because no quantitative data are available for emissions earlier than 1988. However, higher emissions in the past are likely given the history of metal production. Decreases in deposition rates are also likely due to emission control technology installed as a response to regulations such as the Clean Air Act (1970): the soil measurements document that the Clean Air Act is the likely cause of more than 166x reduction in deposition per metric ton of Mn alloy used. These results document that soil measurements can help reconstruct past metal deposition rates. In fact, when developed on easily-identified parent material, soil profiles may be more useful indicators of the past behavior of metal-emitting sources over decadal time scales than atmospheric dispersion models.

TABLE OF CONTENTS

LIST OF FIGURES

LIST OF TABLES

ACKNOWLEDGEMENTS

This work was funded by NSF grant EAR #1052614 to S. Brantley and E. Herndon (Penn State) and the NSF Susquehanna Shale Hills Critical Zone Observatory grant EAR #0725019 to C. Duffy (Penn State).

I have been fortunate to have the technical and emotional support of many people while completing my degree. I am grateful to those who helped with fieldwork, especially Paul Grieve, Joanna Peth, Sarah Sharkey, and Dr. Tim White. I would also like to thank Dr. Dave Stauffer and Dr. Brian Gaudet for help with SCIPUFF, as well as Henry Gong, Laura Liermann, and Melanie Saffer for assistance in the lab. This work benefitted greatly from discussions with those listed above, as well as with Dr. Beth Herndon, Dr. Gary Stinchcomb, Nina Bingham, Xin Gu, and Tiffany Yesavage.

To my advisor, Sue Brantley, thank you for allowing me to pursue this project and for teaching me to always “move forward with courage.” To my officemate and friend, Ashlee Dere, you are the only person I could happily work two feet (0.61 m) away from. To Elizabeth Denis and Emily Woodward, thank you for showing me what true friendship is and to Joe Orlando, thank you for believing in me and for putting up with me through it all. Finally, thank you to my family for your encouragement during my academic pursuits. We may have been separated by many miles, but your love and support have been a sustaining force throughout.

Introduction

Human interactions with and alterations of the global environment have increased so dramatically over the last few centuries that many scientists have deemed our current age the Anthropocene (Crutzen, 2002). Human-driven soil change is now so prevalent that humans are often considered by pedologists to be a soil-forming factor (Amundson and Jenny, 1991; Dudal, 2002). For example, industrial emissions and subsequent deposition of metals has been a significant source of metal loading into soils in the U.S.A. (Nriagu and Pacyna, 1988). While regulations on air and soil metal concentrations now exist in many countries including the U.S.A., the extent of anthropogenic soil change due to past metal inputs from specific industrial activities has not been quantified for many metals. Often, when metal inputs to soils are quantified, only additions to surface horizons are considered (Siccama and Smith, 1979; Siccama and Smith, 1980).

Manganese (Mn), the 12th most abundant element in Earth's crust, is a known neurotoxin and plays a key role in numerous environmental reactions that impact groundwater and bulk soil composition, including the distribution and speciation of several other toxic trace elements (McBride, 1994; Tebo *et al.*, 2004; Mergler *et al.*, 1999). Although on a global scale, 90% of atmospheric Mn emissions may be derived from natural sources (dust, erosion, volcanoes, sea-salt spray, etc.), anthropogenic emissions of Mn may be responsible for the majority of Mn inputs to the atmosphere in industrialized regions (Nriagu and Pacyna, 1988; Nriagu, 1989). Herndon and Brantley (2011) identified widespread, but patchy enrichment of Mn in soils throughout North America and Europe due to industrial sources and was the first to suggest that atmospheric transport is a key process in the modern global Mn cycle.

One metal that has been extensively studied in terms of atmospheric deposition to soils and sediments is Pb (Siccama and Smith, 1978; Gallon *et al.*, 2005). Pb has been a widely-acknowledged for decades as a neurotoxin even at low exposure levels and the existence of several isotopes of Pb has made the study of historic rates of accumulation easier than for other metals (Filippelli and Laidlaw, 2010). Unlike Pb, Mn has no naturally-occurring stable isotopes and, thus, very few studies of long-term historical trends in deposition have been carried out (Cole *et al.*, 1990).

Eramet Marietta Inc. (EMI), a large metallurgical manufacturing facility located just 8 km southwest of Marietta, Ohio, is currently the single largest emitter of Mn into the atmosphere in the United States (U.S. EPATRI, 2010). EMI has emitted more than 4500 metric tons of Mn to the atmosphere since 1988, more than twice as much as the next largest emitter (Fig. 1). Furthermore, Mn air concentrations within a 15 square kilometer radius of EMI have exceeded both background values for urban areas and health-based guidelines (Fig. 2) (ATSDR, 2008; Haynes *et al.*, 2010). Subsequent deposition of this industrially-sourced Mn to the land surface has likely resulted in Mn additions to the soil profile since EMI began operating in 1952. For this reason, the soils near EMI may contain a record of atmospheric deposition and represent a unique opportunity to study Mn behavior in soils near a large point source.

In this study, we assess whether soils can be used to determine the historic deposition rate of a metal from a refinery. Specifically, we a) quantify integrated mass flux of Mn into or out of soils in several locations at a range of distances from the source, and b) compare soil-derived Mn mass flux values with a model of atmospheric deposition that incorporates known emissions and meteorology.

Background

Manganese (Mn) is commonly found in natural systems in fine-grained poorly crystalline mixed valence Mn oxides, which can be very strong oxidizing agents (Post, 1999). Under low oxygen conditions, microorganisms may use Mn oxides as terminal electron acceptors during the oxidation of organic matter or H_2. Furthermore, Mn oxide minerals are known to adsorb or otherwise incorporate other metals such as Cu, Co, Cd, Zn, Ni, Sn, Pb, Ca, Fe, Hg, U, As, and Se (Tebo *et al*., 2004 and the references within). Mn cycling, therefore, plays a key role in the biogeochemical cycling of other elements, including several of public health concern.

Manganese Uses and Emissions

Manganese is one of the most widely used metals in the world. Due to its sulfur-fixing, deoxidizing and alloying properties, Mn is used extensively in iron and steel manufacturing. Upwards of 80-90% of Mn consumed domestically each year is in the steelmaking industry, while minor quantities of Mn are also used in fertilizers and dry cell batteries (Corathers, 2009). Mn is also a component of the fuel additive known as methylcyclopentadienyl manganese tricarbonyl (MMT), which was in use domestically from 1958 until 1977, as well as from 1995 to the present (Frumkin and Solomon, 1997).

Many industries emit Mn. For example, all the facilities in the contiguous U.S. reporting atmospheric emissions of Mn to the EPA during at least one year since 1988 are shown in Fig. 3 by industry type. Primary metals facilities were responsible for 50% of Mn air emissions in the U.S. from 1988 to 2010 (Appendix H). Likewise, anthropogenic emissions of Mn to the atmosphere in the U.S. in 1970 were estimated to be from Mn alloys processing (57%), cast iron processing (17%), and coal combustion (11%), resulting in total emissions of 18000 metric tons (U.S. EPA, 1977). Nriagu and Pacyna (1988) calculated that worldwide anthropogenic emissions of Mn to the atmosphere in 1983 were derived from coal combustion (1080-11880 metric tons, 17% of anthropogenic emissions), oil combustion (58-1790 metric tons, 2 %) non-ferrous metallurgy (415-4250 metric tons, 6%) steel and iron manufacturing (1065-28400 metric tons, 39%) and refuse incineration (252-10000 metric tons, 13%), resulting in net anthropogenic Mn emissions to the atmosphere of 10560-65970 metric tons. Total natural emissions of Mn, including biogenic sources, wind-borne soil particles, volcanoes, sea-salt spray, and forest fires were estimated to be 52000-582000 metric tons (Nriagu, 1989). Based on these values, natural emissions of Mn account for 90% of Mn emissions to the atmosphere yearly.

Manganese Health Effects

Manganese has several essential roles in the human body, including the production of the free-radical killing compound, Mn-superoxide dismutase (ATSDR, 2008). In larger doses, Mn compounds can be powerful neurotoxins. Extended exposure to moderate or high levels of Mn has been shown to cause “manganism”, a neurological disorder that has been likened to Parkinson’s Disease (Mergler et al., 1999). At chronic inhalation exposure levels as low as 27 ug/m^3, motor deficiencies have been detected (ATSDR, 2008). Furthermore, Mn exposure has also been correlated with lower intelligence scores, reduced perceptual reasoning and lower working memory scores in children (Bouchard *et al.,* 2011; Wasserman *et al.,* 2011). Roels *et al.* (1997) argued that Mn toxicity is most likely to occur by inhalation, since ingested Mn is effectively expelled by the liver.

Refinery History and Emissions

Ferroalloy production began at the site currently owned by Eramet Marietta Inc. (EMI) in 1952. The facility currently produces Mn alloys including silicomanganese and ferromanganese.

Formerly, EMI also produced ferrochromium. Since 1988, annual air emissions of Mn compounds reported by EMI to the U.S. Environmental Protection Agency (EPA) ranged from 65-250 metric tons, and have generally decreased, with 2 prominent peaks in 1992 and 2004 (crossed circles in Fig. 4, right axis). Although data are not available for emissions prior to 1988, Mn alloys produced at EMI are consumed in steel manufacturing and, thus, changes in Mn alloy production and subsequent Mn emissions are likely closely related to changes in steel production. EMI emissions, therefore, were presumably higher in the past, and likely peaked around the same time as domestic steel production in the mid-1970s (Fig. 4).

Several processes during ferroalloy production at EMI may emit Mn to the atmosphere. These include storage and transport of Mn ore, crushing, sizing, sintering, furnace smelting, ladle treatment, and casting. Of these activities, furnace smelting produces the largest amount of particulate emissions (EPA, 1985). In addition, high-temperature smelting emits very fine particulates that are potentially respirable and transportable over long distances.

Previous characterization of Mn furnace dust from the production of Mn alloys in other locations has indicated that Mn is typically present as Mn oxides (MnO, MnO_2 or Mn_3O_4) or $MnCO_3$ (Shen *et al.*, 2005). Particulate emissions range from 0.05-0.4 μm in diameter and are composed of the following component oxides: 34% MnO, 25% SiO_2, 8% Al_2O_3, 6% FeO, 2% CaO, and 1% MgO by weight, with other minor constituents (U.S. EPA 1974; U.S. EPA, 1984; Table 5). Silicomanganese production also results in particulate emissions of very similar size and chemical composition.

Previous Studies

Manganese alloy production and its associated industry, steelmaking, have enriched soils in Mn. Boudissa *et al.* (2006) investigated metal concentrations in the air and soils at a range of distances from a closed manganese alloy production facility near Montreal. The group found that surface soils (0-10 cm) contained approximately 266,000, 6,200, and 3,079 ppm Mn at sites 10-800 m from the facility, with high concentrations also found in the subsurface soils (10-25 cm). Boudissa *et al.* (2006) argued that enrichment of Mn very close to the refinery was the result of direct deposition of raw ferromanganese product, while more distant sites were contaminated due to atmospheric deposition of emissions from the refinery, as well as dust erosion and re-deposition from closer to the refinery. Elevated atmospheric concentrations in the vicinity of the closed facility further suggested that Mn-bearing particles continued to be re-suspended out of the soil.

At a distance of 25 km downwind of the refinery, however, the mean concentration of Mn in the air in Montreal dropped by 50% after the plant closed, even as there was a 10% increase in Mn emissions in the area due to the use of the fuel additive MMT (Loranger and Zayed, 1994). This suggests that refinery operations were a significant determinant of Mn air concentrations and likely Mn deposition rates even as far away as 25 km from the source during the time-span of operation.

Mn accumulation has been documented in wetland sediments of Lake Michigan near steel production facilities, the primary users of Mn alloys, in Gary, IN (Perkins *et al.*, 2000), as well as in peat cores obtained from a nearby bog (Cole *et al.*, 1990). Using ^{210}Pb dating, radiocarbon dating, and pollen analysis on peat cores obtained in the Cowles Bog along Lake

Michigan, Cole *et al.* (1990) showed that accumulation rates of Mn increased by nearly 33x from pre-settlement (1339-1656 A.D.) to peak accumulation (1970-1973). The same study noted that accumulation rates of Mn have decreased by approximately 50% since the early 1970's.

Previous Studies around EMI

Previous studies conducted in the greater Marietta area have identified elevated concentrations of Mn and other metals in ambient air (ATSDR, 2009). The Agency for Toxic Substances and Disease Registry (ATSDR) monitored atmospheric concentrations of several elements from 2007-2008 in 5 locations that varied in distance (up to 8 km) and direction from EMI. The study found that average monthly Mn air concentrations exceeded the ATSDR Mn minimal risk level (MRL) ($0.04\ \mu g\ m^{-3}$) at all sites in the study (ATSDR, 2008). Sites located in the same general direction from the industrial complex exhibited similar Mn concentration trends with respect to time, while sites located in opposite directions exhibited inverse trends, suggesting the presence of a large Mn-emitting source in between.

U.S. EPA (2008) used laser ablation inductively coupled plasma mass spectrometry (LA-ICP-MS) to characterize particulate matter collected on air filters at each of the 5 sites in the abovementioned air monitoring study and found that the presence of Mn was closely related to the presence of Cr, Pb, and Zn at all sites. Locations in the same general direction from the industrial complex exhibited similar trends in Mn concentration over time, while sites in different directions were dissimilar, as expected. Correlations were strongest between Mn and Cr and Mn and Pb at the site nearest the industrial complex (< 2 km NNW).

Using scanning electron microscopy, some filters collected in the Marietta air investigation were analyzed to determine particle morphology and Mn-bearing phases. Mn was predominantly present as Mn oxides. Most particles were spherical in shape (77%) and approximately 21% were found to be less than 2.5 μm in aerodynamic diameter, making them both highly transportable and highly respirable (U.S. EPA, 2009).

Atmospheric Dispersion and Atmospheric Dispersion Modeling

Effluents released from an emissions source, such as Mn-bearing compounds from EMI, tend to stay within the atmospheric boundary layer (ABL). This layer of the atmosphere lies nearest Earth’s surface and range from tens of meters up to 5 kilometers in thickness, depending on variables including surface heat flux, wind shear, large-scale weather conditions, and cloud cover (Wyngaard, 2010). In general, the ABL thickness is smallest at night and highest during the day. Summertime ABL thickness is also usually greater than wintertime.

Within the ABL, turbulent conditions prevail on account of fluctuations in variables including temperature, moisture, and flow velocity. This turbulence results in widespread dispersion of released effluents. Depending on the extent of turbulence, the ABL can become very well-mixed such that the concentration of an effluent may be very constant with height within it. Since atmospheric dispersion of effluents strongly influences the concentration of effluent in the air, dispersion modeling, which incorporates meteorological data and emissions statistics, can be used to estimate the levels of airborne hazardous compounds around emitters.

Methods

Choice of Sample Locations

Surface rocks of southeastern Ohio were deposited during the Upper-Paleozoic, likely between the late-Pennsylvanian and early Permian. Five major sequences have been described, including (in order of decreasing age) the Pottsville, Allegheny, Conemaugh, Monongahela, and Dunkard Groups. The first four groups are considered to be Pennsylvanian in age, while the Dunkard Group is assigned to the Permian, with a transitional sequence of both Pennsylvanian and Permian-age rocks in the lower portion (286 ± 12 Ma – 266 ± 17 Ma) (Martin, 1998 and the references within). Approximately 335 meters of rocks are exposed in Washington County, Ohio. Exposed strata in that county belong to the Dunkard Group, with some rocks of the mid-Conemaugh through Monongahela Groups outcropping, especially in low-lying areas. In order to constrain the number of variables in our study, we decided to limit sampling sites to locations overlying the Dunkard Group, the primary lithology located in ridgetop positions of Washington County. In order to achieve this goal, a fine-scale geologic map of Washington County was used (Collins and Smith, 1977).

The Dunkard Group outcrops along a northeast-southwest trending elliptical area of approximately 13000 sq. km in the Appalachian Basin, including parts of Pennsylvania, Maryland, Ohio and West Virginia. It is a coal-bearing unit of up to 360 m in thickness. During the early Permian, lower and upper fluvial plain environments developed in the Dunkard Basin, where lacustrine-deltaic environments had previously prevailed (Martin, 1998). In this regard, the lower portion of the Dunkard Group contains freshwater limestones, and carbonaceous shales and coals, while the upper portion is dominated by sandstones and red mudstones of greater thickness. Cyclic rock sequences identified in the Dunkard Basin have been interpreted as evidence of repeated shifts from alluvial-plain to lacustrine-deltaic-plain depositional environments (Beerbower, 1961).

Measured stratigraphic sections from a range of locations within the Dunkard outcrop belt indicate that fine clastic rocks (shale and mudstone) comprise more than 65 percent of the thickness of each measured section. Sandstones make up 30 percent of measured sections, while coal and limestone account for only about 5 percent and decrease from northeast to southwest (Martin, 1998). Quartz silt, kaolinite, illite, and mixed-layer clay minerals make up the mudstone mineralogy, while the sandstones are rich in quartz, rock fragments of both sedimentary and metamorphic origin, and detrital mica (Martin, 1998). Gilgai and other attributes indicative of subaerial exposure have been found in the red mudstones, suggesting many of these horizons contain paleosols formed in a tropical climate that experienced oscillations between heavy rainfall and no rainfall at all (Martin, 1998).

Field Methods

To assess the extent of Mn deposition to soils near Marietta OH, soil cores (Fig. 5) were primarily collected along a SW-NE trending transect that generally follows the direction of the predominant surface winds in the area (U.S. EPA, 2009). A few additional cores were augered outside this trend, to the N, NW, and SE of EMI. Upland locations were selected for augering in order to increase the likelihood that Mn additions to the soil profile were not attributable to erosion, overland transport, and deposition from adjacent higher locations. In order to increase the likelihood that cores reflected an undisturbed record of Mn deposition since the beginning of EMI operations, sites were chosen near large trees or in locations where land use records indicated that the soil had been undisturbed since at least 1952, the year refinery operations began. In addition, every effort was made to auger soil cores overlying similar bedrock units.

All cores were collected manually in approximately 10 cm increments by hand augering using a stainless steel bucket auger of 5 cm in diameter. The zero depth was defined as the top of the mineral soil. Soil clods were collected when possible at multiple depth intervals within a few cores and stored in crush-free containers for measurement of bulk density. All cores, with the exception of core WES, were augered manually until refusal (assumed to be bedrock).

A few surface mineral soil samples (0-10 cm) were also collected at a range of distances from the refinery.

Laboratory Analyses

All soil samples were air-dried in the laboratory in unsealed plastic bags. Subsamples intended for bulk chemical analysis were ground with mortar and pestle and sieved to less than 150 µm. In order to dissolve silicate minerals, ground samples were fused with lithium metaborate, heated to 1000º C and then diluted with nitric acid (Suhr and Ingamells, 1966). Fusion solutions were analyzed for aluminum (Al), calcium (Ca), chromium (Cr), iron (Fe), potassium (K), magnesium (Mg), manganese (Mn), phosphorous (P), sodium (Na), silicon (Si), titanium (Ti), zinc (Zn) and zirconium (Zr) using an inductively coupled plasma-atomic emission spectrometer (ICP-AES) at Penn State. USGS standard reference material W-2 was analyzed during each instrument run. Based on these analyses, analytical precision on the ICP-AES is estimated to be ±3% for all elements.

Loss on ignition (LOI) was measured on all soil samples by heating approximately 1 g of ground sample to 900º C overnight and measuring the mass before and after combustion.

Soil clod volume was measured using a NextEngine 3D scanner. Analytical precision for volume measurements is estimated to be ±1%. Bulk density was calculated by dividing the mass of each clod by the measured volume. Measured volumes ranged from 1.8-13.0 cm^3.

A few soil samples were also analyzed using a backscatter scanning electron microscope for the presence of zircons, highly-resistant Zr-enriched minerals.

Surface Deposition Model

A public-domain version of SCIPUFF (Secondary Closure Integrated-Puff) was used to model surface deposition of Mn-bearing particulates at each core location for comparison with soil-derived values. SCIPUFF is a Lagrangian atmospheric transport and diffusion model that is often used by the U.S. Department of Defense to track the movement of biohazards (Sykes *et al.,* 2004). The model uses a number of measureable meteorological variables and emissions characteristics to calculate effluent dispersion from an emissions source, as well as subsequent deposition to the land surface.

Mn air emissions statistics for EMI were obtained from the United States Environmental Protection Agency Toxics Release Inventory (U.S. EPATRI, 2010). The emission rate was maintained constant throughout the entire modeled time period, such that the sum of all emissions for the entire year was equal to the reported amount of Mn compounds emitted. A maximum time-step of 15 minutes was used since weather data resolution was 1 hour. Particle size was set to 0.05-0.4 um and a bulk density corresponding to MnO_2 (5.08 g cm^{-3}) was used, since Mn oxides have been identified as the primary Mn-bearing phases in both furnace dust and Marietta air and MnO_2 represents the Mn oxide with the intermediate bulk density (U.S. EPA, 1974; Shen *et al.*, 2005; U.S. EPA, 2009).

Since emissions statistics have only been reported since 1988 and continuous hourly weather conditions are only available for 2005-2013, the entire time period of EMI operation could not be modeled (1952-present). Therefore, only the year 2006 was modeled and it was assumed that this year was representative of a longer time period. This specific year was chosen because the reported precipitation for 2006 was generally consistent with the normal precipitation over the last 30 years (NOAA, 2013a). Hourly surface meteorological information was obtained from the Federal Aviation Authority (FAA) operated Automated Surface Observing System (ASOS) located at the Mid-Ohio Valley Regional Airport in Parkersburg WV, less than 10 km to the southeast of EMI (NOAA, 2013b). Weather parameters (temperature, relative humidity, windspeed, wind direction, precipitation rate, and precipitation type) with hourly resolution were incorporated from the reporting station into the model. Wind direction values were reported to the nearest 10 degrees. Precipitation was binned in the model on a scale of 0-6 where 0 was no rain, 1 represented light rain (0-0.5 mm hr^{-1}), 2 indicated moderate rain (0.5-3.5 mm hr^{-1}), 3 represented heavy rain (>3.5 mm hr^{-1}), 4 represented light snow (0-5 mm hr^{-1}), 5 represented moderate snow (5-20 mm hr^{-1}), and 6 represented heavy snow (>20 mm hr^{-1}).

A simple diurnal boundary layer was used, such that the atmospheric boundary layer height varied between 50 and 1000 m at nighttime and daytime, respectively, and sensible heat flux varied between 0 and 50 W m^2 at nighttime and daytime, respectively. Using the simple boundary layer function, the height of the boundary layer increases linearly in the morning (6 am-12 pm), remains constant at a maximum value (1000 m) during the afternoon hours of 12 pm-6 pm before returning to the minimum value (50 m) (Sykes *et al.*, 2004). Although this modeling approach of the ABL does not rely on measurements of conditions in Marietta, it is consistent with variations in ABL height observed across a wide-range of localities throughout the world over the course of a single day (Seinfeld, 1986).

After running the model, surface deposition values for each core location were extracted from the model using GPS coordinates obtained during sampling. A series of sensitivity tests were also run to show the effect of precipitation, particle size, and bulk density on Mn deposition rate (see Appendix G).

Results

Soil Samples

In total, 11 soil cores were augered on ridgetops (maximum elevation ≈ 340 m) at a range of distances up to 50 km both upwind and downwind from the Mn-emitting refinery (Fig. 5; Table 1). A few surface samples (open squares in Fig. 5) were also collected.

Throughout the field area, exposed rocks varied in color from red to green (Fig. 6). Thickness of augerable regolith varied from 20 to 200 cm, with shallower soils generally occurring at higher elevations. Many of the cores were augered in currently undisturbed non-residential areas (Veto Lake Wildlife Area (VL), Gifford Forest State Park (GF), and Wayne National Forest (IR)). Other cores were sampled in sparsely populated areas, at least 30 m from roads and structures, with one exception (Washington Elementary School (WES)). This site, along with Marietta Middle School (MMS), was chosen because of recent reports from the U.S. EPA suggesting Mn concentrations in air around schools are elevated in the Marietta region (U.S. EPA, 2010). Although on school property, the MMS site fulfilled the other sampling requirements, including location in an upland position in a forested area ~30 m from roads and structures, and did not show evidence of human disturbance within the core itself. WES, however, contained bricks and rusty nails ~70 cm depth, indicating significant disturbance. For this reason, no further sampling was attempted at schools and the data from WES was not included in analysis of Mn deposition.

Soil types and Bulk Density

All soil cores were collected from well-drained soils in the Upshur soil series (Natural Resource Conservation Service (NRCS) (Soil Survey Staff, 2012)). All were described as Upshur silty clay loam soils derived from clayey shale parent material (see Appendix A).

Bulk density measurements were made on soil clods from a range of depths in one core (MMS) and were used to estimate bulk density in all cores. Values ranged from ~1.5 g cm^{-3} near the surface to 2.4 g cm^{-3} in a rock fragment found in the bottom-most core interval. Bulk density versus depth was fit to an equation used previously (Dere *et al.*, in review) for shale soils (Eq. 1; Fig. 7):

$$\rho_b = \rho_b^{\circ} + \frac{(\rho_{b,max} - \rho_b^{\circ})Kz}{1+Kz} \qquad (1)$$

Here ρ_b is the soil bulk density (g cm^{-3}) for a given depth (z) in the profile. ρ_b° and $\rho_{b,max}$ are the bulk density at the surface and in the deepest sample, respectively. K is a fit parameter. Based on measured soil clods from MMS, best estimates for ρ_b°, $\rho_{b,max}$ and K were 1.4 g cm^{-3} , 1.85 g cm^{-3} and 0.1 cm^{-1}, respectively. The bulk density was assumed to vary with depth similarly in all cores (Table 2).

Soil Chemistry

The surface interval (0-10 cm) generally contained the highest observed Mn concentration in each core. Mn concentrations in this interval were highest closest to the refinery (0.25 wt %) at BKR (distance = 1.2 km N, where N refers to direction from refinery) and lower (between 0.02 and 0.10 wt. %) at greater distances (Fig. 8, Table 3). A linear regression for all

Mn concentrations in surface samples (R^2 value of 0.19) from cores more distant than BKR (1.2 km NE) yields a slope that is not significantly different from 0 at the 95% confidence interval (Fig. 8).

In general, Mn concentrations increase from ~0.01-0.02 wt. % at depth upward toward the soil surface, though little increase was observed in the most remote core (IR, 45.0 km NE) (Fig. 9). Significant variations in Mn concentration were observed below 1 m in three cores (MMS (11.2 km NE), VL (14.3 km WSW), GF (46.7 km WNW)).

Mn concentrations also increased in the bottom 10-20 cm of augerable regolith in CLF (10.9 km N) and PR (25.1 km NE) and several physical differences were noted in those same intervals (Appendix A). Specifically, weathered rock fragments with black coatings, inferred to be Mn coatings, were found in the bottom of CLF and PR. Furthermore, light and dark areas potentially indicative of Mn enrichments and depletions were seen in the bottom 20 cm of CLF and below 1 m in GF. In CLF and PR, these bottom intervals were also observed to be more yellow and coarser in texture than upper intervals.

In addition to Mn concentrations, Cr concentrations also increased significantly toward the surface at BKR (Fig. 10). In contrast, although Mn increases toward the soil surface in nearly all cores, Cr actually decreases near the surface in some more distant cores (VL, GF).

For all cores except the closest location and the most distant site to the NE of the refinery, Mn to Cr molar ratios increased toward the soil surface to values of 5 to 16. Mn to Cr ratios greater than 10 were also observed in the bottom 10-20 cm of CLF and PR, while variation was also seen below 1 m depth in MMS, VL, and GF, i.e. at the locations of the Mn concentration spikes shown in Fig. 9. In contrast, the Mn to Cr ratios exhibited in samples throughout both the most distant core to the NE (IR) remained constant at 2.44 ± 0.45 (Fig. 12). In the nearest core BKR, Mn to Cr ratio did not vary widely, though a noticeable break occurred below 60 cm, where values decreased from an average of 3.58 ± 0.34 above to 1.57 ± 0.22 below. Other element-element ratios are reported on a mass basis in Appendix B.

Discussion

Mn Addition Profiles and Surficial Contamination

Based on air concentration measurements and concurrent surface wind analyses, previous studies have suggested that EMI is the dominant source of both Mn and Cr in Marietta air (U.S. EPA, 2008). The highest soil-surface Mn and Cr concentrations were observed at the nearest site to EMI, consistent with EMI as the dominant source of Mn and Cr to soils. Furthermore, the rate of dry deposition for an element is known to depend on the concentration and grain size of particles (Shroeder *et al.,* 1987). As long as the grain size does not vary throughout the study area, air concentrations measured around Marietta are consistent with high Mn deposition to soils near the plant (Figure 8).

Increasing Mn concentrations upward to the surface in soil cores derived from upland locations on mono-lithologic parent material have been referred to as addition profiles (Brantley and White, 2009; Brantley and Lebedeva, 2011). Addition profiles are expected for elements that are input from the atmosphere at significant rates in soil profiles where mixing and removal is not fast. Since all cores were augered at topographic highs, it is likely that upward-increasing Mn is due to atmospheric deposition rather than sources such as lateral sediment transport. Many researchers have identified upward-increasing concentrations of elements in soil and sediment samples that could be attributed to atmospheric deposition (e.g. Boudissa *et al.,* 2006; Esser *et al.*, 1991; Herndon *et al.,* 2011; Parker *et al.*, 1978; Perkins *et al.,* 2000; Pietz *et al.*, 1978). Although it is possible that upward increasing Mn could be indicative of a shift from parent material with a lower Mn content to a parent material with a higher Mn content, the fact that the upward Mn increase is most dramatic near the refinery (BKR) and not present at all at the most distant site to the NE (IR) is consistent with an external Mn source.

The fact that Mn concentrations in the upper 0-10 cm of soil drops from 2400 ppm at a distance of 1.2 km from EMI to 180-1090 ppm at distances 3-48 km away is consistent with other studies. Commonly, heavy metal contamination in surface soils drops off dramatically with distance from the source to near background levels within tens of kilometers (e.g., Parker *et al.*, 1978; Pietz *et al.* 1991). The lack of a relationship between surface Mn concentration and distance from source (Fig. 8) is also consistent with a previous study of Mn concentrations in surficial wetland sediments near the second highest Mn emitting region in the country (Fig. 1), the Chicago-Gary urban-industrial area of northwestern Indiana (Perkins *et al.,* 2000). One reason for a lack of a relationship could be downward migration of Mn. On the basis of comparisons of metal concentrations in the clay-sized fraction of the E and B horizons, Esser *et al.* (1991) previously argued that Mn may have migrated downward in soil profiles studied around Gary Indiana. Perkins *et al.* (2000) argued that wetland sediments exposed to frequent flooding near Gary, IN, also showed evidence of Mn migration downward in the sediments and also concluded that this explained a lack of variation in concentration with distance from source.

Although other studies have attributed a lack of a relationship between surface metal concentration and distance to variations in other characteristics such as vegetation type, vegetation density, clay content, or organic matter content (Esser *et al.*, 1991; Reimann *et al.*, 2009), our study sites were carefully chosen to avoid these variations. Since our cores were augered in well-drained upland soils developed on the same geologic rock type with similar vegetation, it is more likely that post-depositional Mn mobility or the presence of other Mn sources may control surficial Mn content around Marietta (Figure 8), rather than distance from EMI alone. Furthermore, the fact that there is no relationship between surficial Mn content and distance suggests that EMI's footprint of Mn deposition should not be assessed using only surface concentrations.

Mn to Cr ratios

We can also compare the Mn to Cr ratios in soils to that of EMI emissions, since EMI represents the largest source of both metals in the county (EPATRI, 2010). Molar ratios for emissions have not been published for EMI. However, Table 5 shows estimates of Mn to Cr ratios on a molar basis in particulate emissions from facilities that, like EMI, produce ferromanganese (FeMn) and ferrochromium (FeCr) (U.S. EPA, 1974): Mn:Cr varies between 0.1 and 36 (Table 4; U.S. EPA, 1974, U.S. EPA, 2010). Values at the higher end are expected for more recent emissions, since ferrochromium production was suspended in 2008. Assuming MnO_2 and Cr_2O_3 are the primary Mn- and Cr-bearing compounds in furnace emissions from EMI, the molar ratios of Mn to Cr in EMI emissions for 1988-2008 averaged 18 ± 12 (Fig. 13) (U.S. EPA, 1984b; Shen *et al.*, 2005).

These Mn to Cr ratios can be compared to both parent material and the soils closest to the refinery. The Mn to Cr ratio (mol/mol) of the parent material for all the soils is estimated to equal 2.44 ± 0.45, the average of all samples in the most remote soil core IR. With the exception of the Mn concentration spikes, soil samples attain this value in most of the other cores at depth (Fig. 11). In contrast, the Mn to Cr ratio in the upper 60 cm of the soil closest to the refinery equals 3.58 ± 0.34. The ratio returns to near background below this depth, consistent with lack of significant soil mixing below 60 cm.

If EMI emits Mn and Cr in a molar ratio of ~18 and the parent material ratio is expected to be around 2, it may at first appear unusual that the Mn to Cr ratio in surface samples is closer to 18 further from the refinery than nearby. However, particulate diameters from ferrochromium production are larger (up to 1 μm) than those from ferromanganese production (up to 0.75 μm) (U.S. EPA, 1974). Therefore, the net deposition rate of Cr-enriched particles is expected to be faster and more likely to occur closer to the refinery than Mn-enriched particles. This explanation is consistent with the Mn/Cr ratio of particle deposits increasing with distance. We conclude from all the Mn/Cr evidence that both elements have been added to soils around EMI and that the extent of impact extends no deeper than ~60 cm depth.

Elemental Changes with Depth

Increases in wt. % of a mobile element j in a profile can occur because of enrichment of j or because other elements have been lost. The mass transfer coefficient, $\tau_{i,j}$ (eq. 2), is used to study changes in the concentration of a mobile element (i.e. j = Mn) in weathered material ($C_{j,w}$) with respect to the concentration of the same element in the parent material ($C_{j,p}$). The concentration of an immobile element, i, in both the weathered ($C_{i,w}$) and parent material ($C_{i,p}$) is used to account for loss or addition of other elements in the weathered material. The mass transfer coefficient is defined (Brimhall and Dietrich, 1987; Anderson *et al.*, 2002) as:

$$\tau_{i,j} = \frac{C_{j,w}C_{i,p}}{C_{j,p}C_{i,w}} - 1 \qquad (2)$$

$\tau_{i,j} > 0$ indicates enrichment of element j, while $\tau_{i,j} < 0$ indicates depletion.

The net loss or gain of an element in the soil profile relative to parent material can be described by the integrated mass flux ($m_{j,w}$ in eq. 3), which is calculated by integrating the mass transfer coefficient ($\tau_{i,j}$) over depth (z), where $z = 0$ is the land surface and $z = L$ is the bottom of the augerable soil core. Here, ρ_p represents the bulk density of the parent material. Since the parent material for all cores is likely a shale unit, ρ_p was estimated to be 2.6 g cm^{-3} (Jin *et al.*, 2010). The integrated mass flux can be calculated from:

$$m_{j,w} = C_{j,p} \rho_p \sum_{z=0}^{L} \frac{\tau(z)}{\varepsilon(z)+1} dz \qquad (3)$$

The strain factor, $\varepsilon_{i,w}$, is used to account for volume change between the volume of soil (V_w) developed from a given volume of parent material (V_p) assuming an element (here, Zr) is immobile (*i.e.* insoluble). Here, $\varepsilon_{i,w} > 1$ indicates expansion, $\varepsilon_{i,w} < 1$ indicates compaction, and $\varepsilon_{i,w} = 0$ is consistent with iso-volumetric weathering. The strain factor is calculated as follows (Brimhall *et al.,* 1992):

$$\varepsilon_{i,w} = \frac{V_w}{V_p} - 1 = \frac{\rho_p C_{i,p}}{\rho_w C_{i,w}} - 1 \qquad (4)$$

Choice of Parent Material and Immobile Element

Mn concentrations in Dunkard Group rock units may vary widely due to shifts from alluvial-plain to lacustrine-deltaic-plain depositional environments and the resulting shifts in sediment inputs and redox conditions (Beerbower, 1961). Indeed, we observed throughout the study area that exposed rocks varied in color from red to green both on the outcrop and hand-sample scale. These variations may suggest periods of reducing and oxidizing conditions that may have mobilized and immobilized Mn (Fig. 6), resulting in varied Mn contents (Martin, 1998). Furthermore, it is known that the Dunkard Group contains paleosols with Mn carbonate nodules, suggesting that some units may contain very high concentrations of Mn. Beerbower (1961) further suggested that individual rock units within the Dunkard group may be compositionally variable within a few kilometers. For these reasons, the best estimate of the chemical composition of the parent material is the average of multiple intervals from the bottom of each core, i.e., below 60 cm as discussed in the last section. Since only a few cores extended below 1 m in depth and the Mn emissions from EMI have only occurred since 1952, we chose to compare Mn enrichments and depletions in the upper meter of each profile (in some cases cores were shallower than a meter and only the augerable interval was considered). We assumed the parent composition was equal to the average of the 3 deepest sampling intervals of that part of the profile.

Large spikes in Mn concentration were observed in 1 or more of the soil intervals used to calculate average parent material composition for CLF, PR, and GF. In CLF, these spikes occurred in intervals characterized by a coarser texture than surrounding intervals (Appendix A). Since Ramesam (1979) found that sandstones in the Dunkard Group contain higher amounts of Mn than mudstones and shales, these spikes in Mn in CLF are attributed to layers of sandy parent material, rather than downward migration of industrially-sourced Mn. Consistent with this, I observed that this deeper interval was characterized by high Mn but low Cr. In the interval with the Mn spike in PR, a drastic downward change in hue from red to yellow was noticed. Thus changes in the texture and redox environment apparently caused shifts in parent material composition (Appendix A).

Given these issues with respect to changes in parent material in CLF, PR, and GF cores, mass transfer coefficients were calculated for two scenarios. First, we assumed a parent material composition that included these depths with Mn spikes (parent material scenario A). Second, we assumed a parent material that was equal to the average of the 3 samples above the depth of Mn spikes (scenario B). This latter method of calculating parent material excluded the bottom 2 samples in CLF, the bottom sample in PR, and the 3 samples above 1 m in GF. For all other cores, parent material choice did not vary between scenario A and B.

Zirconium (Zr) and titanium (Ti) are often observed to be immobile elements since they are usually present in soils in highly insoluble minerals (Kurtz *et al.*, 2000; Neaman *et al.*, 2006; Brantley and White, 2009). Here, we assume that Zr is the element that is most immobile in the soils based on previous studies. Specifically, in soils on Rose Hills shale in Pennsylvania, Zr was less mobile than Ti (Jin et al., 2010). Zr is less mobile in soils overlying other lithologies as well (Gardner, 1980; Cornu *et al.*, 1990; Neaman *et al.*, 2006). Indeed, backscattered scanning electron microscopy conducted on surface samples from IR documented the presence of zircons, known to be highly insoluble Zr-enriched minerals (Appendix C). In addition, a plot of $\tau_{Zr,Ti}$ (Fig. 14) documents negative mass transfer coefficients for Ti relative to Zr, consistent with loss of Ti relative to Zr.

Mass Transfer Coefficients

Mn is enriched relative to parent material ($\tau_{Zr,Mn} > 0$) near the surface for nearly all cores using parent scenario A (Fig. 15a; Table 4). For example, Mn is enriched in surface soils nearly 9 times above parent material composition in the closest core to the refinery (BKR), while SR, LP, MMS, and VL (all located within 15 km of EMI) are enriched 0.5-2.5 times in the surface. GF

(46.7 km WNW) and CLF (10.9 km N) show depletion of Mn, while IR, located 45.0 km NE in the most remote location, shows slight depletion of Mn (0.2 times in surface). Error bars were calculated following Jin *et al.* (2010) as discussed in Appendix D.

Excluding Mn spikes from inclusion in parent material composition (scenario B) for CLF, PR, and GF, and recalculating mass transfer coefficients for those cores results in enrichment profiles for each of these locations. Specifically, CLF (10.9 km N) and PR (25.1 km NE) are enriched at the surface by 0.5 and 2.7x parent material composition, respectively (Fig. 15b). In contrast to scenario A, IR is the only core that exhibits Mn depletion.

Cr is also enriched in the nearest core to EMI (up to 3x), as well as in the upper 10 cm of LP and PR (Fig. 16). Cr is depleted near the surface in all other cores (Fig. 16). The fact that Cr enrichment (up to 3x) is of a smaller magnitude than Mn enrichment (up to 9x) at BKR is not unexpected, since an average of 18x more Mn is emitted annually from EMI than Cr on a molar basis since 1988 (Fig. 13). As mentioned above, particles highly enriched in Cr are also known to be coarser than particles enriched in Mn (U.S. EPA, 1974), which may explain why Cr addition to soils is only seen very close to the emissions source, while Mn addition is evident farther from the source as well.

Cr depletion in surface intervals distant from EMI suggests that any Cr that has been deposited to the surface is being mobilized out of the soil profile. Cr is likely emitted from ferroalloy production processes and deposited in soils as Cr (III) (U.S. EPA, 1984b), a form considered highly immobile in soils due to organic matter complexation or adsorption onto oxides or silicate clays (McBride, 1994). However, oxidation of Cr (III) to the more mobile (and toxic) Cr (VI) occurs in soils. Indeed, such oxidation can be caused by Mn oxides in natural systems and could in part explain partial Cr depletion observed at MMS, VL, IR and GF (Bartlett and James, 1979). It has been suggested that several Mn (III/IV) oxide minerals may oxidize Cr (III) in the environment, but those with higher surface areas are likely able to oxidize more Cr (III), since adsorption of the resultant Cr (VI) compound may hinder further reaction through armoring (Eary and Ral, 1987). In locations more proximal to EMI, Cr enrichment in the soil documents that anthropogenic addition rates exceed rates of Cr oxidation and loss.

Integrated Mn Mass Flux

Integrated Mn mass flux values, $m_{Mn,w}$, were calculated using eq. 3, an assumed parent bulk density of 2.6 g cm^{-3}, and calculated bulk density values from eq. 1 (Table 1). Values were higher for sites closer to the refinery than those that are more distant: a net addition of Mn was seen at 4 out of 6 locations within 15 km of the refinery (Fig. 17a). Using parent scenario A, integrated mass flux values ranged from a net addition of 77 ± 16 mg Mn cm^{-2} to the upper meter of the soil profile at BKR to a net loss of 83 ± 45 mg Mn cm^{-2} at GF, located 46.7 km to the WNW of EMI. IR, located 45.0 km to the NE of EMI showed a slight net loss of Mn of 3 ± 1 mg Mn cm^{-2}.

Using parent scenario B (i.e., excluding deep spikes in Mn concentration for CLF, PR, and GF), yielded higher integrated mass flux values for those sites (4 ± 1 mg Mn cm^{-2}, 20 ± 2 mg Mn cm^{-2} , and 15 ± 5 mg Mn cm^{-2}, respectively) (Fig. 17b). Net additions of Mn were the same for the two scenarios within error at intermediate distances (Table 1). In fact, only the integrated mass flux for GF scenario B is statistically different than the value derived using scenario A. Unlike scenario A, scenario B suggests that rates of industrial Mn input exceed rates of Mn removal at sites at least as far away as GF (46.7 WNW). Error calculations are shown in Appendix E.

The main implication of using parent scenario B is that the calculated footprint of Mn deposition due to EMI emissions extends considerably farther (at least ~47 km) from EMI than that suggested using parent material A (<25 km). Several studies document the Mn emissions can affect localities 10s of kms distant. For example, Herndon *et al.* (2011) estimated that the geographic extent of deposition from a much smaller Mn source (a steel plant in Burnham, PA) extended ~15 km from the facility. Boudissa *et al.* (2006) showed that Mn deposition due to a ferromanganese refinery resulted in elevated air concentrations and likely deposition at locations at least 25 km in the predominant downwind direction. Likewise, two other studies have suggested that metal contamination in soils due to steel production may extend up to 30 km and 65 km, respectively (Parker *et al.*, 1978; Pietz *et al.*, 1978).

Regardless of scenario, each core location is similar in soil type, parent material, vegetation, topographic position and climate, and the difference in integrated mass flux values for Mn at each location is therefore attributed to the 6th soil-forming factor (humans). Assuming that the excess Mn in BKR has all been added to the soil since EMI began, the average Mn deposition rate from 1952 to present (= m_{Mn} /60) is ~1275 μg Mn cm^{-2} yr^{-1}. This value is much higher than rates of natural Mn deposition. Specifically, the estimates for natural deposition range from a recent rate from remote locations of Bermuda (0.062 μg Mn cm^{-2} yr^{-1}; Duce *et al.*, 1976) to Mn accumulation rates (1.7 μg Mn cm^{-2} yr^{-1}) in Lake Michigan. This latter value was estimated from a sediment core comprising 1200 years of deposition pre-colonial settlement (Cole *et al.*, 1990). Furthermore, the average soil-derived Mn deposition rate calculated here is also a factor of 5 times higher than the only Mn deposition rate reported in the literature near a ferromanganese refinery: 231 μg Mn cm^{-2} yr^{-1}. This latter value was only for dry deposition and was measured in 1965 in the Kanawha Valley of West Virginia. Since wet deposition accounts for 50-66% of Mn deposition from the atmosphere (Duce *et al.*, 1976; Shroeder *et al.*, 1987), the net soil-derived Mn deposition rate at Marietta may only be 2-3 times higher than bulk deposition that occurred near the Kanawha facility in 1965. In the next section, an atmospheric model is used to test whether such a high deposition rate is likely.

Surface Deposition Model

Mn deposition rates were modeled using SCIPUFF for comparison with soil-derived Mn deposition rates. See Appendix G for a discussion of sensitivity tests. Mn deposition rates calculated as both dry and wet deposition by the model for 2006 ranged from 0.001 μg cm^{-2} yr^{-1} at distances of 45 km to 0.209 μg cm^{-2} yr^{-1} at BKR (1.2 km N) (Fig. 18, 19) to 0.487 μg cm^{-2} yr^{-1} within meters of EMI. These modeled rates did not exceed the high end of the range of estimated natural Mn deposition rates (1.7 μg Mn cm^{-2} yr^{-1}; Cole *et al.*, 1990). On the other hand, the model-derived deposition rates within ~5 km of EMI did exceed reported Mn deposition in remote areas of Bermuda (0.062 μg cm^{-2} yr^{-1}) (Duce *et al.*, 1976).

In fact, the model results (Fig. 18) predict much smaller footprints of deposition (<5 km) than recorded by the soil-based measurements (at least 15 and possibly >47 km). In addition, the model-derived rate for BKR for 2006 due to EMI emissions (even after it is added to the background Mn deposition of Duce et al. or Cole et al.) is ~3 orders of magnitude lower than the soil-derived rate close to the refinery (1275 μg Mn cm^{-2} yr^{-1}) (Fig. 19).

At least three explanations are possible for the soil-model discrepancy: i) the soil-derived value is inaccurate; ii) the model does not adequately describe the deposition rate for the model year 2006, or iii) deposition rates were much higher prior to 2006. The fact that the Mn deposition rate measured near a ferromanganese refinery in 1965 in the Kanawha Valley of West Virginia was roughly 3 orders of magnitude higher than the modeled rate for 2006 near EMI provides evidence that explanation (i) is not likely, leaving possible explanations (ii) or (iii) or both. Comparison of model-derived rates with estimates of background Mn deposition supports (ii).

In addition, many lines of evidence suggest that Mn emission rates (and by inference, deposition rates) were higher in the past, thus supporting explanation (iii). For example, 6 facilities that did not exist in 2006 were producing Mn alloys in eastern Ohio and West Virginia in 1971 (U.S. EPA, 1974). In addition, Herndon *et al.* (2011) found that Mn dry deposition rates in industrial and urban locations may have been as high as 1000 $\mu g\ cm^{-2}\ yr^{-1}$ in the 1950's and 1960's, declining by up to 3 orders of magnitude since that time.

The enactment of the Clean Air Act of 1970 resulted in significant improvements in emission controls in the metals industry specifically. For example, in 1968, 2-35 kg Mn were emitted per metric ton of Mn-containing product produced in the U.S.A., whereas in 1980, less than 0.01- 0.65 kg Mn was emitted per metric ton of product (U.S. EPA, 1984). Likely as a direct result, from 1968 to 1976, a decline in ambient Mn concentrations in air of more than an order of magnitude was observed around the Kanawha valley (WV) ferromanganese refinery (U.S. EPA, 1977).

Consistent with cleaner air nationwide after the Clean Air Act, Mn concentrations in air declined by more than 50% at 92 urban locations included in the National Air Surveillance Network (NASN) from 1965 to 1974 (U.S. EPA, 1977). Figure 2 documents an even larger decline in Mn concentrations (up to 2 orders of magnitude) near EMI between 1965 and 1983, suggesting that improvements in air quality were a direct result of controls in the metals industry specifically. In fact, estimated values of dry Mn deposition can be computed from the product of Mn concentration in air (Figure 2) and deposition velocity following Herndon *et al.* (2011), where deposition velocity for Mn-bearing particles is estimated to be 2.63 cm/s based on a compilation of previous studies. Using that approach yields deposition rates around Marietta based on data in Figure 2 that vary from as high as 935 μg Mn cm^{-2} yr^{-1} in 1965 to as low as 5.8 μg Mn cm^{-2} yr^{-1} in 2007. Figure 21 is thus consistent with a decrease in the Mn dry deposition rate by 2 orders of magnitude around Marietta from 1965 to 1983.

In addition to lower emissions per unit of production, production of ferromanganese and silicomanganese (which accounted for nearly 50% of all atmospheric Mn emissions in 1968) declined by 31% between 1965 and 1980 (U.S. EPA, 1984). In addition, domestic Mn alloy consumption also dropped by more than a factor of 3 during this time (Fig. 4) (Jones, 1994). Furthermore, the fact that several other Mn alloy producers existed in southeastern OH in 1971 and closed by 1988, suggests that Mn deposition in that area may have been much higher than similar stand-alone facilities and decreased more sharply than in other locations. In light of all these lines of evidence, it is reasonable to conclude that deposition rates in the OH area were ~3 orders of magnitude higher in the past compared to today's values.

Of course, even if the rate of historical deposition was much higher in the past than it was in 2006, the modeled rate for 2006 could still be inaccurate. In fact, comparison of the modeled bulk Mn deposition rate near BKR (0.209 μg cm^{-2} yr^{-1}) with estimated values of recent dry Mn deposition (5.8-13.3 μg cm^{-2} yr^{-1}) computed from measured Mn concentrations in air from 2007 (Fig. 21) shows that the model may indeed be under-predicting deposition by nearly 2 orders of magnitude. Inaccuracies in the model prediction could be because we assumed that all air emissions occur at a steady rate throughout the year. In fact, the breakdown of higher Mn oxides during smelting results in sudden releases of gases and entrained particles and thus could result in higher Mn deposition intermittently (Person, 1971). Since emissions statistics from EMI are only available with yearly resolution, however, no improvements in the modeling could be made to account for potential sudden releases. Along a different line, the accuracy of the model might also be lacking because we did not include meteorological observations at a range of heights above Earth's surface, which would have more accurately predicted the boundary layer height and the resulting Mn particle dispersion. In other words, Mn particle dispersion and subsequent deposition may not be strongly controlled by surface weather conditions at all and more accurate deposition rates would require more complex upper atmosphere measurements.

In the next section we use estimates of recent Mn deposition rates presented in figure 21, as well as EMI emissions data, Mn alloy consumption data for the U.S.A. (Fig. 4), and soil measurements to calculate an estimate of Mn deposition rates back in time.

Reconstruction of Previous Mn Deposition Rates

Using recent deposition rates in Fig. 21 calculated from air chemistry, I calculated previous Mn deposition rates at BKR by using the trends in Mn emissions from EMI and Mn alloy consumption in the U.S. (Fig. 4, Fig. 22). For the 60 years of EMI operation, 3 different methods were used to estimate Mn deposition rates over different time periods (see Appendix F for variable definitions). Using the first method for the time period where EMI emissions have been reported (1988-2010), deposition at BKR (F_x) was estimated for each year x by scaling to Mn emission rates from EMI for each year ($M_{EMI,x}$):

$$F_x = \frac{F_{2007}}{M_{EMI,2007}} * M_{EMI,x} \qquad (5)$$

Using the estimated value of F_{2007} from Fig. 21 (9.4 µg Mn cm^{-2} yr^{-1}) and $M_{EMI,2007}$ = 86.3 metric tons of Mn yr^{-1} for 2007 (U.S. EPATRI, 2010), the deposition-to-emission ratio, $F_{2007}/M_{EMI,2007,}$ equals ~109 ng Mn cm^{-2} per metric ton of Mn air emissions. For all other years between 1988 and 2010, the value of $M_{EMI,x}$ used in plotting Fig. 4 was multiplied by this factor to estimate the deposition rate at BKR: values ranged from 4.7 to 18.1 µg cm^{-2} yr^{-1}.

To estimate Mn deposition rates at BKR for years prior to 1988, we used eq. (5) and EMI emission rates predicted from U.S. Mn alloy consumption rates (USGS, 2010). These Mn emission rates were predicted using the average Mn emission rates from EMI from 1988-2010 ($M_{EMI,1988\text{-}2010}$ = 103 metric tons of Mn yr^{-1}) and the average U.S. Mn alloy consumption rate ($A_{USA,\ 1988\text{-}2010}$ = 341,913 metric tons of Mn alloys yr^{-1}) during this same time period (Fig. 4). For 1988 to 2010, the emission-to-consumption ratio, $M_{EMI,1988\text{-}2010}/A_{USA,\ 1988\text{-}2010}$, was equal to 0.0003 metric tons of Mn released from EMI per metric ton of Mn alloy consumed domestically. This ratio was then multiplied by reported Mn alloy consumption rates prior to 1988 (A_x ; Fig. 4) to estimate values of air emissions from EMI ($M_{EMI,x}$) ranging from 106-283 metric tons of Mn per year:

$$M_{EMI,x} = \frac{M_{EMI,1988-2010}}{A_{USA,1988-2010}} * A_x \qquad (6)$$

Using this value of $M_{EMI,x}$ and eq. (5), Mn deposition rates were then estimated prior to 1988. Rates ranged up to 31.8 μg Mn cm^{-2} yr^{-1}, i.e., 3x greater than the calculated rate for 2007 (Fig. 4).

As previously noted, a decrease of 1-2 orders of magnitude in Mn air concentrations were observed near EMI and a similar ferroalloy refinery between 1965 and 1983, a fact that has been largely attributed to decreased emissions brought on by actions taken to address the Clean Air Act (1970). For example, the cumulative amount of estimated Mn deposited in Marietta using the methods just described for 1971-2010, $C_{DEP,1971-2010}$, is 376 μg cm^{-2}, even though the soil-derived integrated Mn mass flux value is ~76000 μg cm^{-2}. It is reasonable to assume that Mn air emissions and deposition rates near EMI were likely much higher prior to the regulations: the soil-derived integrated Mn mass flux value suggests that soils near the refinery (BKR) have accumulated 200x more Mn than predicted based on these back-calculated Mn deposition rates.

To estimate a time-averaged Mn deposition rate for 1952-1971 ($F_{avg,1952-1970}$), we therefore calculated the difference between soil-derived integrated Mn mass flux at BKR (m_{Mn}= ~76000 μg cm^{-2}) and $C_{DEP,1971-2010}$ and divided it by the number of years the refinery operated before the Clean Air Act:

$$F_{avg,1952-1970} = \frac{m_{Mn} - C_{DEP,1971-2010}}{(1970 - 1952)} \qquad (7)$$

The calculated value of $F_{avg,\ 1952\text{-}1970}$, 4213 μg cm^{-2} yr^{-1}, is only an order of magnitude higher than the Mn dry deposition rate measured in 1965 near a similar refinery in West Virginia, which is in itself probably only representative of 33-50% of the total (dry + wet) deposition (U.S. DHEW, 1970; Duce *et al.*, 1976). Likewise, the value is of the same order of magnitude as estimates of Mn deposition at industrial locations in the 1950's and 1960's that considered only Mn dry deposition (Herndon *et al*., 2011). Fig. 22 documents that back-calculated Mn deposition rates agree well with other estimates of Mn deposition over time in industrial/urban environments as shown after the Clean Air Act, but deposition rates may have been higher from EMI than in other areas prior to that time. In fact, we can divide the average calculated deposition rates for 1988 to 2010 by the average quantity of Mn alloys consumed ($F_{1971\text{-}2010} / A_{USA,\ 1971\text{-}2010}$) to estimate the deposition-to-consumption ratio for Mn after the Clean Air Act, i.e., 0.034 ng Mn cm^{-2} per metric ton of Mn alloy consumed. In contrast, before the Clean Air Act, we can divide our soil-derived deposition rate for prior to 1970 (4213 μg Mn cm^{-2} yr^{-1}) by the average Mn alloy consumption rate 1952-1971 to calculate a ratio of 5.7 ng Mn cm^{-2} deposited per metric ton of Mn alloy consumed. The soil measurements thus document that the Clean Air Act is the likely cause of reductions in Mn deposition of 166x per metric ton of Mn alloy consumed.

Conclusions

Industrial inputs to soils are often quantified based solely on concentrations of heavy metals in surface horizons (e.g. Pietz *et al.,* 1978; Siccama and Smith, 1979; Siccama and Smith, 1980; Boudissa *et al.*, 2006). Furthermore, trends in atmospheric concentrations and deposition of Mn have received significantly less attention in the literature than trends of more toxic trace elements like As, Cd, Cu, Pb and Zn (Galloway *et al.*, 1982), despite the fact that the cycling of Mn may exert a strong control over the distribution of these elements in the natural environment (McBride, 1994; Tebo *et al.*, 2004). We have shown that anthropogenic inputs of Mn to soils are best considered using the entire soil profile. Furthermore, we showed that these soil measurements can be used with models of atmospheric deposition to provide estimates of metal deposition rates in the past. In Marietta and surrounding areas, Mn concentrations are observed to increase toward the surface in all cores except one located 45 km to the NE. Since cores were augered in ridge top positions and EMI is the largest emitter of Mn to the atmosphere in the area, it is likely the main source of Mn additions to the soil profiles.

Mass additions of Mn of up to 77 μg cm^{-2} to the soil profile were observed 1 km from the refinery, with integrated mass flux values returning to 0 within 25 km. If deep spikes in Mn are excluded from parent material composition, a core ~47 km away also shows positive Mn mass flux values. Indeed, sedimentary rocks and, in particular, the Dunkard Group may have many thin and laterally discontinuous rock units, such that the most difficult aspect of this study was determining parent material composition for each soil profile.

Despite these challenges and despite the fact that EMI has only been in operation for 60 years, evidence of industrial Mn inputs can be observed in the upper 60 cm of soils around the greater Marietta area. This zone, which may extend more than 47 km radially outward from EMI, is the likely footprint for Mn deposition from this refinery. Similar footprints due to a variety of other Mn-emitting industries and of variable size were documented by Herndon and Brantley (2011) throughout the U.S.A. and Europe. We reproduce a version of her Figure 1 here as Figure 23, by superimposing the locations of Mn emitters nationwide over a contour map showing values of m_{Mn}. Primary metals facilities, responsible for nearly 50% of all U.S. Mn air emissions, are shown in purple. The mass flux values were calculated by Herndon *et al.* based on a sparse soil dataset for the nation (n=455). The largest area of high Mn additions is observed to be in the eastern half of the US where the density of Mn emitters is high. The extent of Mn contamination in soils is patchy, reflecting the fact that there are many sources, they are not equally distributed and some soils retain Mn better than others.

Our study also has implications for the effect of U.S. regulations on air and soil quality. After comparing recent estimates of Mn deposition in Marietta with soil-derived integrated mass flux values, we conclude that previous Mn deposition rates were more than 3 orders of magnitude higher than deposition rates near EMI over the last 25 years. This is consistent with a measurement of Mn deposition rate near a similar ferromanganese refinery in 1965, as well as the fact that several other Mn alloy production facilities existed in southeast Ohio and West Virginia in the early 1970's. Higher emission factors prior to the Clean Air Act of 1970 and higher production rates due to higher industrial steel production prior to 1980 are also likely responsible for decreasing Mn deposition rates. Although the pace of Mn deposition around EMI has decreased significantly over the last 60 years, a record of previous emissions remains in the soils. The addition and the geographic extent of addition are best quantified using the integrated mass flux, rather than surficial concentrations alone, since surficial Mn concentrations may not show a trend with distance from the emitting source due to mixing with deeper soils. The integrated mass flux value (m_{Mn}) is a more robust indicator of the metal inputs, as long as the parent material can be identified.

This study could serve as a model for the study of deposition of other metals. These results suggest that soil measurements can help decipher past metal deposition rates and that, in the absence of high resolution meteorological and emissions data, soil measurements may more accurately predict deposition than atmospheric dispersion models.

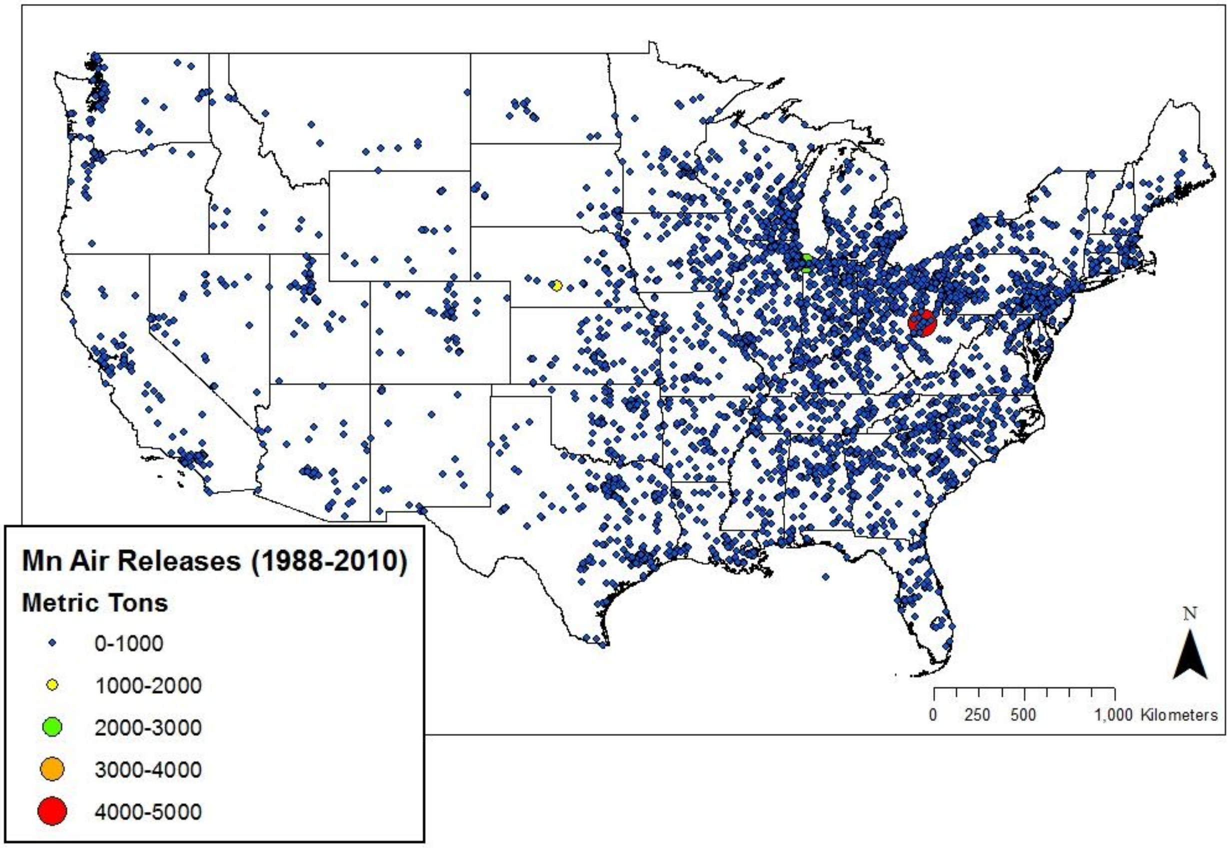

Figure 1-1. Integrated total mass of Mn emitted from 1988-2010 for each facility reporting emissions to the US EPA Toxics Release Inventory in the continental US. EMI, a ferromanganese refinery in Marietta OH (red symbol), released emissions during this time period that were nearly double those of the next largest emitter, US Steelworks in Gary, Indiana (green symbol).

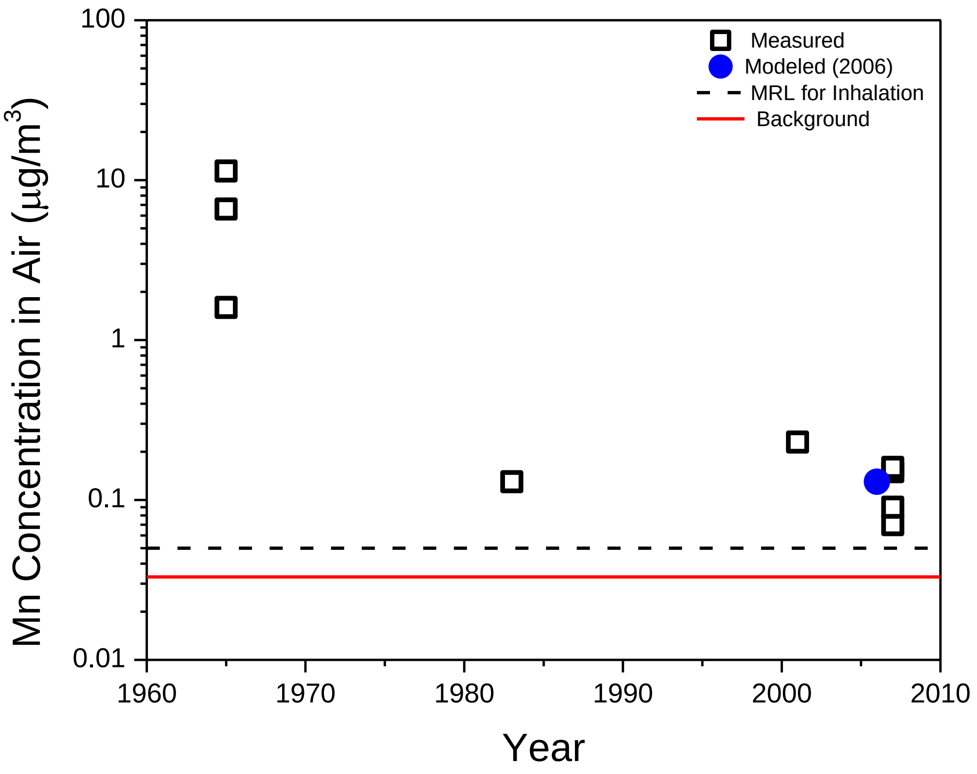

Figure 1-2. Average Mn air concentrations measured (black squares) or modeled (blue circle, Haynes *et al.*, 2010) for multiple locations within the greater Marietta area (< 7 km from EMI) plotted versus time. Although concentrations have decreased with time, all values have exceeded the ATSDR minimal risk level for Mn inhalation, the chronic exposure level that is not likely to result in an observable health effect, thoughout this time period (dashed line) (U.S. EPA, 1984a). Furthermore, values have exceeded estimates of background Mn in urban air (solid red line) (ATSDR, 2007; ATSDR, 2008; ATSDR, 2009; Moore, 1983). Values for 1965 represent average concentrations within a 24-hr period at sites measured to be downwind of EMI at the time, while values from other years are either average monthly or yearly concentrations.

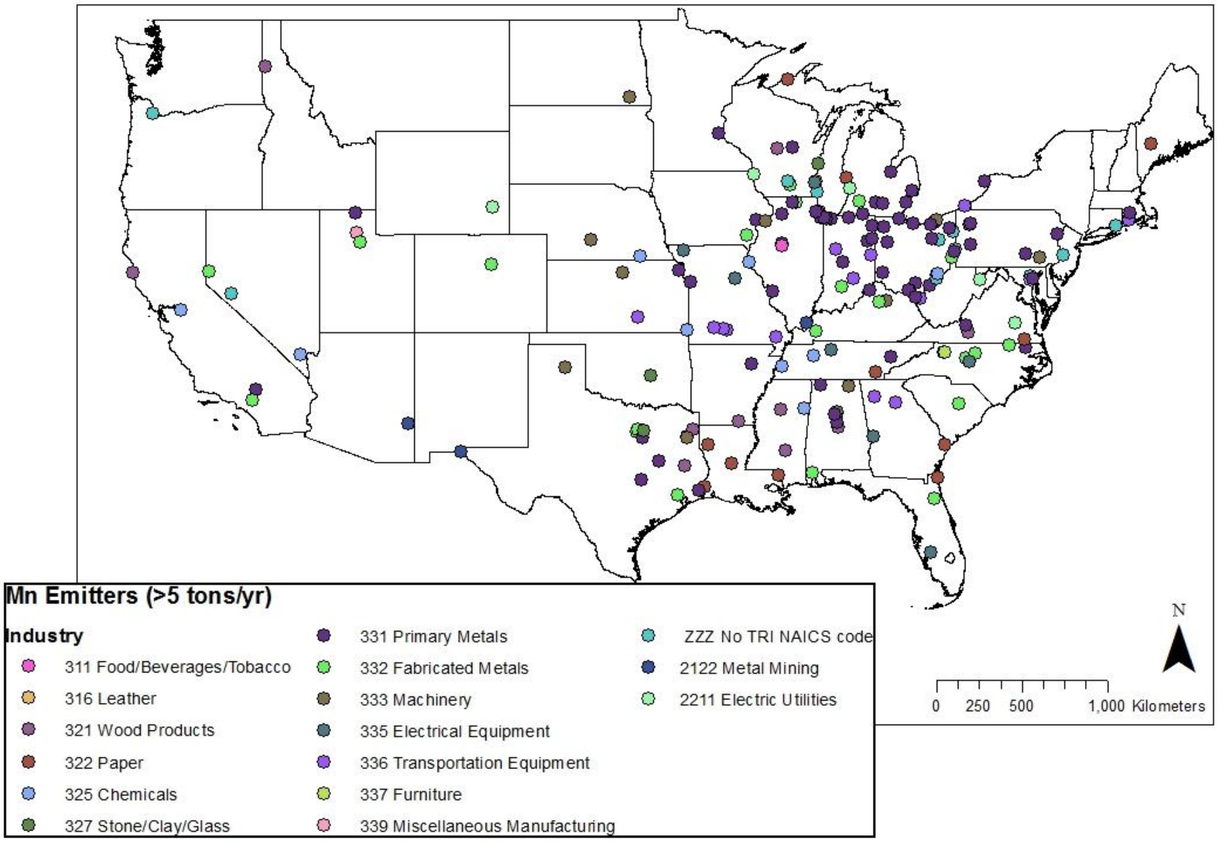

Figure 1-3. Map of the U.S.A. with Mn-emitting facilities reporting emissions of greater than 5 metrics tons per year depicted as dots with colors indicating industry type. Each facility shown has reported Mn emissions to the EPA for at least one year since 1988 (U.S. EPATRI, 2010).

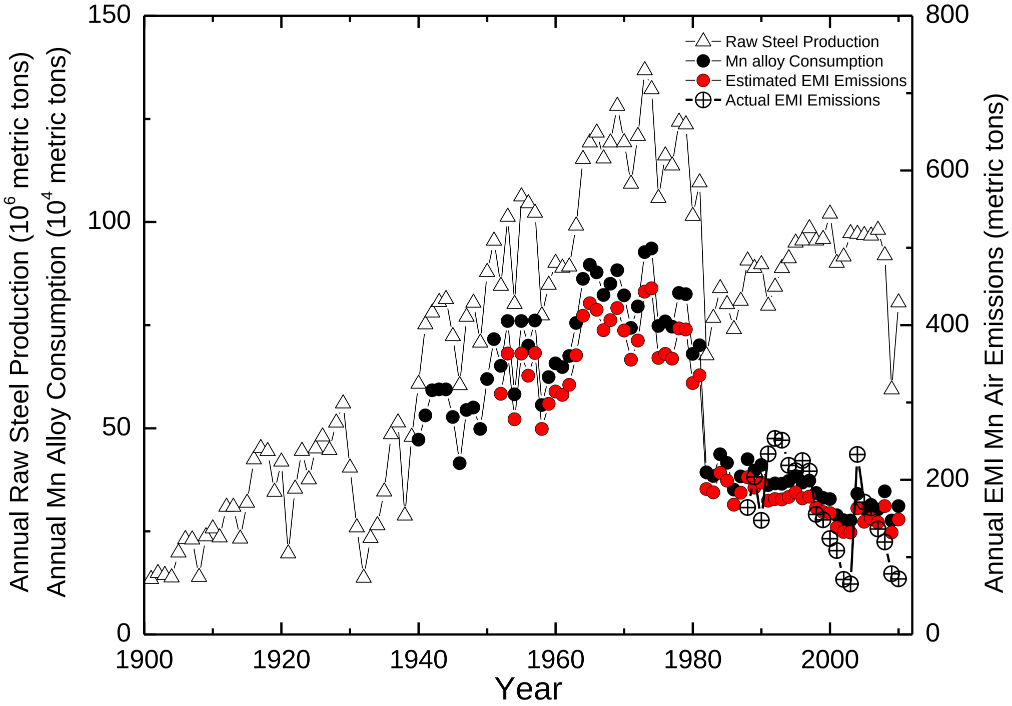

Figure 1-4. Annual raw steel production and annual Mn alloy consumption in the U.S.A., as well as annual EMI Mn air emissions (when reported) plotted versus time. Trends in Mn alloy consumption (closed black circles) followed trends in raw steel production (open triangles) from 1940-2010 because Mn is used in steelmaking (Jones, 1994). Over the period of time where data are reported, 1988-2010, Mn air emissions from EMI (crossed circles) have decreased (EPATRI, 2010). Based on the relationship between Mn alloy consumption and known EMI emissions from 1988-2010 as described in text (eq. 6), EMI emissions were predicted back to its start of operations in 1952 (red closed circles). The enactment of the Clean Air Act in 1970, as well as facility-specific operations changes, likely affected Mn emissions from the refinery.

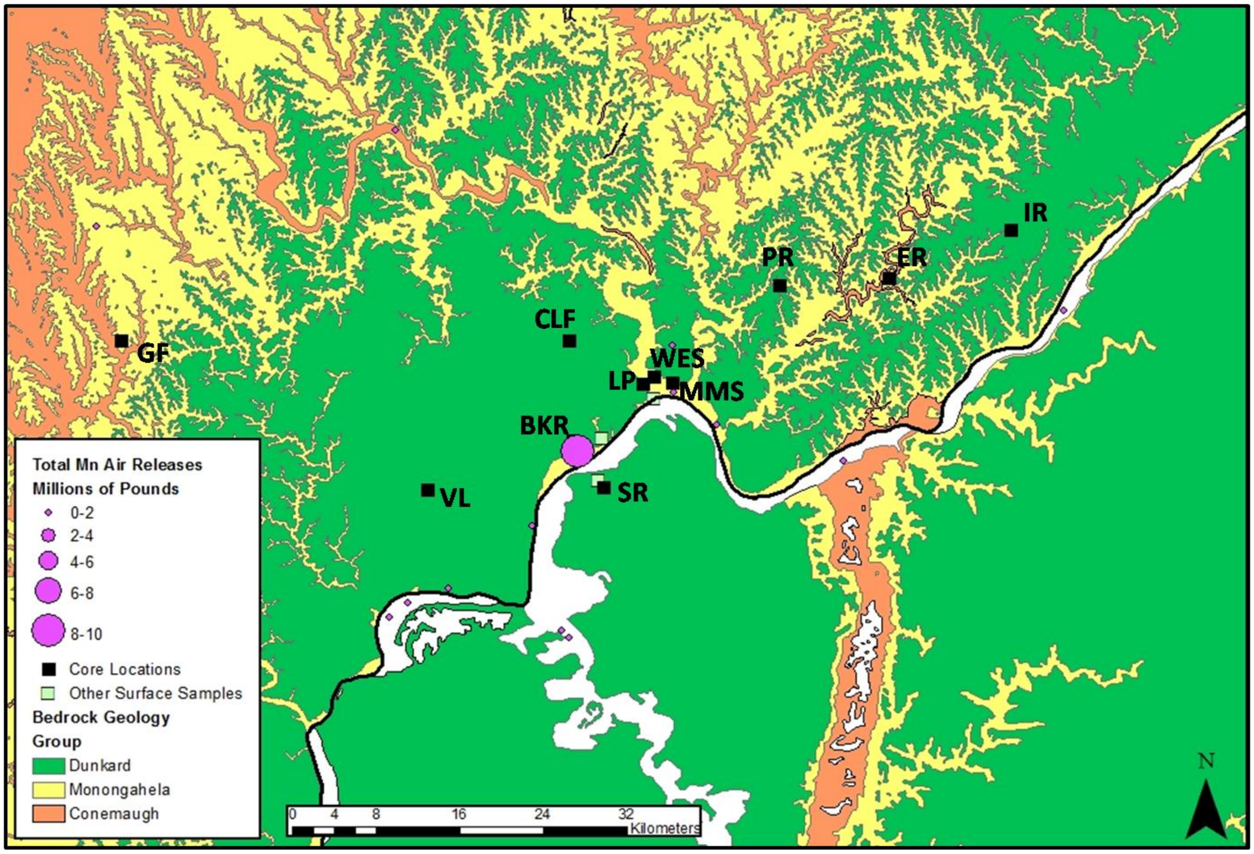

Figure 1-5. A geological map showing the three predominant surficial bedrock formations as well as core locations (black squares) and Mn-emitting sources (pink circles). Black line from NE to SW follows the Ohio River, separating SW Ohio from West Virginia. Pink symbols are scaled to the total integrated Mn air releases from 1988-2010. The largest circle is EMI. Average wind direction is to the northeast. Every effort was made to auger cores in soils overlying the Dunkard Group (green). Three additional 0-10 cm soil samples were obtained and are shown as green squares.

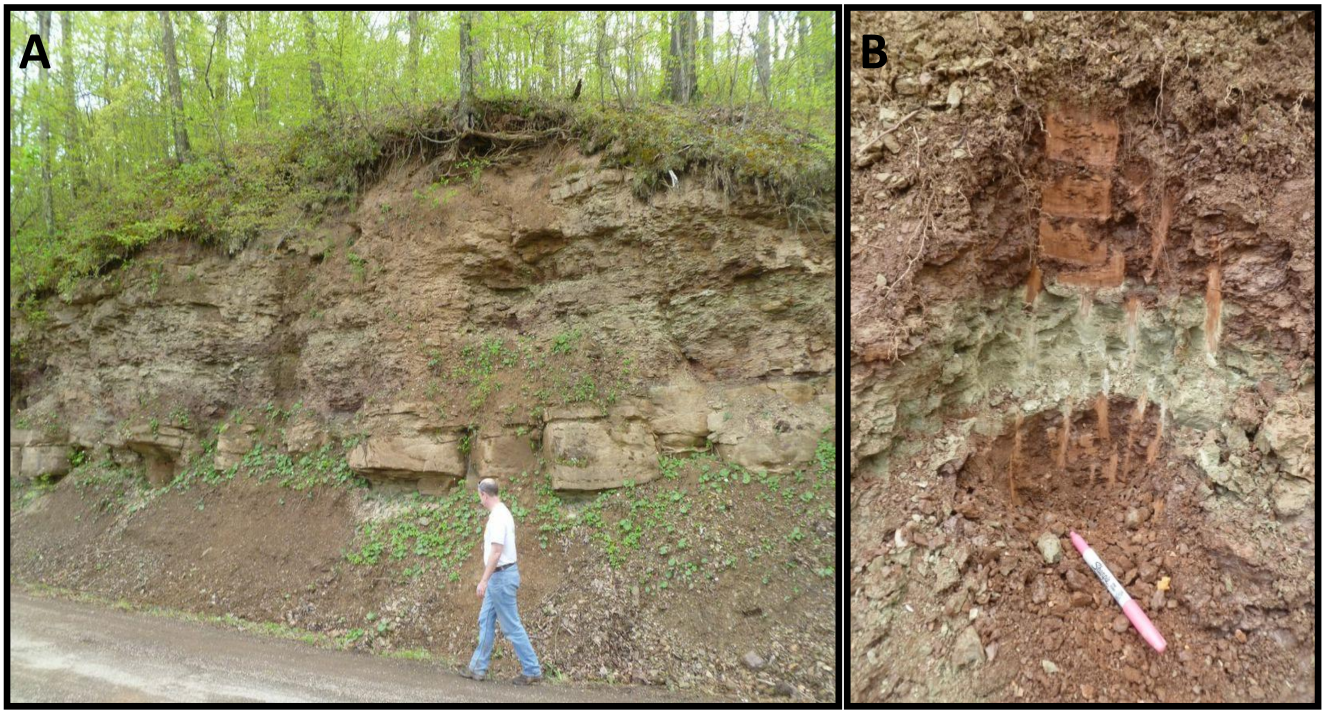

Figure 1-6. Variations in color from red to green were visible both in rock outcrop (A) and in pedons (B) throughout the field area, as shown here for VL. Color changes document periods of oxidizing (red) and reducing (grey-green) conditions, which may have resulted in immobilization and mobilization of Mn respectively (Martin, 1998). More sandy layers are also seen interspersed with clay-rich layers.

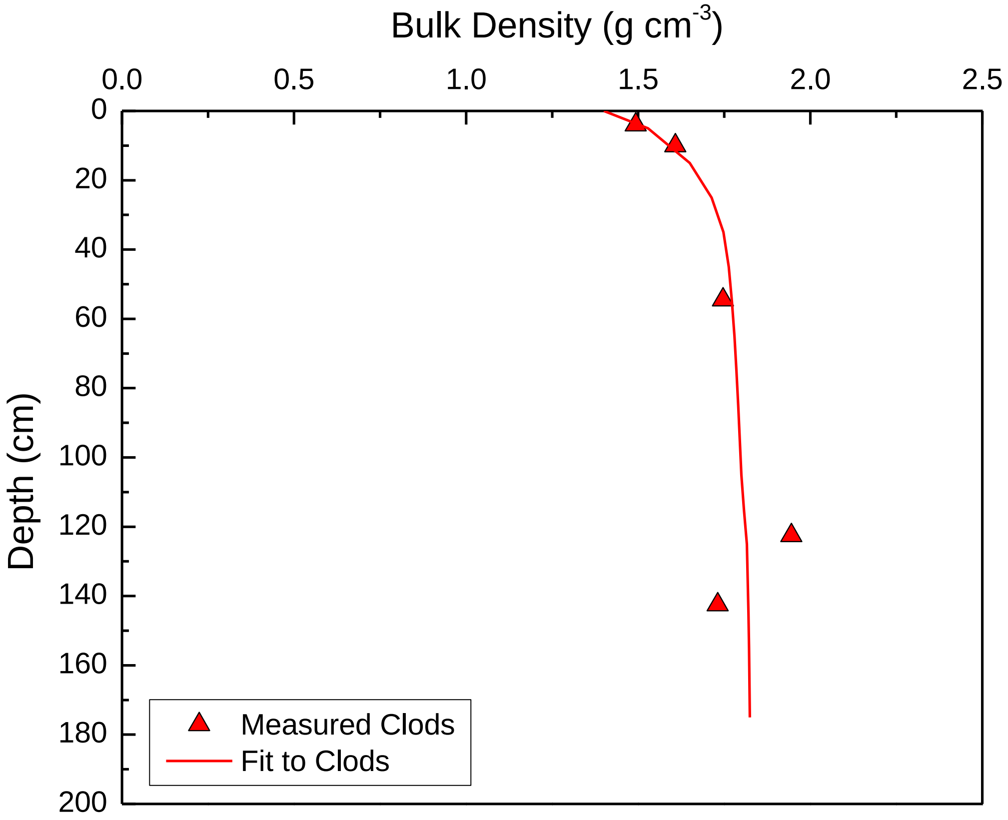

Figure 1-7. Bulk density as a function of depth for MMS. Red triangles are measured values from soil clods from augered cores. Red line was fit to red triangles using equation 1. This equation was used to estimate the bulk density with depth in all soil cores.

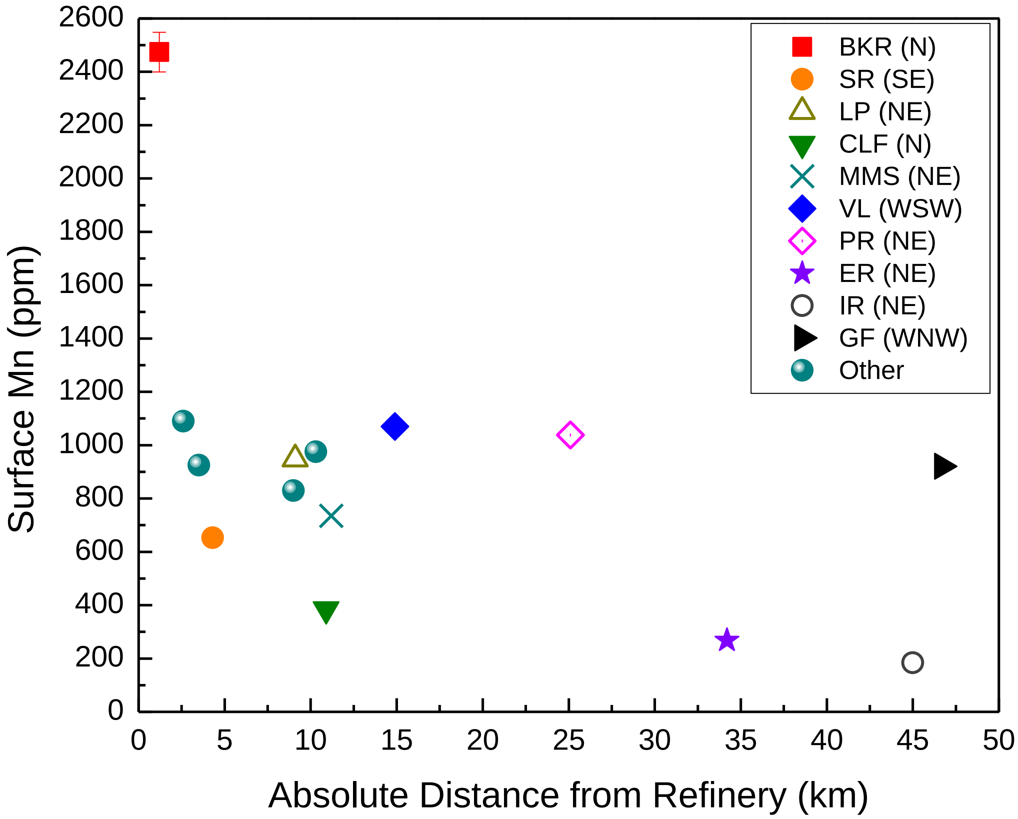

Figure 1-8. Mn concentrations in surface samples (0-10 cm) as a function of distance from EMI with relative direction from the refinery shown in parentheses. All samples are in the predominant downwind direction except for VL and GF. Error bars are shown as an estimate of analytical precision, i.e., 3% of reported values (some are smaller than symbols). For comparison, average Mn in U.S. surface soils is 550 ppm (Shacklette and Boerngen, 1984).

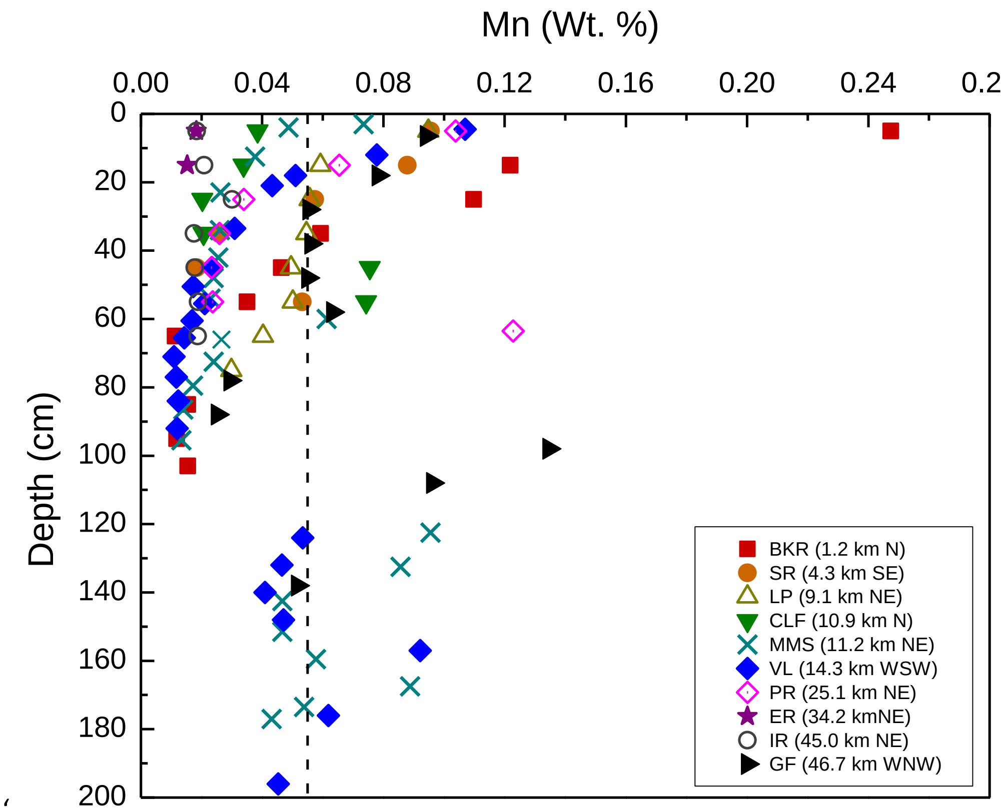

Figure 1-9. Mn concentrations in soil cores, plotted down to augering refusal. Distances and direction from EMI are given in parentheses. Augering refusal was well below 1 m depth at only 3 locations as shown. At each of these locations, Mn concentrations increase and vary below a meter. Mean Mn concentration at 20 cm depth for conterminous US soils is also shown as determined from 1370 soil samples (Shacklette and Boerngen, 1984).

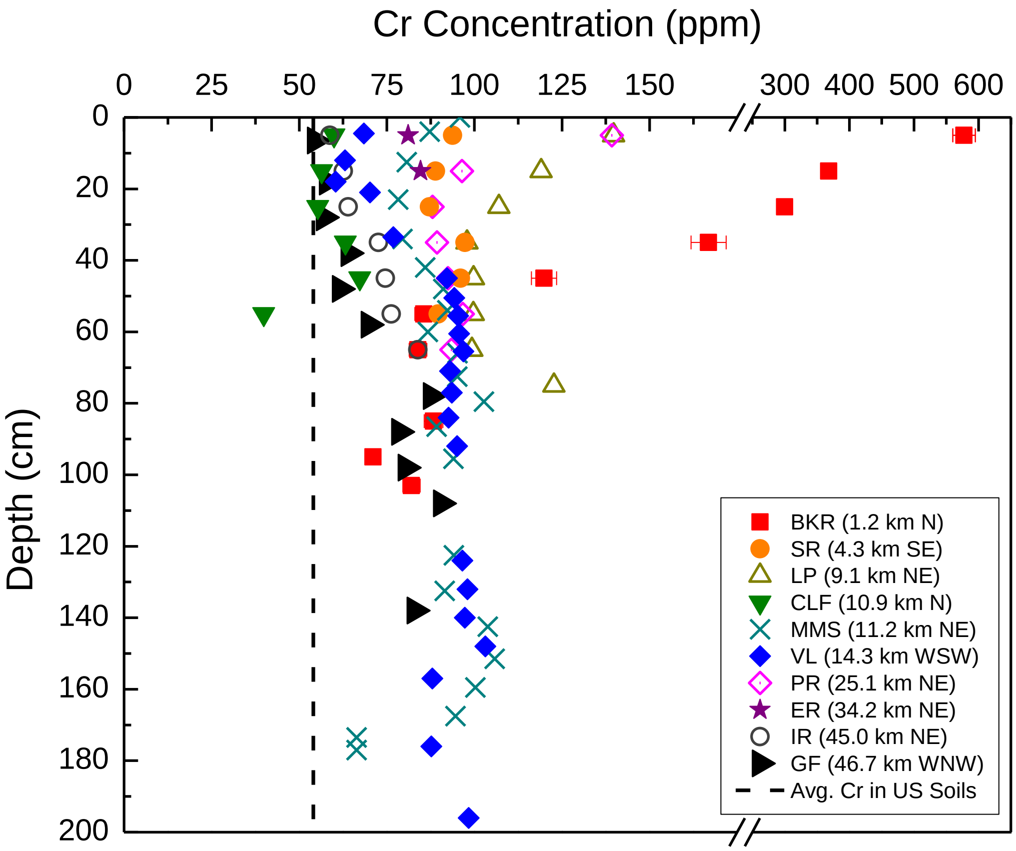

Figure 1-10. Cr concentration as a function of depth at core locations. Absolute distance and relative direction from EMI are given. Mean Cr concentration at 20 cm depth for conterminous US soils is also shown as determined from 1370 soil samples (Shacklette and Boerngen, 1984).

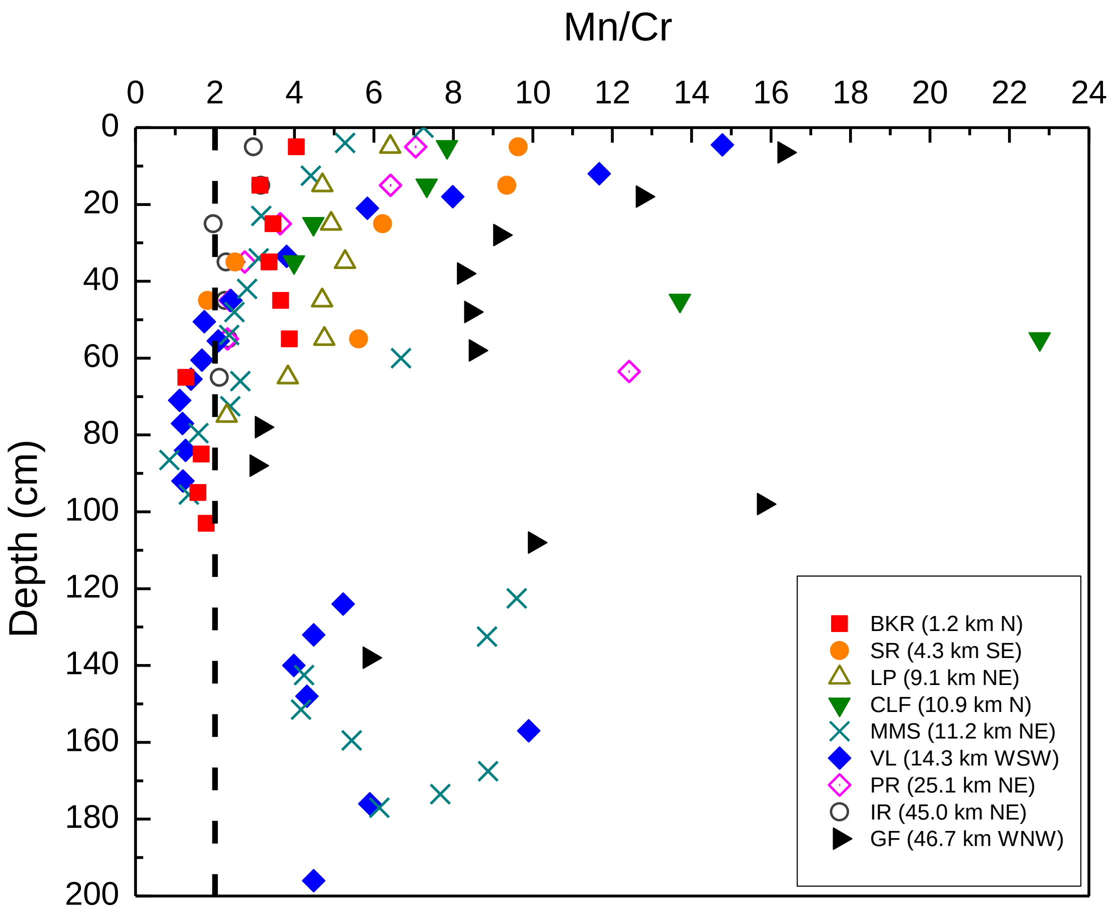

Figure 1-11. Mn to Cr ratio on a molar basis plotted versus depth. Only the ratio at IR stays constant with depth: in other sites the Mn to Cr ratio increases toward the surface. High Mn:Cr values are observed due to spikes in Mn concentration in the bottom-most intervals of CLF and PR, as well as below 1 m depth in MMS, VL, and GF. The Mn;Cr ratio of parent material was estimated as the average for IR and is shown as a dashed line. Estimated average Mn/Cr ratio for EMI emissions equals 18 ± 12 (see text).

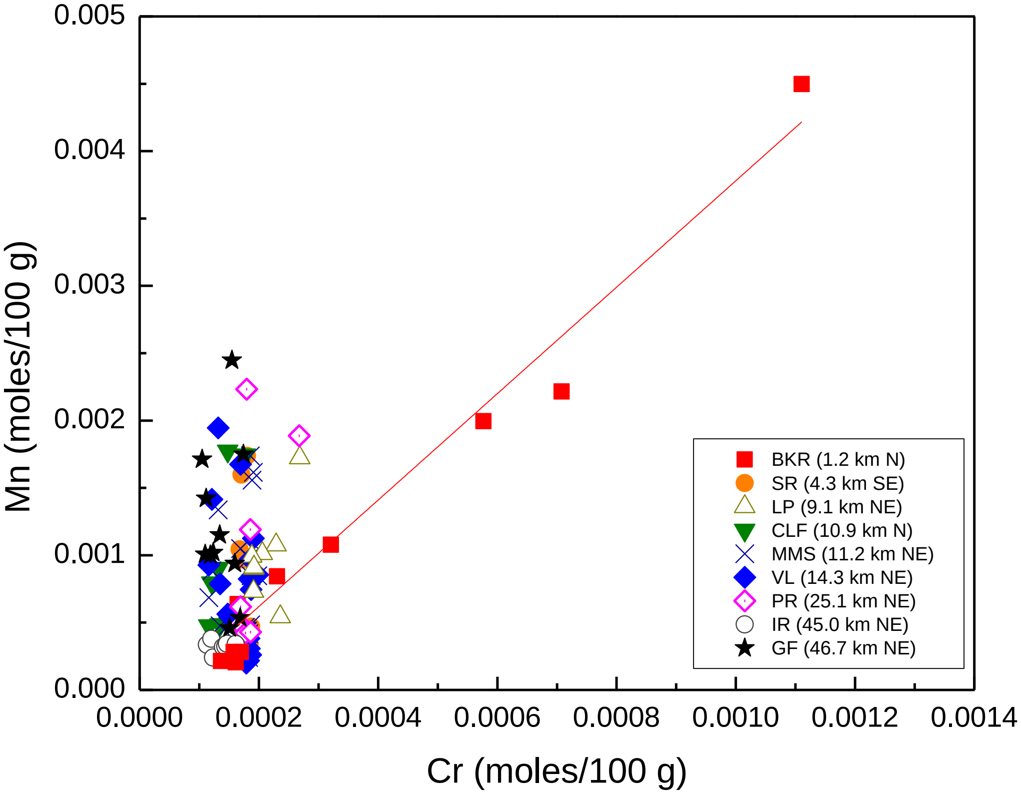

Figure 1-12. Mn concentration varies linearly with Cr concentration only in the upper 60 cm of BKR. Equation for line fit to upper 60 cm of BKR is $y = 3.95\,x$ (R^2=0.985). Below 60 cm in BKR, the Mn:Cr ratio is similar to values for other cores. Sixty cm is inferred to be the maximum depth of anthropogenic additions at BKR. A few samples of LP and PR appear to be trending in the direction of the fit line for BKR.

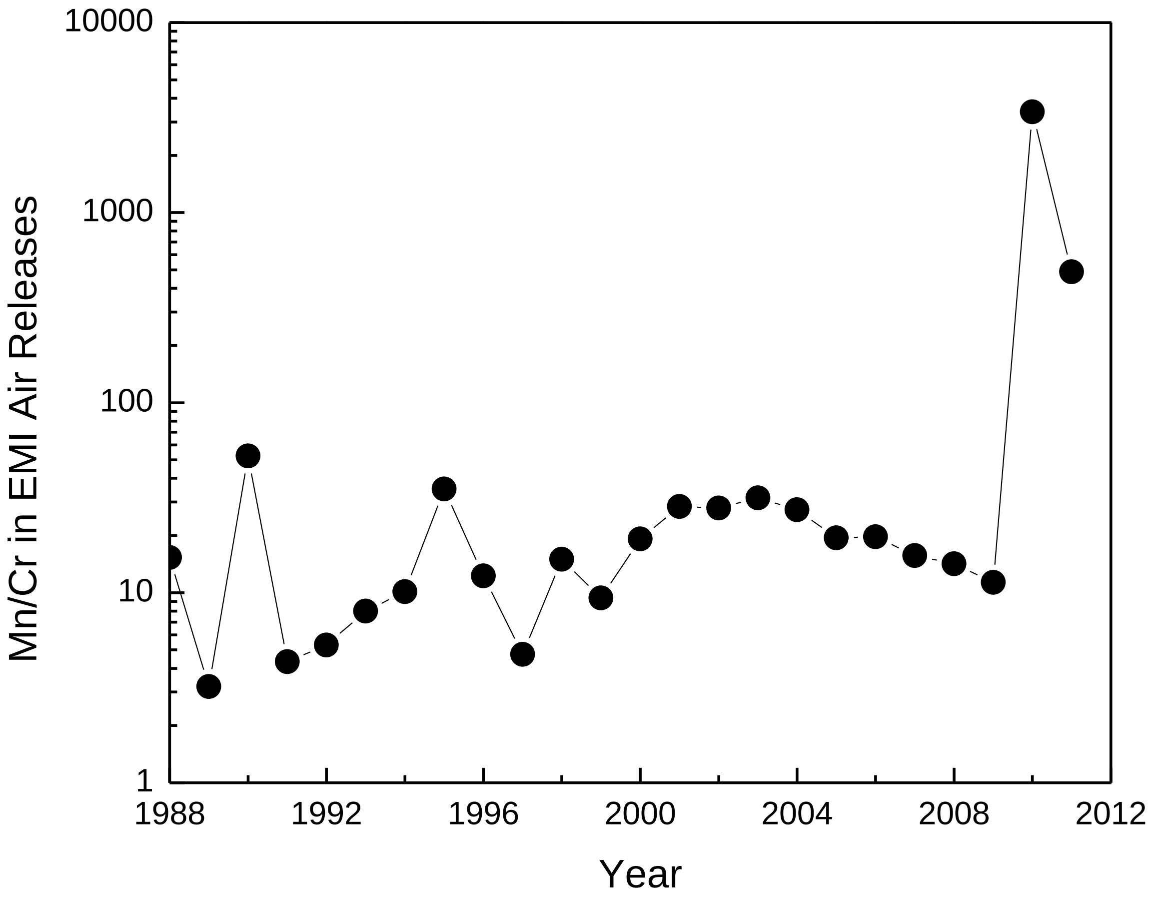

Figure 1-13. Mn:Cr ratios reported for EMI air releases (mol Mn/mol Cr) averaged 18 from 1988 to 2009. Mn:Cr ratios increased by nearly 2 orders of magnitude after production of ferrochromium was discontinued in 2009 (U.S. EPATRI, 2010).

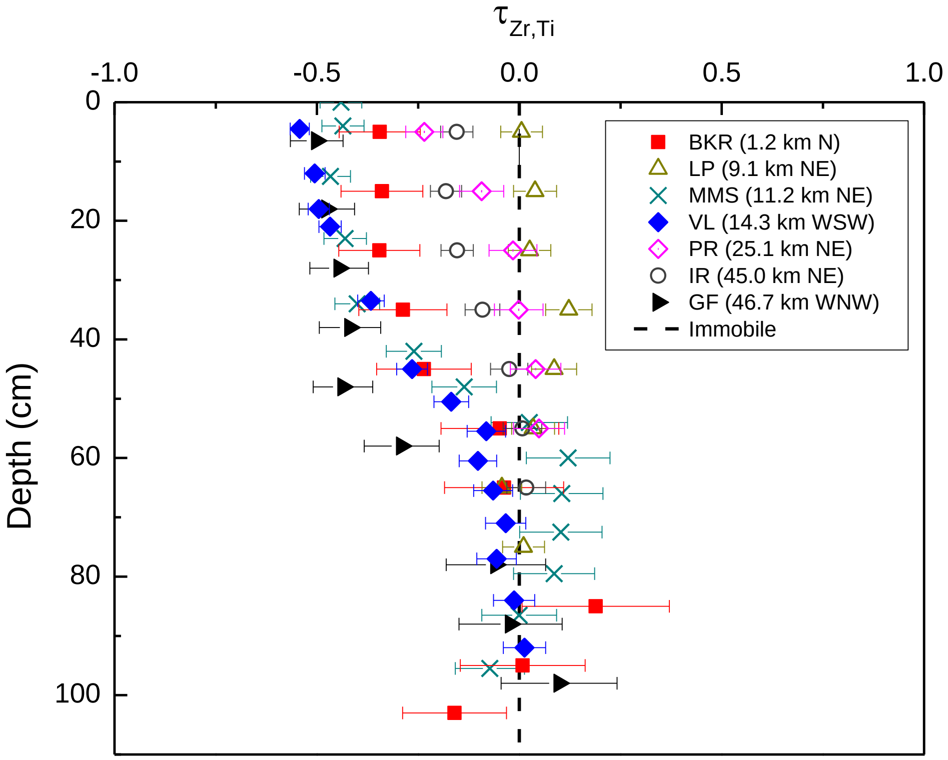

Figure 1-14. Mass transfer coefficients for Ti normalized to Zr using the average of the bottom 3 samples as parent material. For cores >1 m total depth, only the upper m is shown and the average of the 3 samples nearest 1 m were used as parent. Plots show that Ti is more mobile than Zr in the surface of several cores, i.e., that Zr is a better choice for the immobile element. Dashed line indicates τ = 0, i.e., parent composition. For clarity, SR and CLF were not plotted because Ti was immobile with respect to Zr throughout.

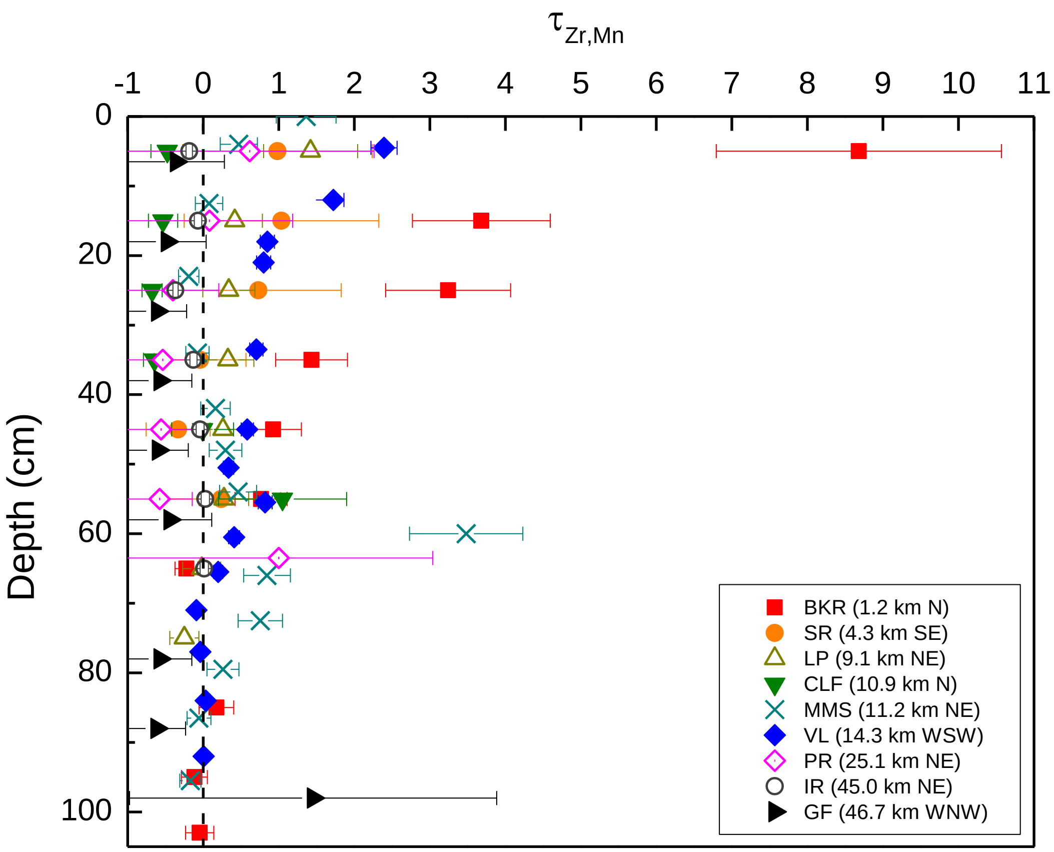

Figure 1-15a. Mn mass transfer coefficients plotted for each core as a function of depth at a range of distances from EMI, where $\tau_{Zr,Mn}>0$ indicates enrichment of Mn above parent composition and $\tau_{Zr,Mn}<0$ indicates depletion. Parent material is defined as the average chemical composition of the 3 bottom-most samples in each core (parent scenario A). For cores deeper than 1 m (MMS, VL and GF), only the upper meter is shown and parent material is defined as the average of the 3 samples closest to 1 m depth.

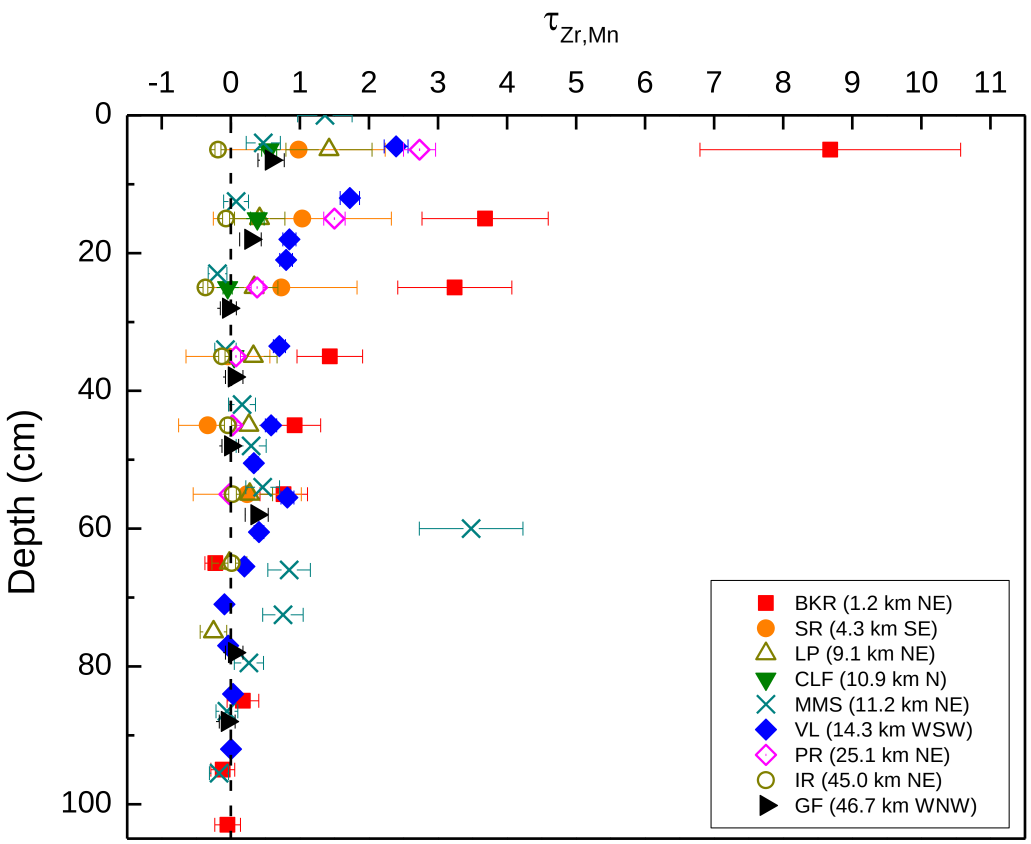

Figure 1-15b. Mn mass transfer coefficients in each core as a function of depth at a range of distances from EMI, where $\tau_{Zr,Mn}>0$ indicates enrichment of Mn above parent composition and $\tau_{Zr,Mn}<0$ indicates depletion. Parent material is defined as the average chemical composition of the 3 bottom-most samples in each core (parent scenario B). For cores deeper than 1 m (MMS, VL and GF), only the upper meter is shown and parent material is defined as the average of the 3 samples closest to 1 m depth. For CLF, PR, and GF, deep spikes in Mn concentration are not included in parent material composition as described in text. Where no error bar is shown, the error is smaller than the symbol.

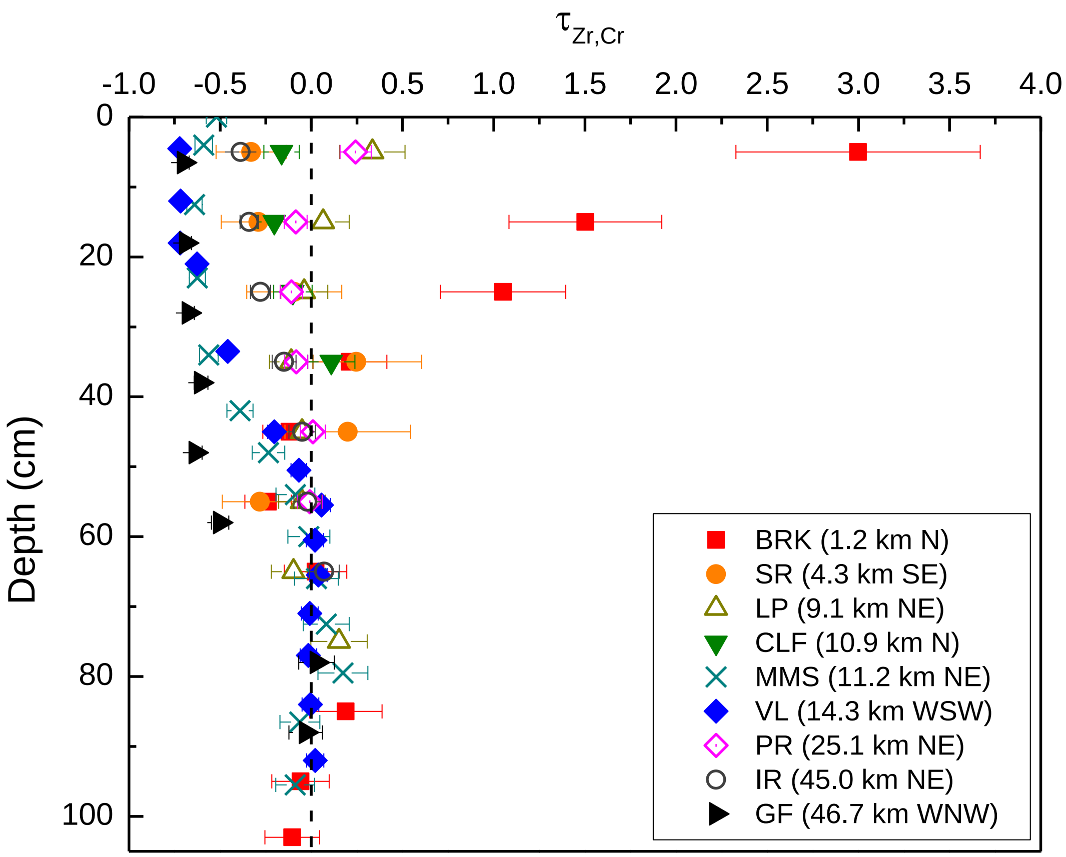

Figure 1-16. Cr mass transfer coefficients in each core as a function of depth at a range of distances from EMI, where $\tau_{Zr,Cr}>0$ indicates enrichment of Mn above parent composition and $\tau_{Zr,Cr}<0$ indicates depletion. Parent material is defined as the average chemical composition of the 3 bottom-most samples in each core. For cores deeper than 1 m (MMS, VL and GF), only the upper meter is shown. Parent scenario B is shown here, though both parent scenarios yielded very similar results.

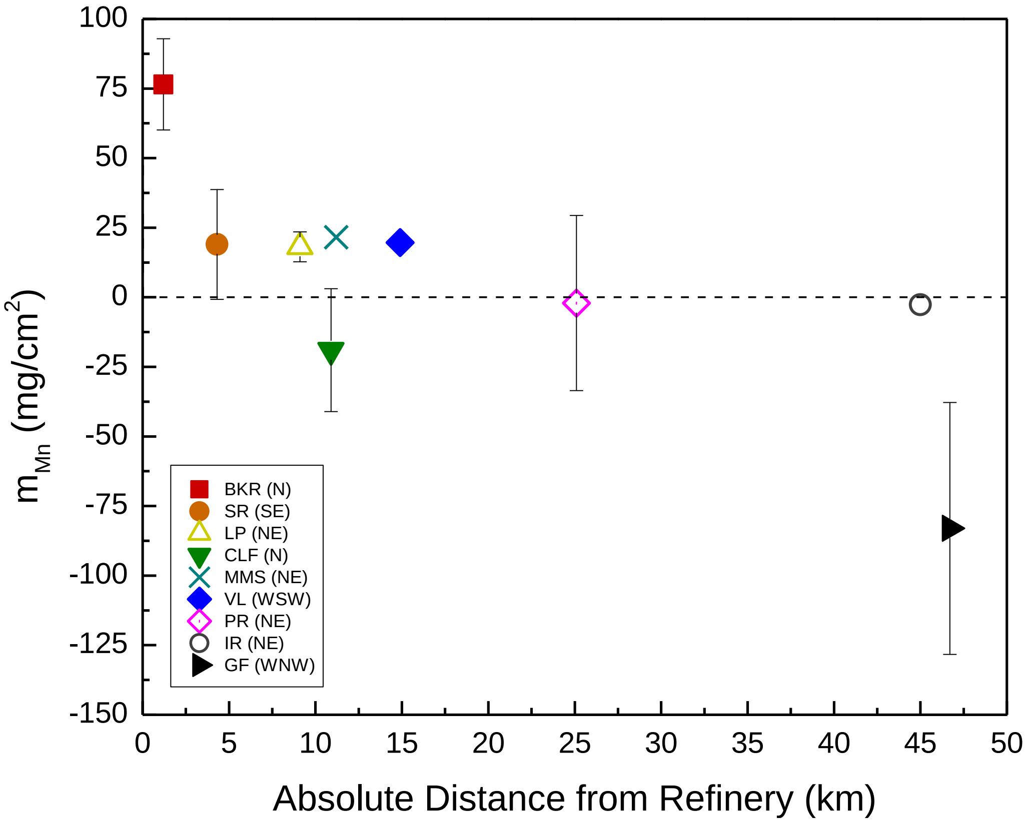

Figure 1-17a. Integrated mass flux of Mn added (positive) or lost (negative) from each soil profile as a function of distance from EMI using parent material scenario A. For cores of greater than 1 m total depth, only the top meter is included (MMS, VL, GF). Values are reported in units of mass of Mn per square cm of land area. Error calculations are shown in Appendix D. Where no error bar is shown, the error is smaller than the symbol.

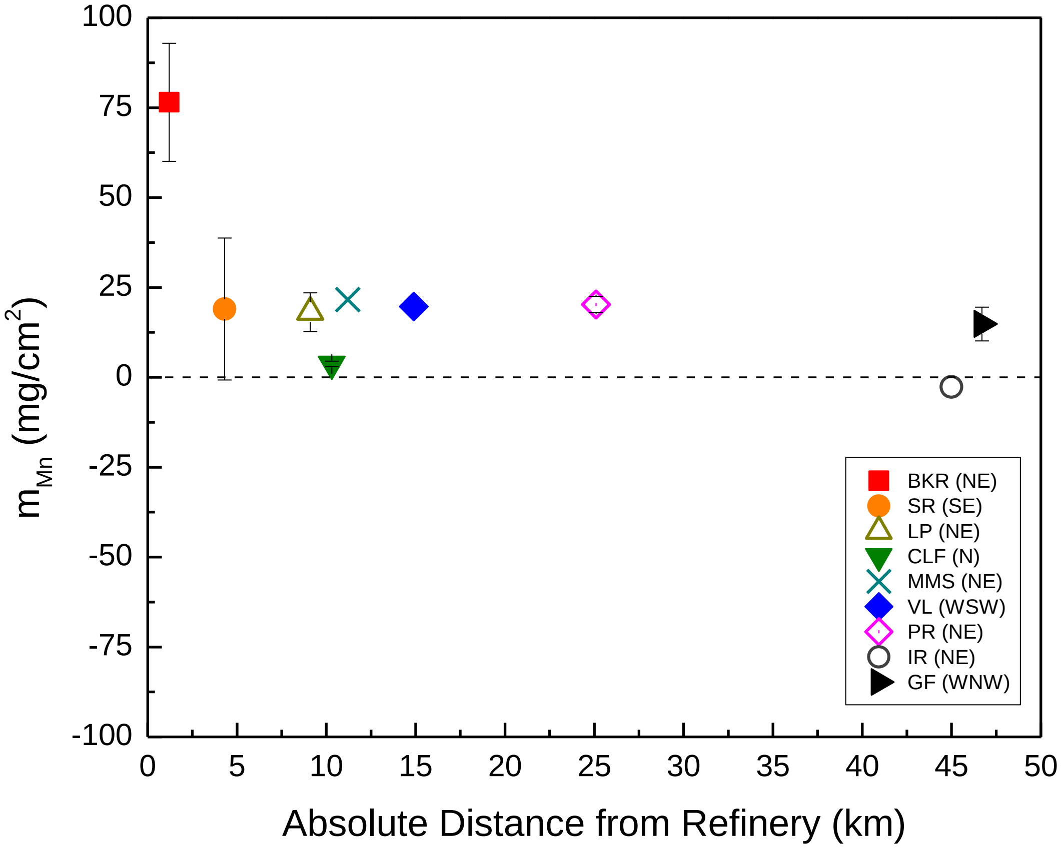

Figure 1-17b. Integrated mass flux of Mn added or lost from each soil profile as a function of distance from EMI using re-calculated values for CLF, PR, and GF (parent material scenario B). For cores of greater than 1 m total depth, only the top m is included (MMS, VL, GF). Positive values indicate net enrichment of Mn in the soil profile, while negative values indicate a net loss. Values are reported in units of mass of Mn per square cm of land area. Where no error bar is shown, the error bar is smaller than the symbol.

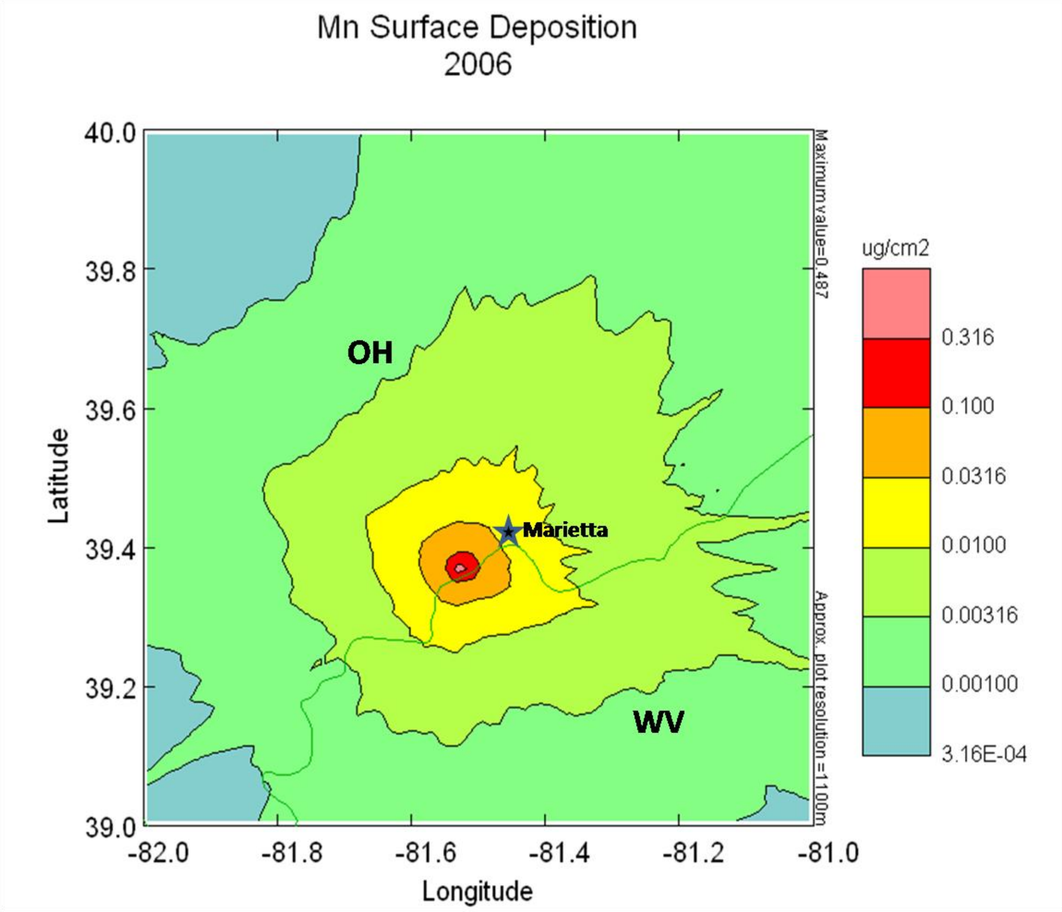

Figure 1-18. Integrated Mn surface deposition for 2006-2007 using SCIPUFF showing the calculated Mn deposition footprint due to EMI operations. Hourly meteorological variables including precipitation, temperature, relative humidity, windspeed and wind direction are incorporated, as well as the EMI Mn emission rate for 2006 (EPA TRI, 2010). No locations exceed the estimated pre-settlement Mn deposition rate of 1.7 μg cm^{-2} yr^{-1} for the Lake Michigan area (Cole *et al.*, 1990). Only deposition within 5 km of the plant exceeds the estimated Mn deposition rate of 0.062 μg cm^{-2} yr^{-1} estimated for Bermuda in 1975 (Duce *et al.*, 1976). Green line is the border between Ohio and West Virginia.

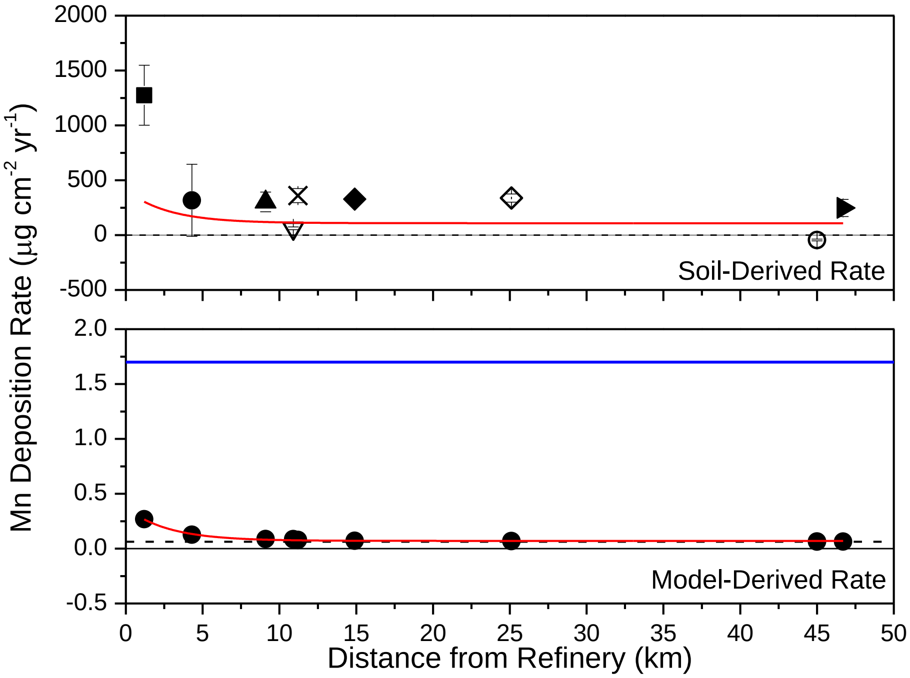

Figure 1-19. Modeled Mn deposition rates from EMI summed with the deposition rate of Mn in remote areas (bottom) for each core location using 2006 EMI Mn emissions and weather conditions. The red line was fit through all model-derived values ($y=0.07051+0.30333e^{(-0.36522x)}$). Soil-derived deposition rates are plotted with the same model fit line at appropriate locations (top): soil rates are at least 3 orders of magnitude higher than modeled rates near the refinery (using parent scenario B). Rate of Mn deposition in remote areas is estimated to be 0.062 µg cm^{-2} yr^{-1} and is shown with the dashed line (Duce *et al.*, 1976) or 1.7 µg cm^{-2} yr^{-1} as shown by solid blue line (Cole *et al.*, 1990). Where no error bars are shown for the soil-derived rate, the error is smaller than the symbol.

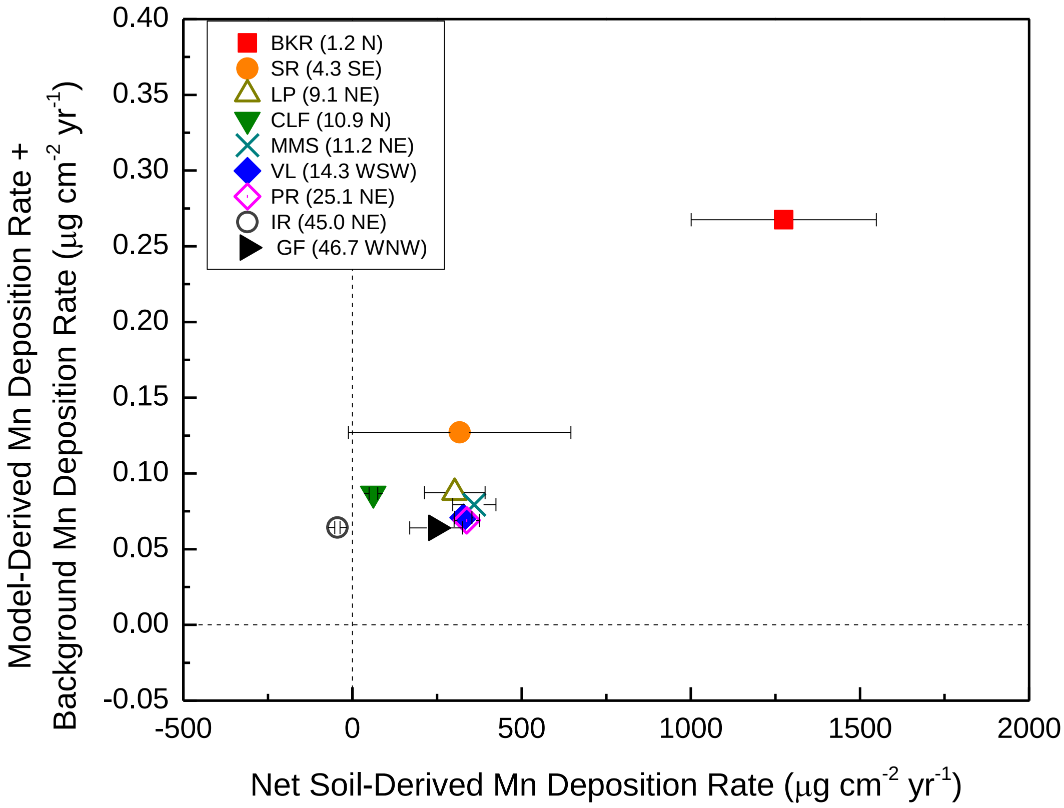

Figure 1-20. Model-derived Mn deposition rates for 2006 summed with the estimated Mn deposition rate due to background levels (0.062 μg cm^{-2} yr^{-1}; Duce *et al.*, 1976) are more than 3 orders of magnitude lower than net soil-derived rates.

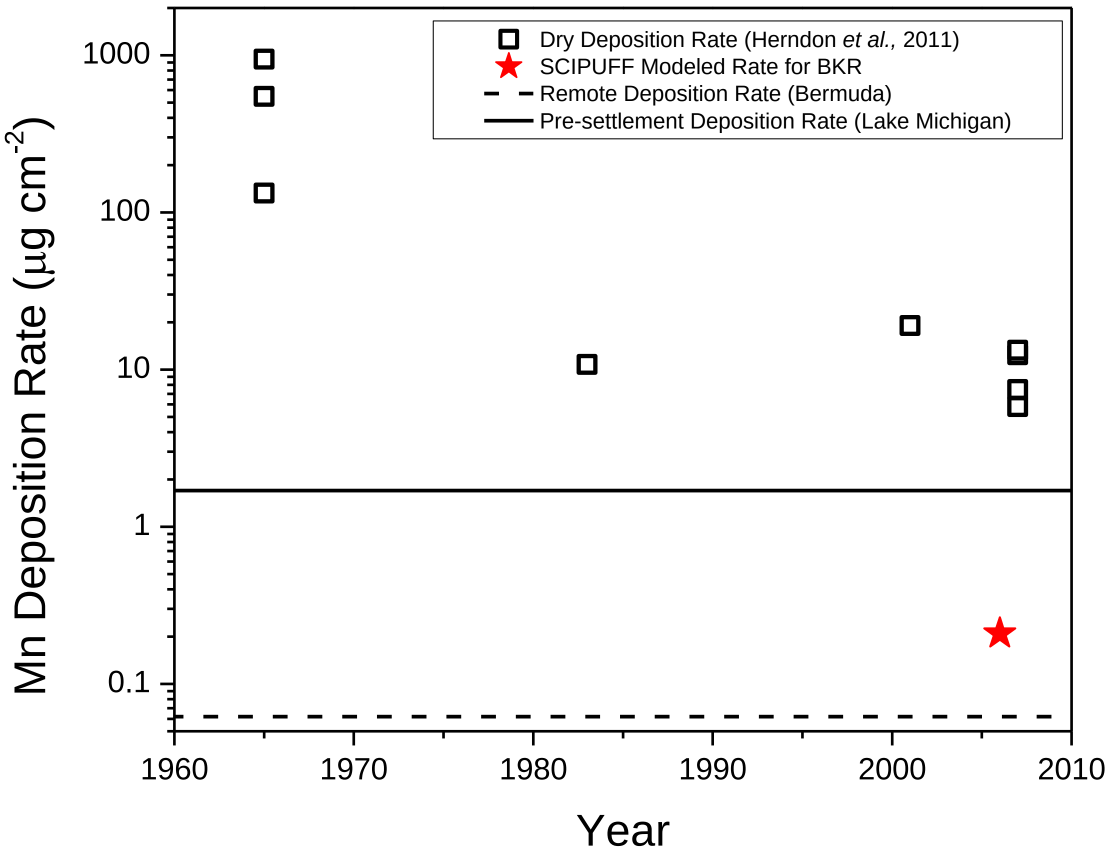

Figure 1-21. Estimated dry deposition rates (open squares) for sites near Marietta over time plotted with modeled bulk deposition rate at BKR (red star). Dry deposition rates are calculated using estimates of Mn dry deposition velocity (2.63 cm s^{-1}) and the measured Mn concentration in air as shown in Fig. 2, following Herndon *et al.* (2011). Modeled bulk Mn deposition rate from this study is up to 2 orders of magnitude lower than estimated rates based on Mn air concentrations, suggesting that the model may be under-predicting recent deposition near the refinery.

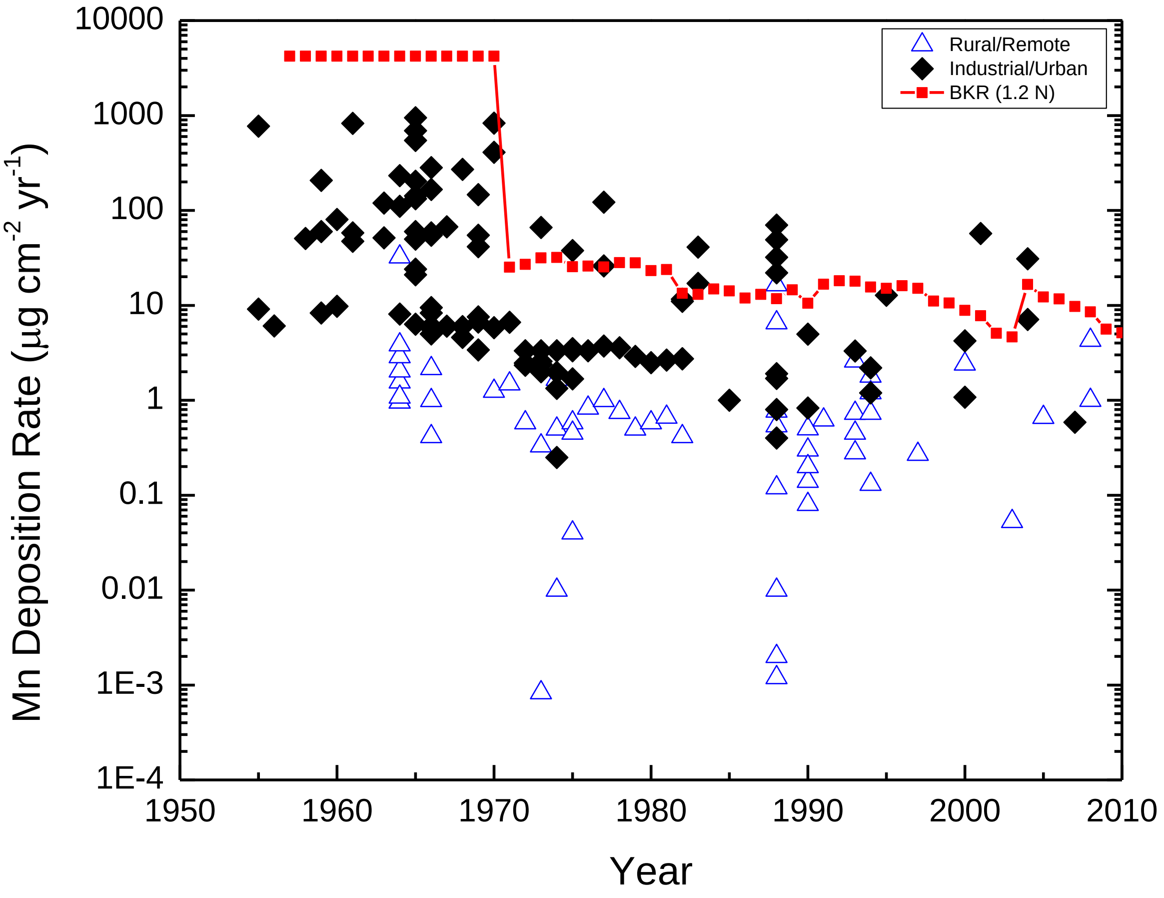

Figure 1-22. Mn deposition rates for BKR calculated for the duration of EMI operations: a) for 1988-2010, deposition rates were calculated based on reported EMI Mn emissions (equation 4, see text); b) for 1971-1987, deposition rates were also based on EMI Mn air releases, estimated based on U.S. Mn alloy consumption (equation 5, see text); c) for 1952-1970, deposition rates were calculated from the soil-derived Mn integrated mass flux value at BKR (equation 6, see text). Back-calculated Mn deposition rates agree well with other estimates of Mn deposition over time in industrial/urban environments as shown after the Clean Air Act, but deposition rates may have been higher near EMI than in other areas prior to that time.

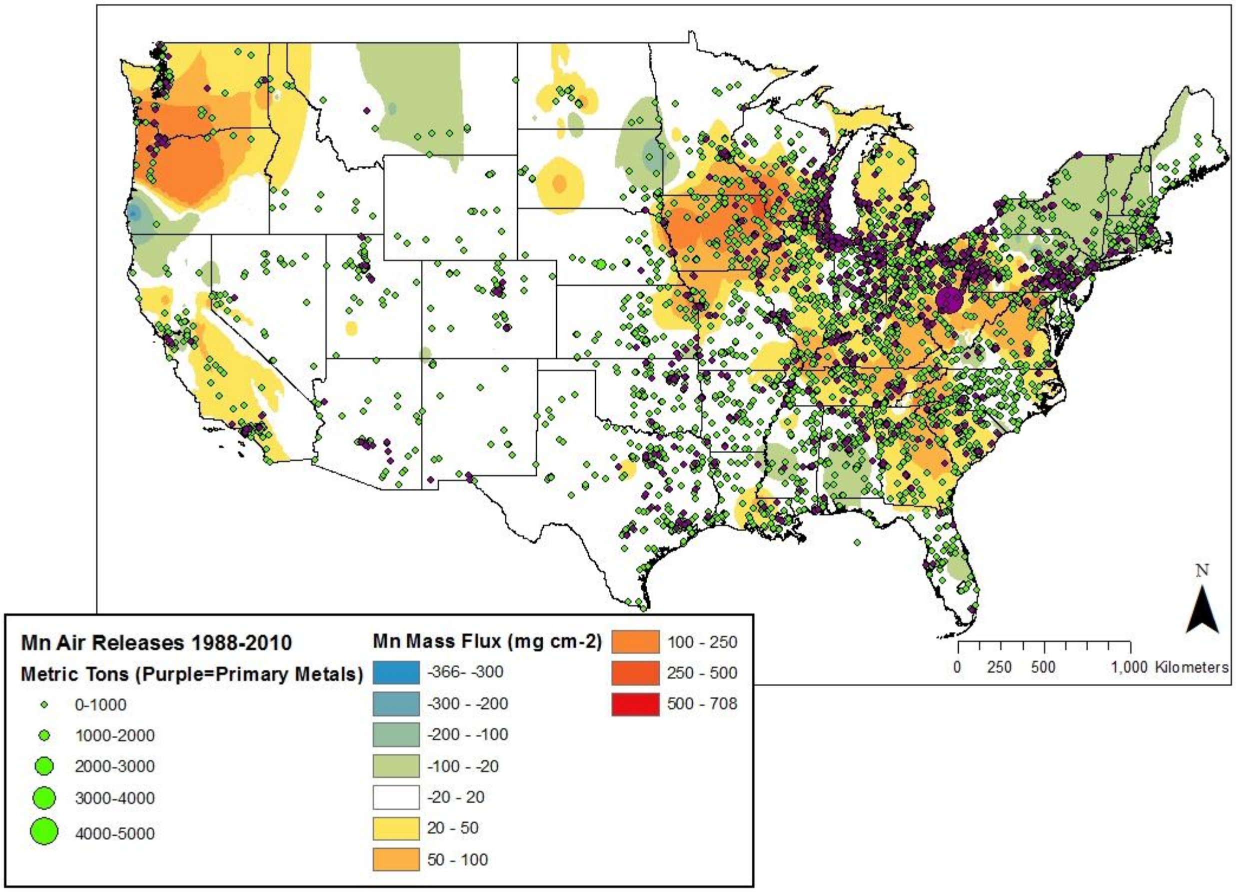

Figure 1-23. Total Mn air releases from facilities (1988-2010) superimposed on interpolated integrated Mn mass flux values throughout the U.S.A. calculated from 455 soil cores in Herndon and Brantley (2011). Purple symbols are primary metals facilities, which were cumulatively responsible for 50% of U.S. Mn air emissions from 1988-2010. The eastern half of the U.S. has more emitters and the largest area of positive integrated Mn mass flux values. Mn contamination is patchy, reflecting the fact that sources are not equally distributed and that some soils better retain Mn than other

Table 1. Summary of Core Locations

Core	Site Name	Distance from EMI (km)	Elevation (m)	Refusal Depth (cm)	Avg. $[Mn]_{Air}^{*}$ ($\mu g/m^3$)	Mn (0-10 cm) (ppm)	$m_{Zr,Mn}$ (mg/cm^2)^	Mn Deposition Rate (2006)[c] ($\mu g/cm^2$)
BKR	Blue Knob Rd	1.2 N	278	106	>1.00	2474	77 ± 16	0.206
SR	Summit Road	4.3 SE	299	60	>1.00	653	19 ± 20	0.065
LP	Lookout Park	9.1 NE	266	80	0.50-0.99	950	18 ± 5	0.025
WES	Washington Elementary	10.3 NE	187	217[a]	0.50-0.99	975	--	--
CLF	Churchtown-Locus Fork	10.9 N	253	60	0.10-0.49	385	-19 ± 22 (4 ± 1)	0.025
MMS	Marietta Middle School	11.2 NE	231	179	0.50-0.99	735	22 ± 4	0.017
VL	Veto Lake Wilderness Area	14.9 WSW	219	202	0.10-0.49	1070	20 ± 2	0.009
PR	Pleasant Ridge	25.1 NE	316	67	0.10-0.49	1038	-2 ± 31 (20 ± 2)	0.007
ER	Eddy's Ridge	34.2 NE	322	20	0.05-0.09	268	--	--
IR	Irish Run	45.0 WNW	340	70	<0.05	184	-3 ± 1	0.002
GF	Gifford Forest	46.7 NE	275	143	0.05-0.09	921	-83 ± 45 (15 ± 5)	0.002

*Predicted 2006 average Mn concentration in air from Haynes *et al.* (2010)

[a] Evidence of recent disturbance in core, including rusty nails and bricks. Augering discontinued before depth of refusal.

[b] Integrated mass transfer coefficient not calculated, since only 2 depth intervals in core.

[c] Modeled surface deposition from this study based on EMI for 2006.

^Where 2 values are given, value in parentheses is calculated using recalculated parent material that excludes Mn spikes in concentration.

Table 2. Calculated soil bulk density*

Soil Depth (cm)	Bulk Density (g cm^{-3})
0	1.40
10	1.63
20	1.70
30	1.74
40	1.76
50	1.78
60	1.79
70	1.79
80	1.80
90	1.81
100	1.81

*Values derived from fit to measured bulk density values from soil clods in MMS (Fig. 7)

Table 3

Elemental concentrations of soil core samples

Depth (cm)	Elemental Concentrations													
	LOI (%)	Al (%)	Ca (%)	Fe (%)	K (%)	Mg (%)	Mn (%)	Na (%)	P (%)	Si (%)	Ti (%)	Cr (ppm)	Zn (ppm)	Zr (ppm)
BKR														
0-10	11.61	4.09	0.07	1.96	1.23	0.23	0.25	0.42	0.04	35.38	0.60	578	56	468
10-20	8.66	4.20	0.06	1.97	1.27	0.24	0.12	0.43	0.03	36.41	0.62	368	46	476
20-30	7.08	4.53	0.06	2.26	1.33	0.27	0.11	0.44	0.03	35.80	0.61	300	66	473
30-40	7.80	4.96	0.05	2.64	1.36	0.30	0.06	0.44	0.03	35.14	0.62	167	66	446
40-50	6.75	5.22	0.06	2.81	1.37	0.33	0.05	0.44	0.02	35.61	0.66	120	66	440
50-60	8.84	5.83	0.07	3.20	1.23	0.39	0.04	0.31	0.03	32.49	0.68	86	66	363
60-70	12.92	8.04	0.10	3.93	1.30	0.62	0.01	0.32	BDL	30.11	0.50	84	66	265
80-90	**11.07**	**8.17**	**0.11**	**4.66**	**1.39**	**0.63**	**0.02**	**0.20**	**BDL**	**27.59**	**0.56**	**88**	**66**	**240**
90-100	**8.59**	**8.11**	**0.12**	**3.74**	**1.37**	**0.60**	**0.01**	**0.34**	**0.03**	**30.43**	**0.48**	**71**	**66**	**244**
100-106	**8.75**	**7.86**	**0.09**	**3.38**	**1.29**	**0.59**	**0.02**	**0.44**	**0.03**	**32.30**	**0.49**	**82**	**66**	**296**
SR														
0-10	13.18	8.00	0.44	5.30	1.98	0.70	0.10	0.40	0.09	27.25	0.55	94	99	253
10-20	12.46	8.74	0.57	5.76	2.14	0.83	0.09	0.38	0.12	26.61	0.53	89	104	227
20-30	13.00	9.64	0.63	6.18	2.52	0.94	0.06	0.29	0.10	24.84	0.47	87	97	174
30-40	**12.81**	**10.74**	**0.85**	**6.74**	**3.38**	**1.10**	**0.03**	**0.21**	**0.15**	**23.82**	**0.44**	**97**	**99**	**141**
40-50	**11.81**	**11.23**	**0.57**	**5.58**	**3.57**	**1.04**	**0.02**	**0.23**	**0.04**	**24.23**	**0.46**	**96**	**87**	**145**
50-60	**11.18**	**9.29**	**1.34**	**3.40**	**2.70**	**0.89**	**0.05**	**0.30**	**0.36**	**26.67**	**0.53**	**90**	**69**	**226**

	LOI (%)	Al (%)	Ca (%)	Fe (%)	K (%)	Mg (%)	Mn (%)	Na (%)	P (%)	Si (%)	Ti (%)	Cr (ppm)	Zn (ppm)	Zr (ppm)
LP														
0-10	18.33	8.05	0.63	4.67	1.84	0.67	0.09	0.15	0.08	25.02	0.52	140	106	220
10-20	11.27	9.62	0.46	5.42	2.10	0.75	0.06	0.16	0.06	27.71	0.58	119	99	234
20-30	10.91	9.32	0.46	5.11	2.01	0.73	0.06	0.19	0.06	27.64	0.57	107	104	233
30-40	10.33	9.64	0.40	5.16	2.08	0.71	0.05	0.18	0.06	28.39	0.61	98	103	231
40-50	11.45	9.80	0.54	5.50	2.20	0.85	0.05	0.12	0.06	27.36	0.57	100	97	220
50-60	**11.76**	**9.72**	**0.65**	**5.44**	**2.41**	**0.99**	**0.05**	**0.10**	**0.07**	**27.20**	**0.54**	**100**	**95**	**220**
60-70	**11.35**	**9.14**	**0.73**	**5.23**	**2.40**	**1.01**	**0.04**	**0.10**	**0.07**	**26.71**	**0.52**	**99**	**95**	**231**
70-80	**11.32**	**9.38**	**1.24**	**5.66**	**2.55**	**1.06**	**0.03**	**0.13**	**0.09**	**27.12**	**0.53**	**123**	**97**	**224**
WES														
Organic	9.61	5.32	0.32	2.92	1.47	0.45	0.10	0.42	0.08	31.54	0.46	71	100	351
0-14	8.49	5.32	0.30	3.06	1.45	0.44	0.10	0.41	0.07	31.04	0.45	71	105	321
14-20	7.69	5.59	0.31	3.29	1.49	0.47	0.10	0.39	0.07	30.84	0.46	69	103	313
20-26	6.66	5.76	0.31	3.24	1.52	0.48	0.10	0.43	0.06	33.02	0.48	59	95	342
26-31	5.75	5.30	0.30	3.05	1.48	0.45	0.09	0.46	0.06	33.21	0.46	63	76	452
31-41	5.87	5.59	0.30	3.09	1.56	0.47	0.09	0.45	0.06	32.50	0.47	58	92	356
41-47	6.77	6.17	0.33	3.36	1.69	0.53	0.11	0.41	0.07	31.15	0.51	68	95	321
47-53	6.50	6.18	0.38	3.41	1.68	0.56	0.10	0.41	0.07	31.72	0.50	57	104	327
53-61	5.58	5.02	0.39	2.87	1.39	0.50	0.08	0.40	0.06	33.36	0.44	52	109	361
61-69	7.15	6.89	0.55	3.68	1.81	0.69	0.11	0.41	0.07	31.80	0.56	72	134	318
69-76	6.34	5.15	0.92	3.09	1.51	0.57	0.09	0.50	0.09	32.45	0.44	51	160	284
76-82	3.84	4.71	0.24	2.52	1.32	0.40	0.06	0.37	0.06	36.97	0.48	51	49	364
82-88	4.27	5.02	0.21	2.70	1.36	0.43	0.04	0.33	0.06	34.46	0.48	60	61	361
88-95	4.54	5.58	0.20	3.26	1.55	0.49	0.04	0.32	0.05	34.14	0.48	59	42	340
95-103	4.69	5.83	0.21	3.36	1.67	0.53	0.03	0.32	0.04	33.14	0.46	61	55	318

	LOI (%)	Al (%)	Ca (%)	Fe (%)	K (%)	Mg (%)	Mn (%)	Na (%)	P (%)	Si (%)	Ti (%)	Cr (ppm)	Zn (ppm)	Zr (ppm)
103-110	4.91	5.72	0.22	3.41	1.67	0.53	0.03	0.34	0.04	33.47	0.42	65	55	286
110-115	4.61	5.60	0.24	3.59	1.62	0.53	0.03	0.37	0.04	34.26	0.40	57	60	285
115-125	4.31	5.25	0.27	3.79	1.53	0.50	0.03	0.44	0.04	34.90	0.39	57	60	320
125-132	3.38	4.41	0.27	3.21	1.37	0.41	0.02	0.48	0.04	35.58	0.37	48	48	351
132-140	3.90	4.80	0.31	3.69	1.31	0.48	0.06	0.46	0.06	34.37	0.33	48	55	330
140-152	2.42	3.94	0.27	2.68	1.14	0.39	0.06	0.44	0.05	38.23	0.24	35	29	200
152-162	2.67	3.92	0.27	2.40	1.09	0.37	0.05	0.45	0.05	38.85	0.22	33	35	214
162-171	2.43	3.51	0.30	2.53	1.00	0.35	0.05	0.44	0.05	38.36	0.20	46	35	168
171-180	1.73	3.19	0.26	1.80	0.93	0.28	0.04	0.46	0.04	40.34	0.17	23	25	163
180-193	1.90	3.14	0.31	2.20	0.90	0.31	0.04	0.44	0.05	41.01	0.19	27	31	146
193-206	1.56	2.92	0.29	1.91	0.89	0.27	0.04	0.47	0.04	40.91	0.20	24	23	175
206-217	1.60	3.09	0.33	1.84	0.92	0.27	0.04	0.52	0.05	41.39	0.18	24	28	164
CLF														
0-10	8.38	4.36	0.08	1.72	1.32	0.24	0.04	0.41	0.04	35.38	0.60	60	37	452
10-20	5.56	4.75	0.08	1.82	1.39	0.26	0.03	0.40	0.03	37.25	0.63	56	39	447
20-30	6.27	5.70	0.05	2.56	1.47	0.33	0.02	0.36	0.02	34.67	0.59	55	48	388
30-40	7.97	**6.67**	**0.03**	**3.02**	**1.49**	**0.37**	**0.02**	**0.31**	**0.03**	**32.48**	**0.58**	**63**	**73**	359
40-50	6.27	**6.83**	**0.02**	**2.70**	**1.33**	**0.38**	**0.08**	**0.40**	**0.03**	**34.37**	**0.56**	**67**	**65**	470
50-60	4.87	**5.03**	**0.01**	**1.92**	**0.86**	**0.33**	**0.07**	**0.35**	**0.02**	**37.82**	**0.38**	**40**	**66**	224
MMS														
Organic	13.68	5.84	0.26	3.96	1.40	0.46	0.07	0.25	0.07	29.50	0.56	96	84	326
0-8	10.13	6.11	0.17	3.83	1.46	0.48	0.05	0.26	0.05	31.34	0.60	87	79	347
8-17	7.87	5.93	0.12	3.34	1.45	0.45	0.04	0.28	0.05	32.23	0.60	81	73	367
17-29	7.92	7.07	0.09	3.87	1.64	0.56	0.03	0.33	0.05	31.49	0.59	78	86	340

	LOI (%)	Al (%)	Ca (%)	Fe (%)	K (%)	Mg (%)	Mn (%)	Na (%)	P (%)	Si (%)	Ti (%)	Cr (ppm)	Zn (ppm)	Zr (ppm)
29-39	8.63	8.00	0.09	4.57	1.86	0.66	0.03	0.33	0.06	28.75	0.54	79	90	296
39-45	10.61	9.30	0.10	5.37	2.14	0.77	0.03	0.25	0.06	26.40	0.52	86	94	230
45-51	9.79	9.85	0.06	6.11	2.21	0.84	0.02	0.27	0.06	25.03	0.51	91	100	194
51-57	9.54	10.58	0.08	6.21	2.45	0.91	0.02	0.18	0.06	24.80	0.52	92	107	165
57-63	9.44	10.50	0.08	10.43	2.32	0.91	0.06	0.18	0.06	22.72	0.49	87	126	143
63-69	9.54	10.96	0.10	7.01	2.59	0.97	0.03	0.19	0.07	23.62	0.51	95	121	151
69-76	9.52	10.88	0.14	6.74	2.59	0.93	0.02	0.19	0.06	23.51	0.48	95	114	143
76-83	**9.93**	**11.69**	**0.17**	**5.50**	**2.73**	**0.93**	**0.02**	**0.19**	**0.06**	**24.31**	**0.47**	**103**	**106**	**143**
83-90	**9.25**	**11.05**	**0.22**	**5.02**	**2.63**	**0.90**	**0.01**	**0.20**	**0.08**	**25.73**	**0.48**	**155**		**89**
90-101	**9.77**	**10.72**	**0.26**	**4.92**	**2.58**	**0.93**	**0.01**	**0.21**	**0.06**	**25.69**	**0.48**	**94**	**96**	**168**
118-127	11.06	9.37	0.57	4.71	2.54	1.29	0.10	0.14	0.09	25.51	0.51	94	108	168
127-138	10.39	9.80	0.63	4.91	2.57	1.33	0.09	0.09	0.11	26.25	0.53	92	94	178
138-147	10.41	9.67	0.61	5.32	2.32	1.40	0.05	0.09	0.09	24.73	0.51	104	90	164
147-156	10.53	10.10	0.58	5.73	2.26	1.45	0.05	0.16	0.09	25.41	0.52	106	114	162
156-163	9.82	10.28	0.61	5.49	2.27	1.48	0.06	0.10	0.09	25.48	0.53	100	121	162
163-172	8.73	9.87	0.65	5.84	2.09	1.30	0.09	0.19	0.09	26.05	0.53	95	91	180
172-175	1.05	8.44	0.28	5.31	1.71	0.94	0.05	0.47	0.05	29.34	0.53	66	83	245
175-179	6.15	8.27	0.23	4.27	1.75	0.90	0.04	0.54	0.05	29.60	0.53	66	93	254
VL														
0-9	8.38	5.17	0.06	2.40	1.18	0.36	0.11	0.41	0.02	34.37	0.64	68	64	402
9-15	6.33	5.48	0.09	2.61	1.23	0.39	0.08	0.40	BDL	34.37	0.62	63	54	364
15-21	6.70	6.16	0.11	2.98	1.27	0.45	0.05	0.37	BDL	32.96	0.61	60	56	352
21-25	9.41	7.36	0.13	3.74	1.42	0.57	0.04	0.36	BDL	30.04	0.56	70	74	307
25-42	11.96	8.42	0.16	4.67	1.63	0.71	0.03	0.28	BDL	27.40	0.51	77	89	232
42-48	13.74	9.30	0.22	5.45	1.93	0.84	0.02	0.19	BDL	25.30	0.48	92	88	189

	LOI (%)	Al (%)	Ca (%)	Fe (%)	K (%)	Mg (%)	Mn (%)	Na (%)	P (%)	Si (%)	Ti (%)	Cr (ppm)	Zn (ppm)	Zr (ppm)
48-53	12.73	9.77	0.26	5.81	2.18	0.90	0.02	0.14	0.03	24.54	0.47	94	93	165
53-58	13.14	9.82	0.94	5.91	3.08	1.17	0.02	0.48	0.03	24.27	0.47	95	97	147
58-63	14.33	9.81	0.29	5.88	2.23	0.91	0.02	0.14	0.04	24.36	0.47	96	95	153
63-68	11.97	10.04	0.27	5.82	2.33	0.89	0.01	0.14	0.04	24.83	0.49	97	96	152
68-74	10.87	10.23	0.24	6.43	2.41	0.91	0.01	0.15	0.05	24.24	0.51	93	112	153
74-80	**10.91**	**10.11**	**0.24**	**6.69**	**2.37**	**0.88**	**0.01**	**0.15**	**0.05**	**24.15**	**0.51**	**94**	**113**	**155**
80-88	**11.79**	**10.26**	**0.24**	**6.83**	**2.33**	**0.88**	**0.01**	**0.16**	**0.05**	**24.00**	**0.52**	**93**	**107**	**152**
88-96	**10.89**	**10.53**	**0.25**	**6.76**	**2.28**	**0.86**	**0.01**	**0.16**	**0.05**	**24.34**	**0.53**	**95**	**111**	**152**
120-128	8.69	11.06	0.50	6.73	2.44	0.86	0.05	0.17	0.14	24.57	0.55	97	141	152
128-136	8.12	11.42	1.01	6.27	2.44	0.90	0.05	0.12	0.36	24.09	0.55	98	115	151
136-144	8.23	10.93	0.97	5.91	2.30	0.85	0.04	0.11	0.35	23.43	0.52	97	99	150
144-152	8.49	11.31	0.92	5.90	2.28	0.82	0.05	0.10	0.33	23.74	0.51	103	98	148
152-162	8.62	11.25	1.09	6.87	2.42	0.82	0.09	0.17	0.38	23.50	0.51	88	119	139
162-190	8.61	12.29	0.65	8.96	2.78	1.07	0.06	0.15	0.19	26.61	0.60	99	137	156
190-202	8.02	11.45	0.56	6.86	2.60	1.01	0.05	0.12	0.08	24.00	0.53	96	132	151
PR														
0-10	19.58	8.94	0.68	5.10	2.13	0.78	0.10	0.24	0.06	23.81	0.53	139	131	220
10-20	11.91	10.64	0.75	5.19	2.49	0.91	0.07	0.22	0.06	25.22	0.59	96	133	207
20-30	10.03	10.94	0.60	6.47	2.64	0.92	0.03	0.19	0.06	25.04	0.60	88	119	194
30-40	9.84	11.18	0.50	6.01	2.68	0.94	0.03	0.19	0.06	25.18	0.60	89	138	191
40-50	**10.15**	**11.20**	**0.49**	**7.19**	**2.71**	**0.94**	**0.02**	**0.17**	**0.06**	**24.22**	**0.59**	**92**	**122**	**180**
50-60	**10.25**	**11.47**	**0.52**	**5.65**	**2.80**	**0.98**	**0.02**	**0.17**	**0.05**	**25.26**	**0.63**	**97**	**132**	**191**
60-67	**10.22**	**10.81**	**0.60**	**5.00**	**2.45**	**0.90**	**0.12**	**0.25**	**0.05**	**26.24**	**0.61**	**93**	**127**	**210**

	LOI (%)	Al (%)	Ca (%)	Fe (%)	K (%)	Mg (%)	Mn (%)	Na (%)	P (%)	Si (%)	Ti (%)	Cr (ppm)	Zn (ppm)	Zr (ppm)
ER														
0-10	10.05	9.03	0.08	4.52	2.20	0.67	0.03	0.28	0.05	27.84	0.58	81	93	284
10-20	11.42	10.09	0.06	5.22	2.42	0.75	0.02	0.24	0.06	26.75	0.59	85	101	262
IR														
0-10	8.66	4.04	0.08	1.68	1.32	0.23	0.02	0.39	0.03	35.57	0.59	59	42	452
10-20	9.34	3.90	0.08	1.74	1.25	0.22	0.02	0.37	0.02	34.10	0.57	63	40	447
20-30	9.88	4.75	0.05	2.06	1.33	0.31	0.01	0.28	0.05	32.65	0.55	64	43	418
30-40	10.09	4.95	0.06	2.39	1.39	0.31	0.02	0.36	0.02	33.37	0.56	73	51	402
40-50	**10.38**	**5.78**	**0.05**	**2.96**	**1.46**	**0.37**	**0.02**	**0.36**	**0.03**	**31.84**	**0.56**	**75**	**63**	**370**
50-60	**9.41**	**6.36**	**0.06**	**3.49**	**1.53**	**0.42**	**0.02**	**0.39**	**0.03**	**31.78**	**0.57**	**76**	**56**	**367**
60-70	**10.26**	**6.52**	**0.07**	**3.88**	**1.59**	**0.45**	**0.02**	**0.42**	**0.03**	**31.88**	**0.58**	**84**	**69**	**369**
GF														
0-13	9.59	3.81	0.30	1.61	1.44	0.25	0.09	0.44	0.05	33.49	0.54	55	49	397
13-23	6.17	4.35	0.22	1.85	1.60	0.27	0.08	0.49	0.04	36.38	0.58	58	48	406
23-33	5.61	4.86	0.22	2.30	1.66	0.33	0.06	0.49	0.02	35.68	0.58	57	45	383
33-43	6.14	5.25	0.20	2.68	1.68	0.37	0.06	0.46	0.02	34.59	0.56	64	62	357
43-53	6.76	5.22	0.20	2.67	1.62	0.38	0.06	0.45	BDL	34.23	0.57	62	48	370
53-63	8.10	6.54	0.25	3.93	1.68	0.54	0.06	0.36	0.03	32.04	0.59	70	54	307
73-83	**13.97**	**8.84**	**0.46**	**5.51**	**2.04**	**1.02**	**0.03**	**0.16**	**BDL**	**26.42**	**0.48**	**88**	**76**	**187**
83-93	**11.48**	**9.38**	**0.52**	**5.75**	**2.16**	**1.10**	**0.03**	**0.13**	**0.04**	**25.61**	**0.47**	**79**		**178**
93-103	**12.34**	**10.04**	**0.69**	**5.93**	**2.40**	**1.25**	**0.13**	**0.10**	**0.05**	**24.44**	**0.44**	**80**		**149**
103-113	13.97	9.64	0.75	5.73	2.53	1.20	0.10	0.11	0.07	24.22	0.45	91	83	149
133-143	14.09	9.21	4.17	4.75	2.63	1.03	0.05	0.12	0.05	22.81	0.47	83	90	144

Table 4. Particulate Emission Chemistry from Ferroalloy Furnaces[a]

Product	**50% FeSi**	**SiMn**	**SiMn**	**FeMn**	**HC FeCr**
Furnace Type	Open	Covered	Covered	Open	Covered
Max Size (μm)	0.75	0.75	0.75	0.75	1
Size Range	0.05-3	0.2-0.4	0.2-0.4	0.05-0.4	0.1-0.4
Element	**Concentration (Moles/100 g emitted)**				
Si	1.04-1.13	0.26	0.41	0.42	0.35
Fe		0.09	0.06	0.08	0.15
Mg		0.03	0.09	0.03	0.38
Ca			0.03	0.04	
Mn		0.44	0.45	0.47	0.04
Al		0.11	0.09	0.16	0.14
Cr				<0.31	0.39
Mn:Cr (mol: mol)				**<36:1**	**1:10**

[a] Adapted from U.S. EPA (1974) and U.S. EPA (1984)

Table 5

Mass transfer coefficients using Zr as immobile element ($\tau_{Zr,j}$) and average of bottom 3 samples nearest 1 m as parent.

Depth (cm)	$\tau_{Zr,j}$ values											
	Al	Ca	Fe	K	Mg	Mn	Na	P	Si	Ti	Cr	Zn
BKR												
0-10	-0.72	-0.64	-0.72	-0.49	-0.78	8.68	-0.27	-0.06	-0.35	-0.34	3.00	-0.97
10-20	-0.71	-0.68	-0.73	-0.48	-0.78	3.68	-0.28	-0.38	-0.34	-0.34	1.50	-0.91
20-30	-0.69	-0.68	-0.68	-0.46	-0.75	3.24	-0.26	-0.29	-0.35	-0.35	1.05	-0.85
30-40	-0.64	-0.71	-0.61	-0.41	-0.71	1.43	-0.21	-0.36	-0.32	-0.29	0.21	-0.78
40-50	-0.62	-0.70	-0.58	-0.40	-0.68	0.92	-0.19	-0.45	-0.30	-0.24	-0.12	-0.72
50-60	-0.48	-0.54	-0.41	-0.35	-0.54	0.77	-0.30	-0.29	-0.23	-0.05	-0.24	-0.58
60-70	-0.02	-0.12	-0.02	-0.05	0.01	-0.22	-0.02	-0.55	-0.02	-0.04	0.02	-0.32
80-90	**0.10**	**0.12**	**0.29**	**0.12**	**0.12**	**0.18**	**-0.34**	**-0.09**	**-0.01**	**0.19**	**0.19**	**-0.02**
90-100	**0.07**	**0.17**	**0.01**	**0.08**	**0.05**	**-0.12**	**0.11**	**0.26**	**0.08**	**0.01**	**-0.06**	**0.07**
100-106	**-0.14**	**-0.24**	**-0.24**	**-0.16**	**-0.14**	**-0.05**	**0.18**	**-0.14**	**-0.06**	**-0.16**	**-0.10**	**-0.04**
SR												
0-10	-0.48	-0.68	-0.32	-0.58	-0.53	0.98	0.08	-0.67	-0.26	-0.22	-0.33	-0.21
10-20	-0.37	-0.53	-0.17	-0.50	-0.38	1.04	0.17	-0.49	-0.20	-0.15	-0.29	-0.08
20-30	-0.09	-0.32	0.16	-0.23	-0.09	0.73	0.17	-0.47	-0.02	-0.02	-0.09	0.12
30-40	**0.25**	**0.12**	**0.55**	**0.27**	**0.32**	**-0.04**	**0.05**	**0.00**	**0.16**	**0.12**	**0.25**	**0.41**
40-50	**0.27**	**-0.27**	**0.25**	**0.31**	**0.21**	**-0.33**	**0.08**	**-0.75**	**0.15**	**0.14**	**0.20**	**0.20**
50-60	**-0.33**	**0.10**	**-0.51**	**-0.37**	**-0.34**	**0.24**	**-0.09**	**0.48**	**-0.19**	**-0.16**	**-0.28**	**-0.39**
LP												
0-10	-0.12	-0.26	-0.12	-0.23	-0.32	1.42	0.39	0.05	-0.05	0.01	0.33	0.13

Depth (cm)	$\tau_{Zr,j}$ values											
	Al	Ca	Fe	K	Mg	Mn	Na	P	Si	Ti	Cr	Zn
10-20	-0.02	-0.50	-0.05	-0.18	-0.29	0.42	0.41	-0.25	-0.02	0.04	0.06	-0.01
20-30	-0.05	-0.50	-0.10	-0.21	-0.30	0.34	0.67	-0.29	-0.01	0.03	-0.04	0.04
30-40	0.00	-0.55	-0.08	-0.17	-0.32	0.33	0.60	-0.20	0.02	0.12	-0.11	0.04
40-50	0.06	-0.38	0.03	-0.08	-0.14	0.26	0.08	-0.17	0.03	0.09	-0.05	0.03
50-60	**0.05**	**-0.24**	**0.02**	**0.00**	**-0.01**	**0.28**	**-0.07**	**-0.06**	**0.03**	**0.03**	**-0.05**	**0.01**
60-70	**-0.05**	**-0.18**	**-0.06**	**-0.05**	**-0.04**	**-0.02**	**-0.13**	**-0.06**	**-0.04**	**-0.04**	**-0.10**	**-0.03**
70-80	**0.00**	**0.43**	**0.05**	**0.05**	**0.05**	**-0.25**	**0.20**	**0.12**	**0.01**	**0.01**	**0.15**	**0.02**
CLF												
0-10	-0.46	3.08	-0.43	-0.08	-0.49	-0.61	-0.17	0.07	-0.25	-0.02	-0.14	-0.57
10-20	-0.40	3.27	-0.39	-0.01	-0.44	-0.65	-0.17	-0.04	-0.20	0.03	-0.18	-0.54
20-30	-0.17	2.21	-0.01	0.20	-0.17	-0.76	-0.16	-0.24	-0.14	0.13	-0.08	-0.34
30-40	**0.04**	**1.02**	**0.26**	**0.32**	**0.01**	**-0.73**	**-0.21**	**0.12**	**-0.13**	**0.19**	**0.14**	**0.08**
40-50	**-0.18**	**0.13**	**-0.14**	**-0.10**	**-0.21**	**-0.26**	**-0.21**	**-0.15**	**-0.30**	**-0.12**	**-0.07**	**-0.27**
50-60	**0.26**	**-0.28**	**0.29**	**0.22**	**0.44**	**0.54**	**0.44**	**0.31**	**0.62**	**0.25**	**0.15**	**0.57**
MMS												
Organic	-0.75	-0.42	-0.63	-0.75	-0.76	1.36	-0.40	-0.52	-0.44	-0.44	-0.52	-0.60
0-8	-0.75	-0.65	-0.67	-0.75	-0.77	0.47	-0.42	-0.62	-0.44	-0.44	-0.59	-0.65
8-17	-0.77	-0.77	-0.72	-0.77	-0.79	0.08	-0.41	-0.68	-0.46	-0.47	-0.64	-0.69
17-29	-0.71	-0.81	-0.66	-0.72	-0.72	-0.19	-0.26	-0.62	-0.43	-0.43	-0.63	-0.61
29-39	-0.62	-0.79	-0.53	-0.63	-0.62	-0.08	-0.14	-0.48	-0.40	-0.40	-0.56	-0.54
39-45	-0.44	-0.68	-0.30	-0.45	-0.44	0.16	-0.15	-0.43	-0.29	-0.26	-0.39	-0.37
45-51	-0.29	-0.76	-0.05	-0.33	-0.27	0.30	0.07	-0.30	-0.21	-0.14	-0.23	-0.21
51-57	-0.11	-0.63	0.14	-0.13	-0.07	0.46	-0.16	-0.19	-0.07	0.02	-0.09	0.00

57-63	0.02	-0.59	1.20	-0.05	0.07	3.48	-0.02	0.01	-0.02	0.12	-0.01	0.35
63-69	0.01	-0.52	0.40	0.01	0.08	0.84	-0.04	0.03	-0.04	0.10	0.03	0.24
Depth (cm)	$\tau_{Zr,j}$ values											
	Al	Ca	Fe	K	Mg	Mn	Na	P	Si	Ti	Cr	Zn
69-76	0.06	-0.32	0.42	0.06	0.10	0.76	0.01	0.07	0.01	0.10	0.08	0.22
76-83	**0.14**	**-0.12**	**0.16**	**0.12**	**0.10**	**0.26**	**0.02**	**0.07**	**0.05**	**0.09**	**0.17**	**0.14**
83-90	**-0.01**	**0.00**	**-0.02**	**-0.01**	**-0.02**	**-0.06**	**0.01**	**0.17**	**0.02**	**0.00**	**-0.06**	
90-101	**-0.11**	**0.10**	**-0.12**	**-0.10**	**-0.07**	**-0.17**	**-0.03**	**-0.22**	**-0.06**	**-0.07**	**-0.09**	**-0.12**
VL												
0-9	-0.81	-0.90	-0.86	-0.81	-0.84	2.39	0.00	-0.81	-0.46	-0.53	-0.72	-0.78
9-15	-0.78	-0.84	-0.84	-0.78	-0.81	1.72	0.07	-0.85	-0.40	-0.50	-0.72	-0.79
15-21	-0.74	-0.81	-0.81	-0.76	-0.78	0.85	0.04	-0.87	-0.41	-0.49	-0.72	-0.78
21-25	-0.64	-0.74	-0.72	-0.70	-0.67	0.80	0.16	-0.83	-0.38	-0.46	-0.63	-0.67
25-42	-0.46	-0.56	-0.54	-0.54	-0.46	0.70	0.17	-0.71	-0.25	-0.35	-0.46	-0.47
42-48	-0.27	-0.27	-0.35	-0.33	-0.22	0.58	-0.02	-0.65	-0.15	-0.25	-0.20	-0.35
48-53	-0.12	-0.02	-0.20	-0.13	-0.05	0.33	-0.16	-0.39	-0.06	-0.15	-0.07	-0.22
53-58	-0.01	2.97	-0.09	0.37	0.39	0.82	2.20	-0.29	0.04	-0.06	0.06	-0.09
58-63	-0.05	0.19	-0.13	-0.04	0.04	0.41	-0.12	-0.11	0.01	-0.09	0.02	-0.14
63-68	-0.02	0.11	-0.14	0.01	0.02	0.20	-0.08	-0.11	0.03	-0.05	0.04	-0.13
68-74	-0.01	0.00	-0.05	0.03	0.04	-0.09	-0.03	-0.03	0.00	-0.01	-0.01	0.01
74-80	**-0.03**	**-0.03**	**-0.02**	**0.00**	**-0.01**	**-0.04**	**-0.04**	**-0.09**	**-0.01**	**-0.04**	**-0.02**	**0.01**
80-88	**0.00**	**-0.01**	**0.02**	**0.01**	**0.01**	**0.03**	**0.03**	**0.02**	**0.00**	**0.01**	**0.00**	**-0.02**
88-96	**0.03**	**0.03**	**0.01**	**-0.01**	**-0.01**	**0.00**	**0.01**	**0.07**	**0.01**	**0.03**	**0.02**	**0.01**
PR												
0-10	-0.29	0.12	-0.24	-0.29	-0.27	0.62	0.08	0.01	-0.17	-0.23	0.30	-0.09
10-20	-0.11	0.31	-0.18	-0.12	-0.09	0.08	0.02	0.04	-0.06	-0.09	-0.04	-0.02
20-30	-0.02	0.11	0.09	-0.01	-0.03	-0.40	-0.06	0.20	-0.01	-0.02	-0.07	-0.07

30-40	0.02	-0.05	0.03	0.03	0.02	-0.53	-0.04	0.19	0.01	0.00	-0.04	0.10
40-50	**0.08**	**-0.02**	**0.30**	**0.10**	**0.07**	**-0.56**	**-0.09**	**0.21**	**0.03**	**0.04**	**0.06**	**0.03**
50-60	**0.04**	**-0.02**	**-0.04**	**0.07**	**0.06**	**-0.58**	**-0.11**	**-0.03**	**0.01**	**0.05**	**0.04**	**0.05**
60-67	**-0.11**	**0.04**	**-0.22**	**-0.15**	**-0.12**	**1.00**	**0.17**	**-0.15**	**-0.04**	**-0.08**	**-0.09**	**-0.08**
Depth (cm)	$\tau_{Zr,j}$ values											
	Al	Ca	Fe	K	Mg	Mn	Na	P	Si	Ti	Cr	Zn
IR												
0-10	-0.47	0.11	-0.60	-0.30	-0.55	-0.19	-0.19	-0.11	-0.09	-0.15	-0.39	-0.45
10-20	-0.48	0.16	-0.58	-0.32	-0.56	-0.07	-0.21	-0.27	-0.12	-0.18	-0.34	-0.47
20-30	-0.33	-0.29	-0.47	-0.23	-0.35	-0.37	-0.36	0.51	-0.09	-0.15	-0.28	-0.40
30-40	-0.27	-0.12	-0.36	-0.17	-0.33	-0.13	-0.16	-0.18	-0.04	-0.09	-0.15	-0.26
40-50	**-0.07**	**-0.16**	**-0.14**	**-0.05**	**-0.11**	**-0.04**	**-0.08**	**-0.01**	**0.00**	**-0.02**	**-0.05**	**0.00**
50-60	**0.03**	**-0.05**	**0.02**	**0.01**	**0.02**	**0.03**	**0.00**	**0.03**	**0.00**	**0.01**	**-0.02**	**-0.10**
60-70	**0.05**	**0.20**	**0.13**	**0.04**	**0.09**	**0.01**	**0.08**	**-0.02**	**0.00**	**0.02**	**0.07**	**0.10**
GF												
0-13	-0.83	-0.77	-0.88	-0.72	-0.91	-0.36	0.46	-0.37	-0.43	-0.50	-0.71	-0.72
13-23	-0.81	-0.83	-0.86	-0.69	-0.90	-0.48	0.57	-0.55	-0.40	-0.48	-0.70	-0.73
23-33	-0.77	-0.83	-0.82	-0.66	-0.87	-0.61	0.67	-0.68	-0.37	-0.44	-0.69	-0.74
33-43	-0.73	-0.83	-0.78	-0.63	-0.84	-0.57	0.69	-0.66	-0.35	-0.42	-0.63	-0.61
43-53	-0.74	-0.83	-0.78	-0.66	-0.84	-0.60	0.60	-0.75	-0.38	-0.44	-0.65	-0.71
53-63	-0.61	-0.75	-0.62	-0.57	-0.73	-0.44	0.51	-0.52	-0.30	-0.29	-0.53	-0.60
73-83	**-0.14**	**-0.24**	**-0.12**	**-0.15**	**-0.17**	**-0.57**	**0.11**	**-0.47**	**-0.05**	**-0.06**	**-0.02**	**-0.08**
83-93	**-0.04**	**-0.10**	**-0.03**	**-0.05**	**-0.06**	**-0.61**	**-0.02**	**0.03**	**-0.03**	**-0.02**	**-0.08**	
93-103	**0.23**	**0.43**	**0.19**	**0.25**	**0.28**	**1.46**	**-0.12**	**0.55**	**0.10**	**0.10**	**0.13**	

References

Amundson R., and Jenny H. (1991) The place of humans in the state factor theory of ecosystems and their soils. *Soil Science* **151**, 99-109.

Agency for Toxic Substances and Disease Registry (2008) Manganese, Toxicological Profile. Department of Health and Human Services.

Agency for Toxic Substances and Disease Registry.http://www.atsdr.cdc.gov/sites/washington_marietta/index.html; **2009.**

Anderson S.P., Dietrich W.E., Brimhall G.H. (2002) Weathering profiles, mass-balance analysis, and rates of solute loss: Linkages between weathering and erosion in a small, steep catchment. *Geological Society of America Bulletin* **114**, 1143-1158.

Bartlett R. and James B. (1979) Chromium behavior in soils III: oxidation. *Journal of Environmental Quality* **8**, 31-35.

Beerbower J.R. (1961) Origin of cyclothems in the Dunkard Group (Upper Pennsylvanian-Lower Permian) in Pennsylvania, West Virginia, and Ohio. *Geological Society of America Bulletin* **72**, 1029-1050.

Bouchard M.F., Sauve S., Barbeau B., Legrand M., Brodeur M., Bouffard T., Limoges E., Bellinger D.C., Mergler, D. (2011) Intellectual impairment in school-age children exposed to manganese from drinking water. *Environmental Health Perspectives* **119**, 138-143.

Boudissa S.M., Lambert J., Muller C., Kennedy G., Gareau L., Zayed J. (2006) Manganese concentrations in the soil and air in the vicinity of a closed manganese alloy production plant. *Sci. Total. Environ.* **361**, 67-72.

Brantley S.L. and Lebedeva M. (2011) Learning to read the chemistry of regolith to understand the critical zone. *Annual Review of Earth and Planetary Sciences* **39**, 387-416.

Brantley S.L. and White A.F. (2009) Approaches to modeling weathered regolith. *Review in Mineralogy and Geochemistry* **70**, 435-484.
Brimhall G.H. (1992) Deformational mass transport and invasive process in soil evolution. *Science* **255**, 695-702.

Brimhall G.H., Dietrich W.E. (1987) Constitutive mass balance relations between chemical composition, volume, density, porosity, and strain in metasomatic hydrochemical systems: results on weathering and pedogenesis. *Geochem. Cosmochim. Acta* **51**, 567-587.

Cole K.L., Engstrom D.R., Futyma R.P., Stottlemyer R. (1990) Past atmospheric deposition of metals in Northern Indiana measured in a peat core from Cowles Bog. *Environmental Science and Technology* **24**, 543-549.

Collins H.R., Smith B.E. (1977) *Geology and Mineral Resources of Washington County, Ohio*. Ohio Division of Geological Survey, Columbus.

Corathers L.A. (2009) Minerals Yearbook: Manganese. US Geological Survey.

Cornu S., Lucas Y., Lebon E., Ambrosi J.P., Luizao F., Rouiller J., Bonnay M., Neal C. (1999) Evidence of titanium mobility in soil profiles, Manaus, central Amazonia. *Geoderma* **91**, 281-295.

Crutzen P.J. (2002) Geology of mankind. *Nature* **415**, 23.

Dere A.L., White T.S., April R.H., Reynolds B., Miller T.E., Knapp E.P., McKay L.D., Brantley S.L. (in review) Climate dependence of feldspar wweathering in shale soils along a latitudinal gradient. *Submitted to Geochimichia et Cosmochimica Acta.*

Duce R.A., Hoffman G.L., Ray B.J., Fletcher I.S., Wallace G.T., Fasching J.L. Sr., Pitrowicz R., Walsh P.R., Hoffman E.J., Miller J.M., Heffter J.L. Trace metals in the marine atmosphere: sources and fluxes. In *Marine Pollutant Transfer* (Edited by Windom and Duce), pp. 77-119. Heath, Lexington, MA, U.S.A.; **1976.**

Dudal R. (2005) The sixth factor of soil formation. *Eurasian Soil Science* **38**, S60-S65.

Eary L.E., and Ral D. (1987) Kinetics of chromium (III) oxidation to chromium (VI) by reaction with manganese dioxide. *Environmental Science and Technology* **21,** 1187-1193.

Egli M., Fitze P. (2000) Formulation of pedogenic mass balance based on immobile elements: a revision. *Soil Sci.* **165**, 437–443.

Esser K.B., Helmke P.A., Bockheim J.G. (1991) Heavy metals in the environment: Trace element contamination of soils in the Indiana Dunes. *Journal of Environmental Quality* **20**, 492-496.

Filippelli G.M. and Laidlaw M.A. (2010) The elephant in the playground: confronting lead-contaminated soils as an important source of lead burdens to urban populations. *Perspectives in Biology and Medicine* **53**, 31-45.

Frumkin H. and Solomon G.S. (1997) Manganese in the U.S. gasoline supply. *American Journal of Industrial Medicine* **31**, 107-115.

Gallon C., Tessier A., Gobeil C., Beaudin L. (2005) Sources and chronology of atmospheric lead deposition to a Canadian Shield lake: Inferences from Pb isotopes and PAH profiles. *Geochimica et Cosmochimica* **69**, 3199-3210.

Galloway J.N., Thornton J.D., Norton S.A. Volchok H.L. (1982) Trace metals in atmospheric deposition: a review and assessment. *Atmospheric Environment* **16**, 1677-1700.

Gardner L.R. (1980) Mobilization of Al and Ti during weathering – isovolumetric geochemical evidence. *Chemical Geology* **30**, 151-165.

Haynes E.N., Heckel P., Ryan P., Roda S., Leung Y.K., Sebastian K., Succop P. (2010) Environmental manganese exposure in residents living near a ferromanganese refinery in Southeast Ohio: A pilot study. *NeuroToxicology* **31**, 468-474.

Herndon E.M., Jin L., Brantley S.L. (2011) Soils reveal widespread manganese enrichment from industrial inputs. *Environ. Sci. Technol.* **45**, 241-247.

Jin L.J., Ravella R., Ketchum B., Bierman P.R., Heaney P., White T., Brantley S.L. (2010) Mineral weathering and elemental transport during hillslope evolution at the Susquehanna/Shale Hills Critical Zone Observatory. *Geochimica et Cosmochimica Acta* **74**, 3669-3691.

Jones, T.S. Manganese material flow patterns. Bureau of Mines Information Circular 9399 US Department of the Interior; **1994**.

Kurtz A.C., Derry L.A., Chadwick O.A., Alfano M.J. (2000) Refractory element mobility in volcanic soils. *Geology* **28**, 683-686.

Lin H. (2006) Temporal stability of soil moisture spatial pattern and subsurface preferential flow pathways in the Shale Hills catchment. *Vadose Zone Journal* **5**, 317-340.

Loranger S. and Zayed J. (1994) Manganese and lead concentrations in ambient air and emission rates from unleaded and leaded gasoline between 1981 and 1992 in Canada: A comparative study. *Atmospheric Environment* **28**, 1645-1651.

Martin W.D. (1998) *Geology of the Dunkard Group (Upper Pennsylvanian-Lower Permian) in Ohio, West Virginia, and Pennsylvania.* Ohio Division of Geological Survey, Columbus.

Mergler D., Baldwin M., Belanger S., Larribe F., Beuter A., Bowler R., Panisset M., Edwards R., Geoffrey A., Sassine M., Hudnell K. (1999) Manganese neurotoxicity, a continuum of dysfunction: results from a community based study. *NeuroToxicology* **20**, 327-342.

McBride M.B. *Environmental Chemistry of Soils.* Oxford University Press: New York, U.S.A.; 1994.

Miller W.P, McFee W.W., Kelly J.M. (1983) Mobility and retention of heavy metals in sandy soils. *Journal of Environmental Quality* **12**, 579-584.

Moore F.L. Letter from F.L. Moore, Elkem Metals Co., Marietta, OH to L.S. Erdreich, Environmental Criteria and Assessment Office, U.S. EPA, Cincinnati, OH, 1983.

National Oceanographic and Atmospheric Administration (NOAA) (2013a) Quality-controlled local climatological data. U.S. Department of Commerce, National Oceanic and Atmospheric Administration, National Environmental Satellite Data and Information Service, National Climatic Data Center. http://cdo.ncdc.noaa.gov/qclcd/

National Oceanographic and Atmospheric Administration (NOAA) (2013b) Advanced hydrologic prediction service observed precipitation. U.S. Department of Commerce, National Oceanic and Atmospheric Administration, National Weather Service. http://water.weather.gov/precip/

Neaman A., Chorover J., Brantley S.L. (2006) Effects of organic ligands on granite dissolution in batch experiments at pH 6. *American Journal of Science* **306**, 451-473.

Nriagu J.O. (1989) A global assessment of natural metal sources of atmospheric trace metals. *Nature* **338**, 47-49.

Nriagu J.O. and Pacyna J.M. (1988) Quantitative assessment of worldwide contamination of air, water and soils by trace metals. *Nature* **333**, 134-139.

Parker G.R., McFee W.W., Kelly J.M. (1978) Metal distribution in forested ecosystems in urban and rural northwestern Indiana. *Journal of Environmental Quality* **7**, 337-342.

Perkins S.M., Filippelli G.M., Souch C.J. (2000) Airborne trace metal contamination of wetland sediments at Indiana Dunes National Lakeshore. *Water, Air, and Soil Pollution* **122**, 231-260.

Person R.A. (1971) Control of emissions from ferroalloy furnace processing. *Journal of Metals*, 17-29.

Pietz R.I., Vetter R.J., Masarik D., McFee W.W. (1978) Zinc and cadmium contents of agricultural soils and corn in Northwestern Indiana. *Journal of Environmental Quality* **7**, 381-385.

Post J.E. (1999) Manganese oxide minerals: Crystal structures and economic and environmental significance. *Proceedings Natl. Acad. Sci. USA* **96**, 3447-3454.

Ramesam V. (1979) Chemistry and mineralogy of <2µm size fraction of non-marine cyclothems, Dunkard Group, Upper Pennsylvanian-Lower Permian, in Ohio, U.S.A. *Journal of the Geological Society of India* **20**, 548-558.

Reimann C., Englmaier B., Flem B., Gough L., Lamothe P., Nordgulen O., Smith D. (2009) Geochemical gradients in soil O-horizon samples from southern Norway. *Applied Geochemistry* **24**, 62-76.

Roels H., Meiers G., Delos M., Ortega I., Lauwerys R., Buchet J.R., Lison D. (1997) Influence of the route of administration and the chemical form ($MnCl_2$, MnO_2) on the absorption and cerebral distribution of manganese in rats. *Archives of Toxicology* **71**, 223-230.

Schroeder W.H., Dobson M., Kane D.M., Johnson N.D. (1987) Toxic trace elements associated with airborne particulate matter: a review. *Journal of Air Pollution Control Association* **37**, 1267-1285.

Seinfeld J.H. (1986) *Atmospheric Chemistry and Physics of Air Pollution.* John Wiley and Sons, New York.

Shacklette H.T., Boerngen J.G. (1984) Element concentrations in soils and other surficial materials of the conterminous United States. U.S. Geol Survey Professional Paper 1270. Washington, DC: U.S. Gov. Print Office.

Shen R., Zhang G., Dell'Amico M., Brown P., Ostrovski O. (2005) Characterisation of manganese furnace dust and zinc balance in production of manganese alloys. *ISIJ international* **9,** 1248-1254.

Siccama T.S., Smith W.H. (1978) Lead accumulation in a northern hardwood forest. *Environmental Science and Technology* **12**, 593-594.

Siccama T.S., Smith W.H. (1980) Changes in lead, zinc, copper, dry weight, and organic matter content of the forest floor of white pine stands in Central Massachusetts over 16 years. *Environmental Science and Technology* **14**, 54-56.

Soil Survey Staff, Natural Resources Conservation Service, United States Department of Agriculture. Web Soil Survey. Available online at http://websoilsurvey.nrcs.usda.gov/. Accessed [10/1/2012].

Suhr N.H., Ingamells, C.O. (1966) Solution technique for analysis of silicates. *Analytical Chemistry* **38**, 730-734.

Sykes R.I., Parker S.F., Henn D.S. (2004) SCIPUFF Version 2.1. Technical Documentation, Titan/ARAP Report No. 728.

Tebo B.M., Bargar J.R., Clement B.G., Dick G.J., Murray K.J., Parker D., Verity R., Webb S.M. (2004) Biogenic manganese oxides: properties and mechanisms of formation. *Annu. Rev. Earth Planet. Sci.* **32**, 287-328.

U.S. Department of Health, Education and Welfare (1970) *Kanawha Valley Air Pollution Study*. National Air Pollution Control Administration Publication No. APTD 70-1, Raleigh.

U.S. Environmental Protection Agency (1974) *Engineering and Cost Study of the Ferroalloy Industry*. Report No. EPA-450/2-74-008, Triangle Park.

U.S. Environmental Protection Agency (1977) *National trends in trace metals in ambient air: 1965-1974, Office of Air Quality Planning and Standards.* Report No. EPA-450/1-77-003, Triangle Park.

U.S. Environmental Protection Agency (1984a) *Health Assessment Document for Manganese: Final Report*. Report No. EPA-600/8-83-013f.

U.S. Environmental Protection Agency (1984b) *Locating and Estimating Air Emissions from Sources of Chromium.* Report No. EPA-450/4-84-007g, Triangle Park.

U.S. Environmental Protection Agency (1985) *Locating and Estimating Air Emissions from Sources of Manganese.* Report No. EPA-450/4-84-007h, Triangle Park.

U.S. Environmental Protection Agency (2008) *Laser Ablation and Inductively Coupled Plasma Mass Spectrometry Analysis of Glass Fiber Filters Collected at Multiple Locations in the Marietta, Ohio Area from April to October 2007.* National Enforcement Investigations Center, Report number VP0591E04, Washington D.C.

U.S. Environmental Protection Agency (2009) *Scanning Electron Microscopy of HiVol Filters Collected in 2007: Marietta, Ohio.* National Enforcement Investigations Center, Report number VP0591, Washington D.C.

U.S. Environmental Protection Agency (2010). *School Air Toxics Initiative: The Ohio Valley Educational Center (Marietta, OH), Warren Elementary School (Marietta, OH), and Neale Elementary School (Marietta, OH),* accessed 5/23/2013 at http://www.epa.gov/air/sat/pdfs/MariettaTechReport.pdf.

U.S. Environmental Protection Agency Toxic Release Inventory, http://www.epa.gov/triexplorer/; 2010

U.S. Geological Survey. Manganese statistics, *in* Kelly, T.D., and Matos, G.R., comps, Historical statistics for mineral and material commodities in the United States: U.S. Geological Survey Data Series 140, http://pubs.usgs.gov/ds/2005/140/; 2013.

Wasserman G.A., Liu X., Parvez F., Factor-Litvak P., Ahsan H., Levy D., Kline J., van Geen, A., Mey J., Slavkovich V., Siddique A.B., Islam T., Graziano J.H. (2011) Arsenic and manganese exposure and children's intellectual function. *NeuroToxicology* **32**, 450-457.

Wyngaard J.C. (2010) *Turbulence in the Atmosphere*. Cambridge University Press, New York.

Appendix A. Soil Characteristics

Sample	Mn Conc. (wt. %)	Hue	Value	Chroma	Texture and Observations
BKR					
0-10	0.25	2.5 YR	6	3	Silt Loam
10-20	0.12	2.5 YR	7	4	Silt Loam
20-30	0.11	2.5 YR	7	4	Silty Clay Loam
30-40	0.06	2.5 YR	7	4	Silty Clay Loam
40-50	0.05	2.5 YR	7	4	Silty Clay Loam
50-60	0.04	2.5 YR	7	6	Silty Clay Loam
60-70	0.01	10 YR	7	6	Gravelly Silty Clay
80-90	0.02	10 YR	7	6	Gravelly Clay
90-100	0.01	10 YR	7	4	Gravelly Clay
100-106	0.02	10 YR	7	6	Gravelly Clay
SR					
0-10	0.10	10 YR	6	4	Gravelly Clay Loam
10-20	0.09	10 YR	6	4	Gravelly Loam
20-30	0.06	10 YR	6	4	Gravelly Loam
30-40	0.03	2.5 Y	7	4	Clay Loam
40-50	0.02	2.5 Y	7	3	Clay Loam with flat rocks (10%)
50-60	0.05	2.5 Y	7	3	Clay Loam with flat rocks (10%)
LP					
0-10	0.09	7.5 YR	5	4	Silty Clay Loam
10-20	0.06	7.5 YR	6	4	Silty Clay Loam
20-30	0.06	7.5 YR	6	4	Silty Clay Loam

30-40	0.05	7.5 YR	6	4	Silty Clay Loam
40-50	0.05	7.5 YR	6	4	Silty Clay Loam
Sample	**Mn Conc. (wt. %)**	**Hue**	**Value**	**Chroma**	**Texture and Observations**
50-60	0.05	7.5 YR	6	4	Silty Clay Loam
60-70	0.04	2.5 YR	6	4	Silty Clay Loam
70-80	0.03	2.5 YR	5	6	Silty Clay Loam
CLF					
0-10	0.04	10 YR	7	2	Silt Loam
10-20	0.03	10 YR	7	4	Silt Loam
20-30	0.02	10 YR	7	4	Loam
30-40	0.02	7.5 YR	7	6	Silt Loam
40-50	0.08	10 YR	6	4	Loam
50-60	0.07	10 YR	7	4	Sandy Loam, Dark coatings on peds, Increase in mica
MMS					
Organic	0.07	7.5 YR	6	3	Clay Loam
0-8	0.05	7.5 YR	6	3	Silty Clay Loam
8-17	0.04	7.5 YR	6	3	Silty Clay Loam
17-29	0.03	7.5 YR	6	3	Silt Loam
29-39	0.03	5 YR	6	6	Silty Clay Loam
39-45	0.03	5 YR	6	6	Silty Clay Loam
45-51	0.02	5 YR	5	6	Silty Clay Loam, Some clay films, Red and white peds
51-57	0.02	5 YR	5	6	Silty Clay Loam, Some clay films
57-63	0.06	5 YR	5	6	Silty Clay Loam, Clay films
63-69	0.03	5 YR	5	6	Silty Clay Loam
69-76	0.02	5 YR	5	6	Silty Clay Loam, Clay films, Red and white peds
76-83	0.02	5 YR	6	6	Silty Clay Loam

83-90	0.01	7.5 YR	6	4	Silty Clay Loam
90-101	0.01	7.5 YR	6	4	Silty Clay Loam, Red and white peds

Sample	Mn Conc. (wt. %)	Hue	Value	Chroma	Texture and Observations
118-127	0.10	5 YR	6	4	-
127-138	0.09	5 YR	6	4	-
138-147	0.05	2.5 YR	5	6	-
147-156	0.05	2.5 YR	5	6	-
156-163	0.06	2.5 YR	5	6	-
163-172	0.09	2.5 YR	5	6	-
172-175	0.05	5 YR	4	4	-
175-179	0.04	5 YR	5	4	-
VL					
0-9	0.11	10 YR	6	4	Silty Clay Loam
9-15	0.08	7.5 YR	7	4	Silty Clay Loam
15-21	0.05	7.5 YR	6	4	Silty Clay Loam
21-25	0.04	7.5 YR	6	6	Silty Clay Loam
25-42	0.03	5 YR	5	6	Silty Clay Loam
42-48	0.02	5 YR	6	6	Silty Clay Loam
48-53	0.02	5 YR	6	6	Silty Clay Loam
53-58	0.02	5 YR	5	6	Silty Clay Loam
58-63	0.02	5 YR	5	6	Silty Clay Loam
63-68	0.01	5 YR	5	6	Silty Clay Loam
68-74	0.01	2.5 YR	5	6	Silty Clay Loam
74-80	0.01	2.5 YR	5	6	Silty Clay Loam
80-88	0.01	2.5 YR	4	6	Silty Clay Loam
88-96	0.01	2.5 YR	5	6	Silty Clay Loam
120-128	0.05	2.5 YR	5	6	-

128-136	0.05	2.5 YR	5	6	-
136-144	0.04	2.5 YR	5	6	-
Sample	**Mn Conc. (wt. %)**	**Hue**	**Value**	**Chroma**	**Texture and Observations**
144-152	0.05	2.5 YR	5	6	-
152-162	0.09	5 YR	5	6	-
162-190	0.04	5 YR	4	6	-
190-202	0.05	5 YR	4	6	-
PR					
0-10	0.10	7.5 YR	5	4	Loam
10-20	0.07	10 YR	6	4	Loam
20-30	0.03	5 YR	5	6	Loam
30-40	0.03	5 YR	5	6	Clay Loam
40-50	0.02	5 YR	5	6	Clay Loam
50-60	0.02	7.5 YR	6	4	Loam
60-67	0.12	2.5 YR	7	4	Clay Loam
IR					
0-10	0.02	2.5 Y	7	3	Silty Clay Loam
10-20	0.02	2.5 Y	7	4	Silty Clay Loam
20-30	0.01	2.5 Y	7	4	Silty Clay Loam
30-40	0.02	2.5 Y	7	4	Silty Clay Loam
40-50	0.02	10 YR	6	6	Silty Clay Loam
50-60	0.02	10 YR	7	6	Silty Clay Loam
60-70	0.02	10 YR	7	6	Silty Clay Loam
GF					
0-13	0.09	2.5 Y	6	3	Silt Loam

13-23	0.08	2.5 Y	7	4	Silt Loam
23-33	0.06	10 YR	7	6	Silt Loam
Sample	**Mn Conc. (wt. %)**	**Hue**	**Value**	**Chroma**	**Texture and Observations**
33-43	0.06	10 YR	7	6	Silt Loam
43-53	0.06	10 YR	7	6	Silty Clay Loam
53-63	0.06	10 YR	7	6	Silty Clay loam
73-83	0.03	7.5 YR	6	6	Silty Clay
83-93	0.03	7.5 YR	6	6	Silty Clay
93-103	0.13	5 YR	6	6	Silty Clay
103-113	0.10	5 YR	6	6	-
133-143	0.05	2.5 Y	7	4	-

Appendix B. Element-element ratios on a mass basis

Depth (cm)				
BKR	**Mn/Al**	**Mn/Fe**	**Mn/Cr**	**Mn/Zn**
0-10	0.060	0.127	4.284	44.354
10-20	0.029	0.062	3.311	26.536
20-30	0.024	0.049	3.659	16.679
30-40	0.012	0.022	3.555	9.013
40-50	0.009	0.016	3.866	7.042
50-60	0.006	0.011	4.096	5.324
60-70	0.001	0.003	1.343	1.712
80-90	0.002	0.003	1.749	2.347
90-100	0.001	0.003	1.662	1.794
100-106	0.002	0.005	1.883	2.347
SR				
0-10	0.012	0.018	10.191	9.622
10-20	0.010	0.015	9.887	8.453
20-30	0.006	0.009	6.580	5.888
30-40	0.002	0.004	2.650	2.596
40-50	0.002	0.003	1.918	2.123
50-60	0.006	0.016	5.942	7.741
LP				
0-10	0.012	0.020	6.785	8.977
10-20	0.006	0.011	4.976	5.967
20-30	0.006	0.011	5.208	5.375
30-40	0.006	0.011	5.580	5.322
40-50	0.005	0.009	4.967	5.104
50-60	0.005	0.009	5.025	5.267
60-70	0.004	0.008	4.059	4.240
70-80	0.003	0.005	2.432	3.071
CLF				
0-10	0.009	0.022	6.421	10.531
10-20	0.007	0.019	6.006	8.768
20-30	0.004	0.008	3.670	4.199
30-40	0.003	0.007	3.267	2.817
40-50	0.011	0.028	11.226	11.695
50-60	0.015	0.039	18.643	11.269
MMS				
Organic	0.013	0.019	7.666	8.698

	Mn/Al	**Mn/Fe**	**Mn/Cr**	**Mn/Zn**
0-8	0.008	0.013	5.579	6.174
8-17	0.006	0.011	4.668	5.135
17-29	0.004	0.007	3.351	3.033
29-39	0.003	0.006	3.279	2.911
39-45	0.003	0.005	2.972	2.725
45-51	0.002	0.004	2.634	2.393
51-57	0.002	0.004	2.492	2.140
57-63	0.006	0.006	7.070	4.857
63-69	0.002	0.004	2.791	2.189
69-76	0.002	0.004	2.525	2.105
76-83	0.001	0.003	1.674	1.621
83-90	0.001	0.003	0.900	0.000
90-101	0.001	0.003	1.417	1.385
118-127	0.010	0.020	10.151	8.871
127-138	0.009	0.017	9.359	9.118
138-147	0.005	0.009	4.490	5.181
147-156	0.005	0.008	4.407	4.106
156-163	0.006	0.011	5.756	4.777
163-172	0.009	0.015	9.389	9.809
172-175	0.006	0.010	8.117	6.460
175-179	0.005	0.010	6.493	4.655
VL				
0-9	0.021	0.045	15.626	16.776
9-15	0.014	0.030	12.344	14.341
15-21	0.008	0.017	8.446	9.065
21-25	0.006	0.012	6.172	5.857
25-42	0.004	0.007	4.024	3.465
42-48	0.003	0.004	2.541	2.660
48-53	0.002	0.003	1.832	1.852
53-58	0.002	0.004	2.205	2.164
58-63	0.002	0.003	1.765	1.775
63-68	0.001	0.002	1.475	1.488
68-74	0.001	0.002	1.173	0.975
74-80	0.001	0.002	1.250	1.030
80-88	0.001	0.002	1.329	1.147
88-96	0.001	0.002	1.259	1.079
120-128	0.005	0.008	5.530	3.788
128-136	0.004	0.007	4.744	4.052
136-144	0.004	0.007	4.212	4.140
144-152	0.004	0.008	4.562	4.804

152-162	0.008	0.013	10.470	7.769
	Mn/Al	**Mn/Fe**	**Mn/Cr**	**Mn/Zn**
162-190	0.005	0.007	6.235	4.500
190-202	0.004	0.007	4.743	3.441
PR				
0-10	0.012	0.020	7.456	7.941
10-20	0.006	0.013	6.787	4.931
20-30	0.003	0.005	3.851	2.861
30-40	0.002	0.004	2.905	1.873
40-50	0.002	0.003	2.517	1.910
50-60	0.002	0.004	2.447	1.789
60-67	0.011	0.025	13.144	9.642
IR				
0-10	4.560	0.011	3.137	4.349
10-20	5.356	0.012	3.335	5.212
20-30	2.789	0.006	2.069	3.079
30-40	3.546	0.007	2.415	3.446
40-50	3.076	0.006	2.382	2.822
50-60	2.966	0.005	2.472	3.356
60-70	2.876	0.005	2.234	2.706
GF				
0-13	24.686	0.058	17.270	19.190
13-23	17.983	0.042	13.498	16.341
23-33	11.395	0.024	9.700	12.386
33-43	10.677	0.021	8.735	9.086
43-53	10.557	0.021	8.929	11.448
53-63	9.669	0.016	9.050	11.661
73-83	3.323	0.005	3.353	3.887
83-93	2.692	0.004	3.213	-
93-103	13.400	0.023	16.723	-
103-113	9.985	0.017	10.626	11.553
133-143	5.607	0.011	6.224	5.707

Appendix C. Backscatter Scanning Electron Microscope Image of Zircon Grains

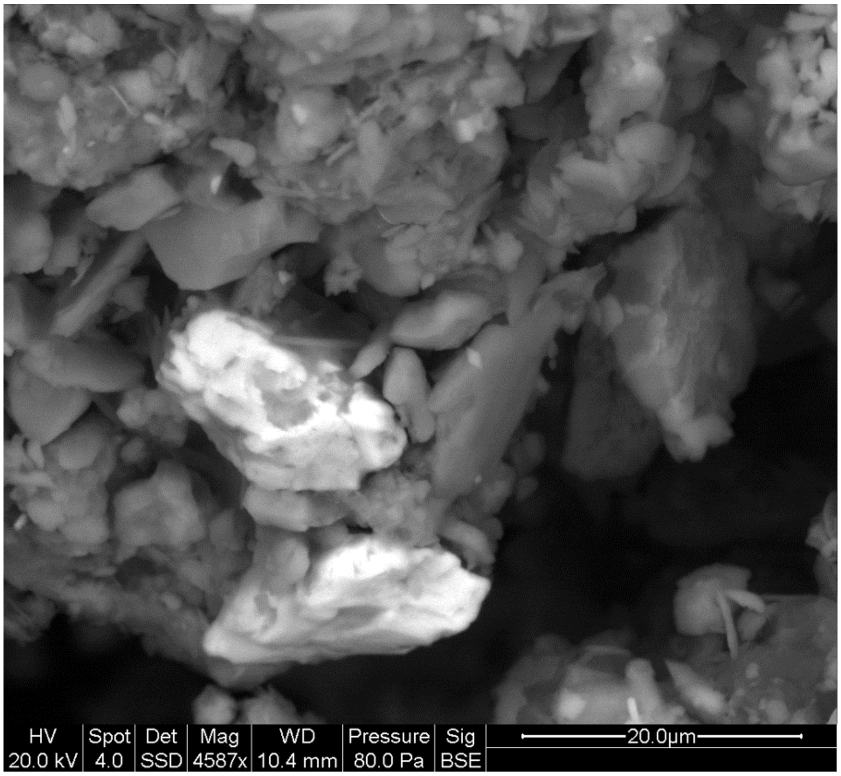

Chemical composition of grain was determined to be 28 wt. % Zr, 23 wt. % Si, 3 wt. % Al, and 48 wt. % O.

Appendix D: Error Calculation for Integrated Mass Transfer Coefficients ($\tau_{i,j}$)

$$\left(\frac{\Delta\tau}{\tau+1}\right)^2 = \left(\frac{\Delta C_{j,w}}{C_{j,w}}\right)^2 + \left(\frac{\Delta C_{i,p}}{C_{i,p}}\right)^2 + \left(\frac{\Delta C_{j,p}}{C_{j,p}}\right)^2 + \left(\frac{\Delta C_{i,w}}{C_{i,w}}\right)^2$$

Appendix E: Error Calculation for Integrated Mass Flux (m_j)

$$m_j = C_{j,p}\,\rho_p \sum_{z=0}^{z=L} \frac{\tau(z)}{\varepsilon(z)+1}\Delta z$$

If $f = \sum_{z=0}^{z=L} \frac{\tau(z)}{\varepsilon(z)+1}\Delta z$, then $m_j = C_{j,p}\,\rho_p\, f$

$$\left(\frac{\Delta m_j}{m_j}\right)^2 = \left(\frac{\Delta C_{j,p}}{C_{j,p}}\right)^2 + \left(\frac{\Delta \rho_p}{\rho_p}\right)^2 + \left(\frac{\Delta f}{f}\right)^2$$

$$\left(\frac{\Delta\left(\frac{\tau(z)}{\varepsilon(z)+1}\Delta z\right)}{\left(\frac{\tau(z)}{\varepsilon(z)+1}\Delta z\right)}\right)^2 = \left(\frac{\Delta\tau}{\tau}\right)^2 + \left(\frac{\Delta(\varepsilon(z)+1)}{(\varepsilon(z)+1)}\right)^2$$

$$(\Delta f)^2 = \sum\left(\Delta\left(\frac{\tau(z)}{\varepsilon(z)+1}\Delta z\right)\right)^2 = \sum\left(\left(\left(\frac{\Delta\tau}{\tau}\right)^2 + \left(\frac{\Delta(\varepsilon(z)+1)}{(\varepsilon(z)+1)}\right)^2\right)\left(\frac{\tau(z)}{\varepsilon(z)+1}\Delta z\right)^2\right)$$

$$\left(\frac{\Delta f}{f}\right)^2 = \frac{\sum\left(\left(\frac{\tau(z)}{\varepsilon(z)+1}\Delta z\right)^2\left(\left(\frac{\Delta\tau}{\tau}\right)^2 + \left(\frac{\Delta(\varepsilon(z)+1)}{(\varepsilon(z)+1)}\right)^2\right)\right)}{\left(\sum\frac{\tau(z)}{\varepsilon(z)+1}\Delta z\right)^2}$$

$$\left(\frac{\Delta(\varepsilon(z)+1)}{(\varepsilon(z)+1)}\right)^2 = \left(\frac{\Delta C_{i,p}}{C_{i,p}}\right)^2 + \left(\frac{\Delta \rho_p}{\rho_p}\right)^2 + \left(\frac{\Delta C_{i,w}}{C_{i,w}}\right)^2 + \left(\frac{\Delta \rho_w}{\rho_w}\right)^2$$

$$\left(\frac{\Delta\tau}{\tau+1}\right)^2 = \left(\frac{\Delta C_{j,w}}{C_{j,w}}\right)^2 + \left(\frac{\Delta C_{i,p}}{C_{i,p}}\right)^2 + \left(\frac{\Delta C_{j,p}}{C_{j,p}}\right)^2 + \left(\frac{\Delta C_{i,w}}{C_{i,w}}\right)^2$$

Appendix F. Table of Variables Used to Reconstruct Deposition History

Variable	Units	Definition
$\boldsymbol{F_{x}}$	mg cm^{-2} yr^{-1}	Calculated Mn deposition rate
$\boldsymbol{F_{2007}}$	mg cm^{-2} yr^{-1}	Calculated average Mn deposition rate for 2007 from Fig. 21 (Herndon *et al.*, 2010*)*
$\boldsymbol{M_{EMI,x}}$	*metric tons* yr^{-1}	Mass of Mn emitted by EMI, known for each year (x) from 1988-2010, calculated using eq. 6 for years prior
$\boldsymbol{M_{EMI,1988\text{-}2010}}$	*metric tons* yr^{-1}	Average Mn emissions per year from EMI (1988-2010)
$\boldsymbol{A_{x}}$	*metric tons* yr^{-1}	Reported U.S. Mn alloy consumption per year
$\boldsymbol{A_{USA,1988\text{-}2010}}$	*metric tons* yr^{-1}	Average U.S. Mn alloy consumption (1988-2010)
$\boldsymbol{F_{avg,1952\text{-}1970}}$	mg cm^{-2} yr^{-1}	Average Mn deposition rate calculated from 1952-1970
$\boldsymbol{m_{Mn}}$	*mg* cm^{-2}	Area-normalized Mn mass flux at BKR (~76000 mg cm^{-2})
$\boldsymbol{C_{DEP}}$	*mg* cm^{-2}	Cumulative amount of calculated Mn deposited 1971-2010 (ΣF_x, where x=1971-2010)

Appendix G. SCIPUFF Sensitivity Tests

Sensitivity tests were run to assess the effect of precipitation, particle size and bulk density on Mn deposition rates modeled using SCIPUFF. Increasing precipitation from no rain to heavy rain throughout the entire year resulted in an increase in Mn deposition rates of about an order of magnitude (Fig. G1). Mn deposition rates calculated using the observed precipitation were closer to the no rain scenario, an expected result since observed precipitation resulted in dry conditions ~85% of the year. Varying particle size, while holding all other inputs constant, showed that Mn deposition rates are at a minimum in the size range of reported particle emissions (0.05-0.4 μm) and that deposition rates increase both above and below this particle size diameter, as well as on the lower and higher end of the range (Fig. G2a, G2b). Reducing bulk density from 5.08 g cm^{-2} to 1.00 g cm^{-2} resulted in decreased Mn deposition rates. These results suggest that if particles aggregate in the atmosphere to form masses of greater effective particle size, higher deposition rates would be observed in the vicinity of the refinery.

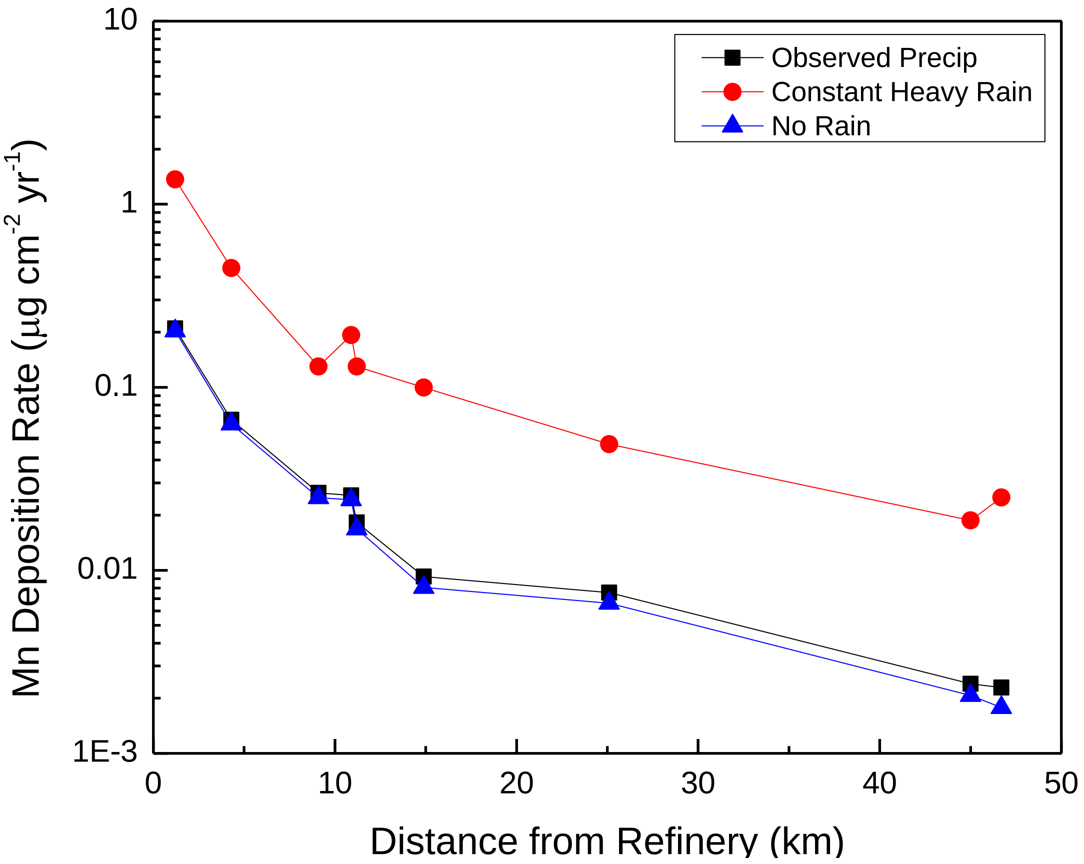

Figure G1. Modeled Mn deposition rates differ by an order of magnitude between constant heavy rain and no rain throughout the year at each core location. Using observed precipitation, Mn deposition rates are only slightly greater than using the no rain scenario, reflecting the fact that observed precipitation (~100 cm) occurred during only about 15% of the year. All other inputs were held constant including particle size, bulk density and emission rate. Observed precip scenario is the same as modeled scenario presented in figures 18-20.

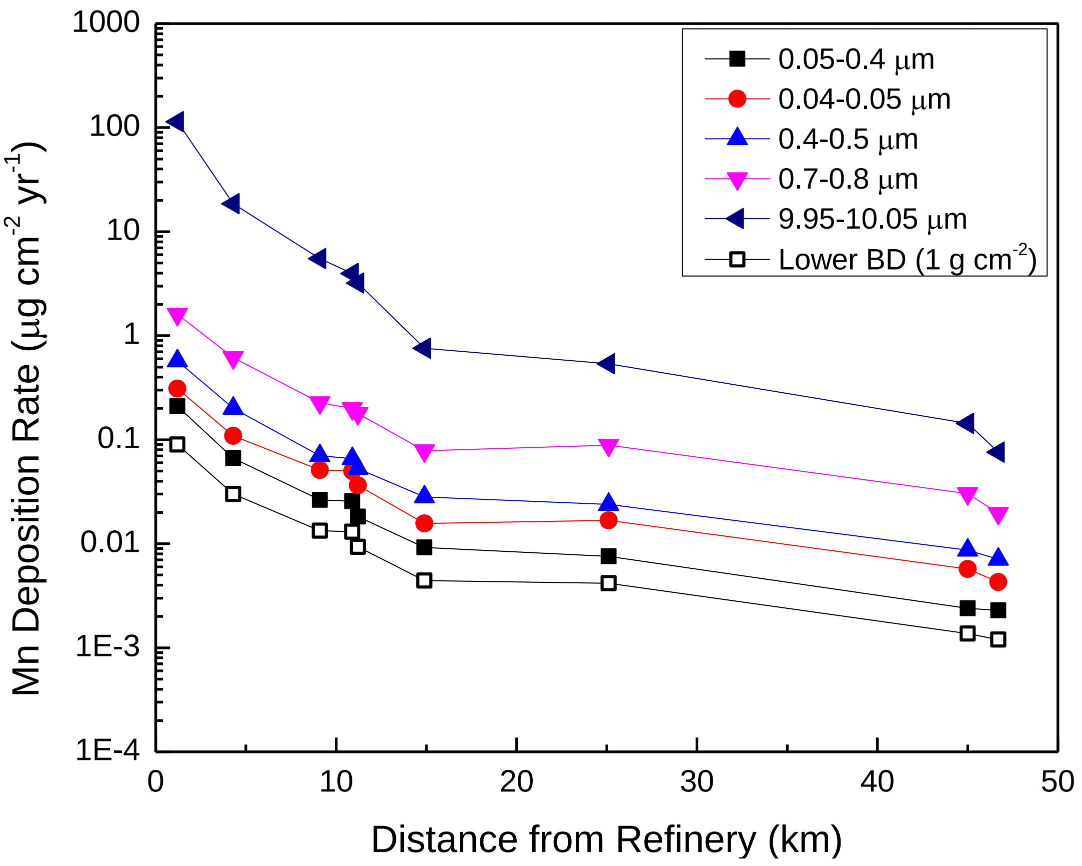

Figure G2a. Using the 2006 emission rate, a bulk density of 5.08 g cm^{-2}, and observed precipitation, model-derived Mn deposition rates for particle sizes on the low end (red circles) and high end (blue upward triangles) of size range reported for particulate emissions from ferromanganese production (closed black squares) are higher than for the entire reported range. Deposition rates increase with increasing particle above this size range to nearly 3 orders of magnitude higher than the modeled rate using the reported particle size range (0.05-0.4 µm). Using the same reported particle size range, but lowering bulk density from 5.08 g cm^{-2} to 1.00 g cm^{-2} decreases modeled Mn deposition rates (open black squares).

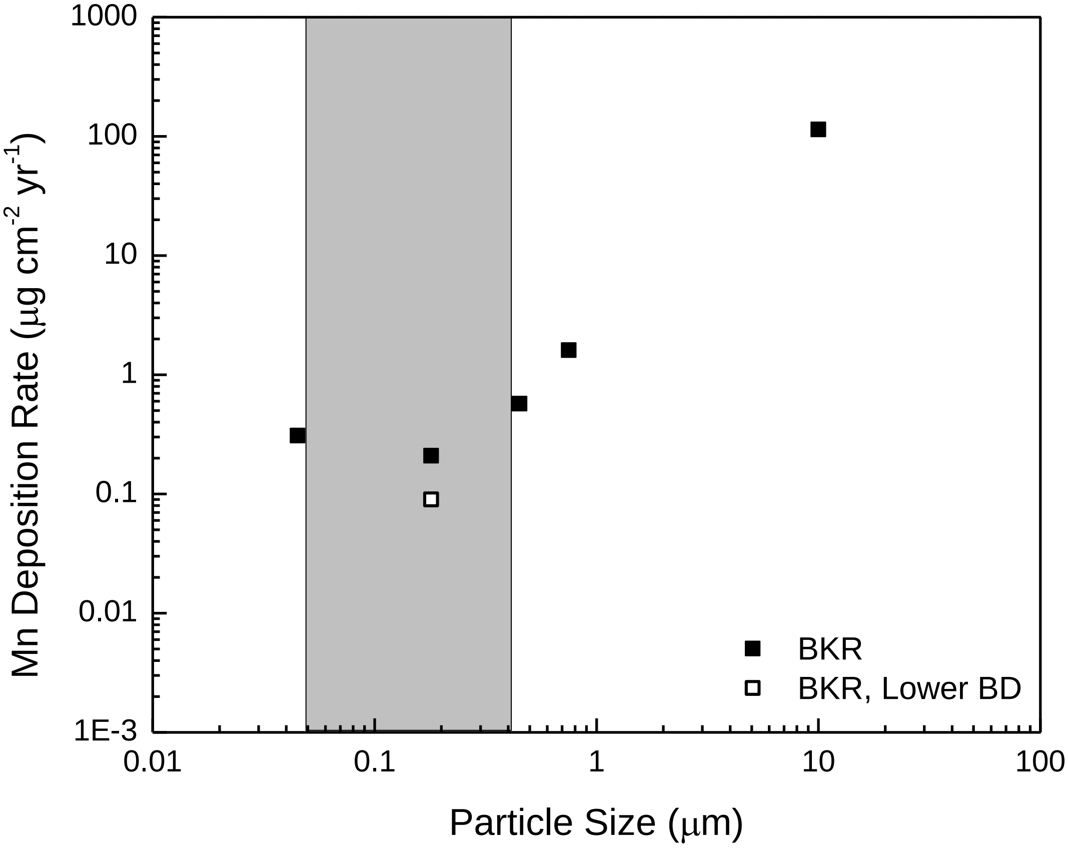

Figure G2b. Modeled Mn deposition rates at BKR are at a minimum within the range reported for particulate emissions from ferromanganese production (grey box). Reducing bulk density to 1.00 g cm^{-3} from 5.08 g cm^{-3} results in a lower Mn deposition rate.

Appendix H. US Mn Air Emissions by Industry Type 1988-2010

Industry	Number of Mn-emitting Facilities	Total Mn Air Emissions 1988-2010 (metric tons)*	% of US Mn Air Emissions 1988-2010*
331 Primary Metals	1040	16722 (4361)	49.88 (13.01)
332 Fabricated Metals	1065	3376	10.07
336 Transportation Equipment	599	2508	7.48
333 Machinery	651	2389	7.13
325 Chemicals	335	2325	6.93
2211 Electric Utilities	401	2181	6.51
322 Paper	147	1433	4.27
ZZZ No TRI NAICS code	275	714	2.13
327 Stone/Clay/Glass	127	655	1.95
335 Electrical Equipment	54	284	0.85
321 Wood Products	51	219	0.65
339 Miscellaneous Manufacturing	50	187	0.56
2122 Metal Mining	271	158	0.47
311 Food/Beverages/Tobacco	69	118	0.35
3273 Cement	62	91	0.27
337 Furniture	58	50	0.15
324 Petroleum	43	43	0.13
334 Computers/Electronic Products	33	36	0.11
316 Leather	7	19	0.06
562 Hazardous Waste/Solvent Recovery	37	7	0.02
326 Plastics and Rubber	43	6	0.02
2121 Coal Mining	13	4	0.01
323 Printing and Publishing	4	0	0.00
315 Apparel	3	0	0.00
4246 Chemical Wholesalers	2	0	0.00
313 Textiles	2	0	0.00
4247 Petroleum Bulk Terminals	2	0	0.00
Sum	**5444**	**33525**	**100.00**

* Values in parentheses are only for Eramet Marietta, Inc.